

STB FILE COPY

AD-A230 684



Analysis of Space Radiation Effects in Gallium Arsenide
and Cadmium Selenide Semiconductor Samples
Using Luminescence Spectroscopic Techniques

THESIS

Brad Lee Shaffer
Captain, USA

AFT/CSO/END/00D 02

S DTIC
ELECTE
JAN 08 1991
E D

DEPARTMENT OF THE AIR FORCE
AIR UNIVERSITY

AIR FORCE INSTITUTE OF TECHNOLOGY

Wright-Patterson Air Force Base, Ohio

DISTRIBUTION STATEMENT A

Approved for public release;
Distribution Unlimited

91 1 3 071

AFIT/GSO/ENP/90D-02

Analysis of Space Radiation Effects in Gallium Arsenide
and Cadmium Selenide Semiconductor Samples
Using Luminescence Spectroscopic Techniques

THESIS

Brad Lee Shaffer
Captain, USA

AFIT/GSO/ENP/90D-02

DTIC
ELECTE
JAN 08 1991
S E D

Approved for public release; distribution unlimited

AFIT/GSO/ENP/90D-02

Analysis of Space Radiation Effects in Gallium Arsenide
and Cadmium Selenide Semiconductor Samples
Using Luminescence Spectroscopic Techniques

THESIS

Presented to the Faculty of the School of Engineering
of the Air Force Institute of Technology
Air University

In Partial Fulfillment of the
Requirements for the Degree of
Master of Science (Space Operations)

Brad Lee Shaffer, B.S.
Captain, USA

December, 1990

Accession For	
NTIS GRA&I	<input checked="" type="checkbox"/>
DTIC TAB	<input checked="" type="checkbox"/>
Unannounced	<input type="checkbox"/>
Justification	
By _____	
Distribution/	
Availability Codes	
Dist	Avail and/or Special
A-1	

Approved for public release; distribution unlimited



Preface

I am grateful for the opportunity to examine these unique semiconductor samples. They represent the first semiconductor materials purposely exposed to and retrieved from the space environment for analysis. The educational experience has been extremely rewarding.

It is important at this time to recognize an individual who's assistance was instrumental in the completion of this work, Greg Smith, physics laboratory technician. If not for his constant help and sage advice I would still be putting the apparatus together. I would also like to thank my advisors, Dr. R. L. Hengehold and Dr. Y. K. Yeo, for their assistance and mentorship, and Maj. Morlan, Operations Research Department, for his editorial talents. Other individuals that need recognition are: Bill Evans, Leroy Cannon, and Rick Patton, Physics Department, for their logistical support and technical assistance, and Lt. Michele Jones and Mr. Charles Hurley, WPAFB Materials Laboratory, for preparation and management of the M0006 samples. Finally, I would like to thank Dr. D. Sparlin, University of Missouri-Rolla Physics Department, for sparking my interest in solid state physics, and for his memorable teachings, undying devotion to his students, and personal interest in their successful completion of the difficult curriculum.

No married individual could possibly hope to complete such an arduous task without the support of his roommate and family. I must thank my wife, Debbie Jo, for taking up the slack left by my preoccupation. She was my source of motivation and inspiration, and only through her support was I able to complete this research. And thanks to my children, Kenneth, Joshua, and Danielle, for understanding.

I would like to dedicate this work to an outstanding man, superb soldier, and highly professional Noncommissioned Officer. His firm and fair leadership, comprehensive engineering knowledge and skills, and commanding personality made him widely loved, respected and remembered by subordinates, peers, and superiors alike ... CSM (Ret) Kenneth Lamar Snaffer.

Brad Lee Shaffer

Table of Contents

	Page
Preface	ii
Table of Contents	iv
List of Figures	vii
List of Tables	x
Abstract	xi
I. Research Problem and Methods	1
1.1 Background	1
1.2 Problem Statement	4
1.3 Research Objective	4
1.3.1 Sub-objectives	4
1.3.2 Scope	4
1.4 Methodology	5
II. Literature Review - Luminescence	6
2.1 Introduction	6
2.2 Luminescence	6
2.2.1 Energy Band Theory.	7
2.3 Cathodoluminescence	10
2.3.1 Electron Penetration	11
2.3.2 Specific Energy Losses	13
2.4 Photoluminescence	13
2.4.1 Penetration Depths	15
2.5 Conclusion	16

	Page
III. Literature Review - Low Earth Orbit Space Environment and Radiation	
Effects on Semiconductors	17
3.1 Introduction	17
3.2 Low Earth Orbit Environment	17
3.2.1 Galactic Radiation	18
3.2.2 Solar Radiation	23
3.2.3 Trapped Radiation	24
3.2.4 Atmospheric Considerations	29
3.2.5 Summary	40
3.3 Radiation Effects On Semiconductors	42
3.3.1 General Effects	42
3.3.2 Gallium Arsenide	47
3.3.3 Cadmium Selenide	49
3.3.4 Summary	50
3.4 Conclusion	50
IV. Apparatus and Procedures	52
4.1 The System	52
4.1.1 Sample Information	52
4.1.2 System Overview	53
4.1.3 Vacuum System	53
4.1.4 Cryogenic Transfer System	58
4.1.5 Sample Finger	58
4.1.6 Sample Handling	59
4.1.7 Electron Gun	59
4.1.8 Optical System	60
4.1.9 Signal detection and Processing system	63
4.2 Procedure	63

	Page
4.2.1 Chamber Evacuation	63
4.2.2 Sample Cooling	65
4.2.3 Electron Beam Alignment	66
4.2.4 Spectrometer Alignment	67
4.2.5 Optics Alignment	67
4.2.6 Luminescence Measurements	68
V. Results and Discussion	69
5.1 Results	69
5.1.1 LEC, undoped, semi-insulating, GaAs (Cominco)	69
5.1.2 Sample #12; CdSe:S, high resistance	71
5.1.3 Sample #13; CdSe:S, low resistance	73
5.1.4 Sample #14; <i>p</i> -GaAs:Zn, 6.42×10^{18} Zn/cm ³ . .	77
5.1.5 Sample #15; <i>n</i> -GaAs, 1.42×10^{16} /cm ³	77
5.1.6 Sample #16; compensated GaAs, epitaxial, high resistance	82
5.1.7 Sample #17; <i>n</i> -GaAs:Si, $2-4 \times 10^{18}$ Si/cm ³	82
5.1.8 Sample #18; GaAs:Si, $N = 2.9 \times 10^{18}$ /cm ³	87
5.1.9 Sample #19; GaAs:Si, $N = 2.1 \times 10^{18}$ /cm ³	87
5.1.10 Sample #20; GaAs:Si, $N = 0.92 \times 10^{18}$ /cm ³	91
5.1.11 Sample #21; GaAs:Si, $N = 0.66 \times 10^{18}$ /cm ³	91
5.2 Discussion	91
VI. Conclusions and Recommendations	97
6.1 Conclusions	97
6.2 Recommendations	97
Bibliography	99
Vita	106

List of Figures

Figure	Page
1. Long Duration Exposure Facility Altitude History	2
2. Radiative Transitions	8
3. Cathodoluminescence Depth Profile	14
4. Momentum Required for Penetration to the Earth's Surface	20
5. Differential Energy Spectra for Protons in a 463-km Orbit	21
6. Differential Energy Spectra for Helium Nuclei in a 463-km Orbit	22
7. Charged Particle Movement Along Magnetic Field Lines	25
8. The Inner And Outer Radiation Belts	26
9. Contours Of Constant Intensity Of Electrons With Energies Greater Than 0.5 MeV	28
10. Total Intensity F Of The Earth's Magnetic Field	30
11. Southern Atlantic Anomaly	31
12. Concentrations Of Major Atmospheric Constituents During Daytime	32
13. Concentrations Of Major Atmospheric Constituents During Nighttime	33
14. Concentrations Of Major Atmospheric Constituents For An Exospheric Temperature Of 1300 Degrees K	35
15. Ground Trace For 30 Degree Inclination, 170 km Orbit Through The South Atlantic Anomaly With Electron Energies Greater Than 0.5 MeV Shown	36
16. LDEF Orientation In Space	38
17. LDEF Structure	39
18. LDEF Accumulated Direct Solar Dose	41
19. Range-Energy Curves For Penetrating Radiations	45
20. System Diagram	54
21. Vacuum System	55

Figure	Page
22. Upper Chamber Housing	56
23. Lower Chamber Housing	57
24. Optical System	61
25. Cathodoluminescence Spectra Of Cominco; LEC, Undoped, Semi-insulating GaAs	72
26. Cathodoluminescence Spectra of Sample #12; High-Resistance, Sulfur Contaminated CdSe, Control and Exposed Samples	74
27. Cathodoluminescence Spectra of Sample #13; Low-Resistance, Sulfur Contaminated CdSe, Control and Exposed Samples	76
28. Cathodoluminescence Spectra of Sample #14; Zn-doped (<i>p</i> -type) GaAs (6.42×10^{18} Zn/cm ³) Control And Exposed Samples	78
29. Cathodoluminescence Spectra of Sample #15; Undoped (<i>n</i> -type) GaAs (1.42×10^{16} /cm ³) Control Sample at 100 μ A	80
30. Cathodoluminescence Spectra of Sample #15; Undoped (<i>n</i> -type) GaAs (1.42×10^{16} /cm ³) Exposed Sample at 2 keV	81
31. Cathodoluminescence Spectra of Sample #17; Si-Doped (<i>n</i> -type) GaAs ($2-4 \times 10^{18}$ Si/cm ³) Control Sample at 3 keV - 100 μ A, and 1 keV - 5 μ A	83
32. Cathodoluminescence Spectra of Sample #17; Si-Doped (<i>n</i> -type) GaAs ($2-4 \times 10^{18}$ Si/cm ³) Exposed Sample at 3 keV - 100 μ A, and 1 keV - 5 μ A	84
33. Cathodoluminescence Spectra of Sample #17; Si-Doped (<i>n</i> -type) GaAs ($2-4 \times 10^{18}$ Si/cm ³) Control And Exposed Samples at 3 keV Beam Energy	85
34. Cathodoluminescence Spectra of Sample #17; Si-Doped (<i>n</i> -type) GaAs ($2-4 \times 10^{18}$ Si/cm ³) Control And Exposed Samples at 2 keV Beam Energy	86
35. Cathodoluminescence Spectra of Sample #18; Si-Doped GaAs (2.9×10^{18} /cm ³) Control And Exposed Samples	88
36. Cathodoluminescence Spectra of Sample #19; Si-Doped GaAs (2.1×10^{18} /cm ³) Control Sample at 100 μ A	89
37. Cathodoluminescence Spectra of Sample #19; Si-Doped GaAs (2.1×10^{18} /cm ³) Exposed Sample at 100 μ A	90

Figure	Page
38. Cathodoluminescence Spectra of Sample #19; Si-Doped GaAs ($2.1 \times 10^{18}/\text{cm}^3$) Control And Exposed Samples at 1 keV and $100 \mu\text{A}$. . .	92
39. Cathodoluminescence Spectra of Sample #20; Si-Doped GaAs ($0.92 \times 10^{18}/\text{cm}^3$) Control Sample at 2 keV	93
40. Cathodoluminescence Spectra of Sample #20; Si-Doped GaAs ($0.92 \times 10^{18}/\text{cm}^3$) Exposed Sample at 2 keV	94
41. Cathodoluminescence Spectra of Sample #20; Si-Doped GaAs ($0.92 \times 10^{18}/\text{cm}^3$) Control And Exposed Samples	95

List of tables

Table		Page
1.	Electron Beam Energies and Penetration Depths In GaAs	12
2.	Relative Abundances of Radiation Nuclei	19
3.	Ambient Particle Flux Change Due To Satellite Passage	40
4.	LDEF Sample Descriptions	70

Abstract

Analysis of space radiation effects in gallium arsenide and cadmium selenide semiconductor samples using luminescence spectroscopic techniques. The M0006 semiconductor samples were placed into a 28.5 degree inclination, 480 km altitude, near-circular orbit aboard the Long Duration Exposure Facility satellite and exposed to direct space environment for a period of 11 months, and were shielded by 0.313 inches of aluminum for another 58 months. The samples were examined for changes using cathodoluminescence and photoluminescence in various wavelength regions from 0.5 to 1.8 microns. Samples were cooled to approximately 10 degrees Kelvin in a vacuum of 10^{-8} torr. Cathodoluminescence was performed with 1-3 keV electron energies at beam currents of 5-100 microamperes (2.5×10^{14} to 5.0×10^{15} electrons/cm²-sec). The photoluminescence excitation source was a 20 mW Argon laser. Changes were detected in some of the sample pairs which could be attributed to radiation induced effects. The changes primarily manifested themselves in three different categories: 1) decrease or increase of luminescent intensity; 2) shifts in peak locations; and 3) quenching of a peak. Special changes noted by sample and category were: #12 (CdSe:3), 1) exposed sample increased five times in luminescent intensity, and the luminescence lines shifted slightly towards shorter wavelengths; #13 (CdSe:S), 1) the exposed sample had about five times greater luminescence than the control sample, additionally, the exciton related emission increased much more strongly than the donor-acceptor pair emission did for the exposed sample; #14 (p-GaAs:Zn), no changes; #15 (n-GaAs), 1) the relative intensity of carbon donor-acceptor pair emission increased slightly than that of the carbon free-to-bound transition from the exposed sample; #16 (GaAs), compensated material provided no signal in either control or exposed samples to evaluate; #17 (n-GaAs:Si), 3) the 1.479 eV Si donor-acceptor pair transition and 0.77 eV arsenic antisite related lines were quenched; #18 (GaAs:Si), 1) decrease in luminescence intensity, 2) peak shift

towards longer wavelengths; #19 (GaAs:Si), 1) decrease in luminescence intensity; #20 (GaAs:Si), 2) peak shift towards longer wavelengths from 1.489 eV for control sample to 1.476 eV for the exposed sample; #21 (GaAs:Si), exposed sample was too damaged from unmounting process to be examined.

Analysis of Space Radiation Effects in Gallium Arsenide
and Cadmium Selenide Semiconductor Samples
Using Luminescence Spectroscopic Techniques

I. Research Problem and Methods

1.1 Background

Space radiation is thought to produce defects in semiconductors and reduce their reliability. With the purpose of gaining a better understanding of this interaction, several semiconductor samples were placed into space aboard the Long Duration Exposure Facility (LDEF) scientific satellite. Their exposure will enable scientists to examine in their laboratories, for the first time, the effects of long term exposure to space radiation on semiconductors.

The LDEF carried 57 experiments into space, including 8 gallium arsenide and 2 cadmium selenide semiconductor samples. On 7 April 1984, the space shuttle Challenger positioned the satellite into a 28.5 degree inclination, 480 kilometer altitude, near-circular orbit. The satellite's attitude was three-axis gravity gradient stabilized (one end of its cylindrical-like shape always faced the earth, the other end faced away, and it did not rotate around any of its three axis). When the satellite was rescued from a decaying orbit on 12 January 1990, the LDEF appeared to be in the same stable attitude it was originally positioned in five years and nine months earlier (17:35). Figure 1 shows that the altitude of the satellite was fairly constant throughout the length of the mission until the last year when it's altitude decayed very rapidly.

The gallium arsenide and cadmium selenide semiconductor samples are part of the Space Environment Effects experiment M0006. The purpose of the experiment

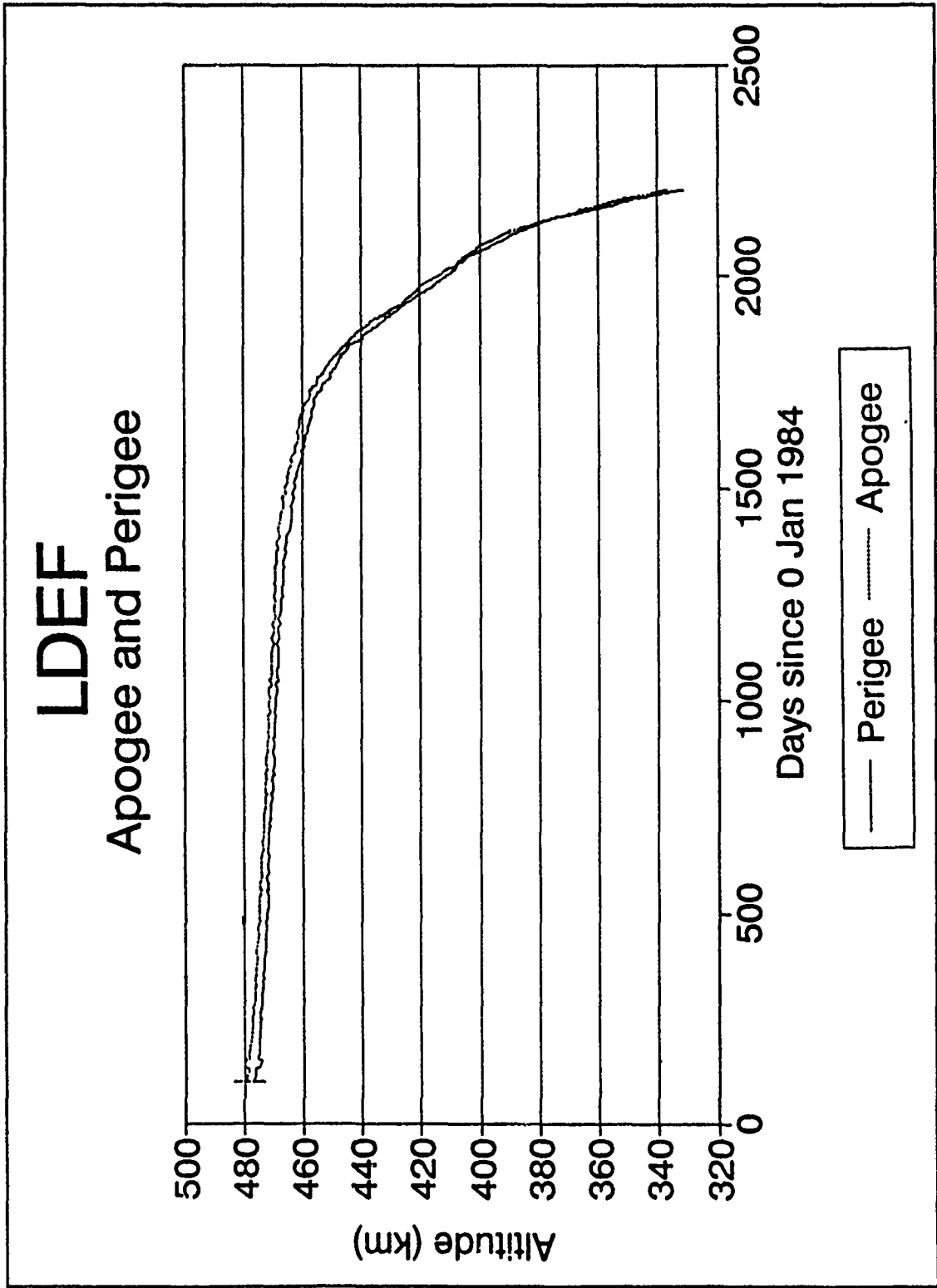


Figure 1. Long Duration Exposure Facility Altitude History (40)

was to examine the effects of long-term exposure to the near-earth space environment on advanced electro-optical sensor and radiation sensor components. The samples were hard-mounted in an Experimental Exposure Control Canister which measured 96.5 cm by 127 cm wide, and 15.24 cm deep. The sealed canister prevented contamination of the samples until returned to the laboratory. The canister was programmed to open its cover two weeks after deployment in space, and close it eleven months later (53:185). In this manner, the samples would be directly exposed for a specific period of time. It is believed that the canister operated as programmed.

While in the near-earth orbit, the samples were exposed to several types of radiation: geomagnetically trapped electrons and protons, galactic cosmic-ray ions and solar-flare particles, and their associated secondary interaction products. These radiations vary in energies from keV to GeV and beyond, and in intensities from one geographic region to the next (1:67) (18:483). The type of radiation most likely to cause change in the samples was geomagnetically trapped protons and electrons. This is because LDEF's orbit, although about 85% radiation free, had one area of intense trapped proton radiation over the South Atlantic. The LDEF passed through this region on the average of 6 out of 16 orbits each day (16:303) (18:484).

Satellite semiconductor detector systems are susceptible to degradation by space radiation. It can cause physical changes to materials in general, or induce a charge in electronic circuits. In the case of semiconductor detectors, it can interfere with detector operations by exceeding flux and/or energy capacities of the system, or by physically degrading the responsiveness and reliability of the device.

Future satellites will employ detectors with greater sensitivity and resolution that will undoubtedly cost more and will be expected to operate longer. In order for these detectors to meet the challenge, a greater understanding of the effects produced by space radiation will be required. The information provided by this initial examination will constitute the first step of a long journey towards producing a new generation of radiation-hardened semiconductor detectors.

1.2 Problem Statement

To date, the LDEF samples had not been analyzed. A "first cut" analysis of the samples must be made using non-destructive spectroscopic techniques to detect physical changes in the materials. High resolution luminescent spectroscopy has proven to be an ideal technique for determining impurity and defect characteristics of materials. The results of this research will direct future analysis efforts.

1.3 Research Objective

Using luminescence spectroscopic techniques, determine what characteristic changes have occurred in the spectra of the exposed samples compared to the control samples, and identify what caused those changes.

1.3.1 Sub-objectives

1. Using cathodoluminescence, generate spectral output for undoped reference, control, and exposed samples. Compare these outputs and locate differences that may have occurred.
2. If no changes are detected in meeting sub-objective 1, use photoluminescence and generate spectral output for the undoped, control, and exposed samples. Compare these outputs and locate differences that may have occurred.
3. If changes have occurred, characterize the radiation environment and attempt to determine the cause of the changes.

1.3.2 Scope This thesis will entail a pragmatic initial analysis of the spectral output by visual inspection to identify changes. Identification of the cause(s) for spectral differences will be accomplished by comparison against known radiation effects data, and drawing inferences of similarities or trends.

1.4 Methodology

Analysis of the samples will be accomplished using high-resolution cathodoluminescence and/or photoluminescence spectroscopic techniques. Spectroscopy provides a spectrum of the material, which is then used to determine impurity and defect characteristics. Because the control and space exposed samples are pieces of the same semiconductor wafers, spectroscopy will reveal changes caused by the space radiation.

Luminescence is the process of stimulating radiation emission from a luminescent material as the result of some energy absorption. The radiated emission is in the form of photons, or light. This luminescent light can be captured and the luminescent intensity plotted as a function of wavelength; this process is known as spectroscopy. If the excitation energy is provided by a beam of electrons, the emission is called cathodoluminescence. If the excitation energy is provided by photons, the luminescence is called photoluminescence (47:2-3).

In cathodoluminescence, the penetrating electrons lose their kinetic energy through collisions with lattice electrons. Energy obtained via collisions excites the lattice electrons into a higher energy state, where they remain for a very short period of time. When the electrons return to the lower energy state, they emit photons characteristic of the difference of energy between the two electronic states.

The same basic process occurs for photoluminescence except the energy is carried into the lattice by photons. The emission process is the same as for cathodoluminescence described above.

II. Literature Review - Luminescence

2.1 Introduction

This chapter reviews the literature on luminescence to provide the reader with the basic concepts that underlie this research effort. Understanding these concepts will assist the reader in the discussion and conclusion sections of this thesis. The major topics discussed in this review are luminescence, cathodoluminescence, and photoluminescence. A separate chapter will review the most recent literature of radiation effects on semiconductor materials.

2.2 Luminescence

Luminescence is the phenomenon of emission of photons with characteristics unique to the radiating material (45:2). In order for luminescence to occur, the material must be excited. There are several methods of excitation, but this research will involve only two: cathodoluminescence, and photoluminescence. Cathodoluminescence depends on excitation by energetic electrons or cathode rays; photoluminescence depends on excitation by electromagnetic radiation or photons (77:2).

Luminescent emission results from electronic state transitions, which is characteristic of the source material. Because the same transitions can be created by different excitation methods, the resulting spectral emissions are normally independent of the method of the excitation. The generation of unique transition spectra is known as emission spectroscopy (77:3).

Some materials are dependent on the existence of impurities or defects within the structure in order for luminescence to occur. In general, imperfections include the following: impurity atoms, lattice defects, dislocations, and foreign particles (cosmic ray nuclei) (22:58) (45:2).

The explanation of luminescence requires the introduction of allowed energy states within the forbidden energy band separating the conduction band and the highest valence band. These states may be produced by chemical impurities, interstitials, or vacancies in the lattice, and are physically centered about the lattice imperfections. If an electron wandering through the crystal loses energy in the neighborhood of such an imperfection, it can be trapped by the localized state. Similarly, holes may be 'trapped' by these sites when an electron is released from the site and fills an empty state in the valence band. In an energy level scheme, electron traps occur near the conduction band, and hole traps occur near the valence band. Traps which lie deep enough within the forbidden region to act in both capacities are frequently called 'recombination centers,' since a hole and an electron may recombine there. Recombination centers are chiefly responsible for achieving equilibrium in a stimulated crystal because direct recombination, in which the entire gap energy must be lost during a very short interaction time, is highly improbable. When a transition involving a trap results in the emission of light, the trap may be referred to as a 'luminescent center.' Luminescent centers close to the conduction or valence bands make possible the emission of light of energy near E_g , the band gap energy. Such emission will therefore occupy a wavelength region on the long wavelength side of hc/E_g , the main absorption edge of the crystal. Luminescence so produced is called 'edge emission.' (58:15-16)

2.2.1 Energy Band Theory. Isolated atoms are surrounded by electrons at discrete energy levels. When the atoms are brought close together, as in a semiconductor crystal, the energy levels will split into distinct bands. The bands are separated by an energy gap where electrons are forbidden to reside. Defects or impurities in the crystal can introduce allowed energy levels into the energy gap, also known as the forbidden gap.

In the excitation of electrons from the valence band to the conduction band, electrons are permitted to cross the energy gap provided their energy is greater than the gap energy. Vacancies will be left in the valence band after electrons have departed. These vacancies are referred to as holes. In the process of returning to the valence band, the electron's energy is either absorbed by the crystal or lost through radiation.

In general, impurities that occupy lattice sites and possess extra electrons not involved in covalent bonding with adjacent lattice atoms are called donors, or *n*-type impurities. Impurities with insufficient numbers of electrons to satisfy covalent bonding demands with adjacent lattice atoms are called acceptors, or *p*-type impurities. Donor impurity levels are usually found on the conduction band side of the forbidden gap, and acceptor levels are found on the valence band side (See Figure 2) (22:65).

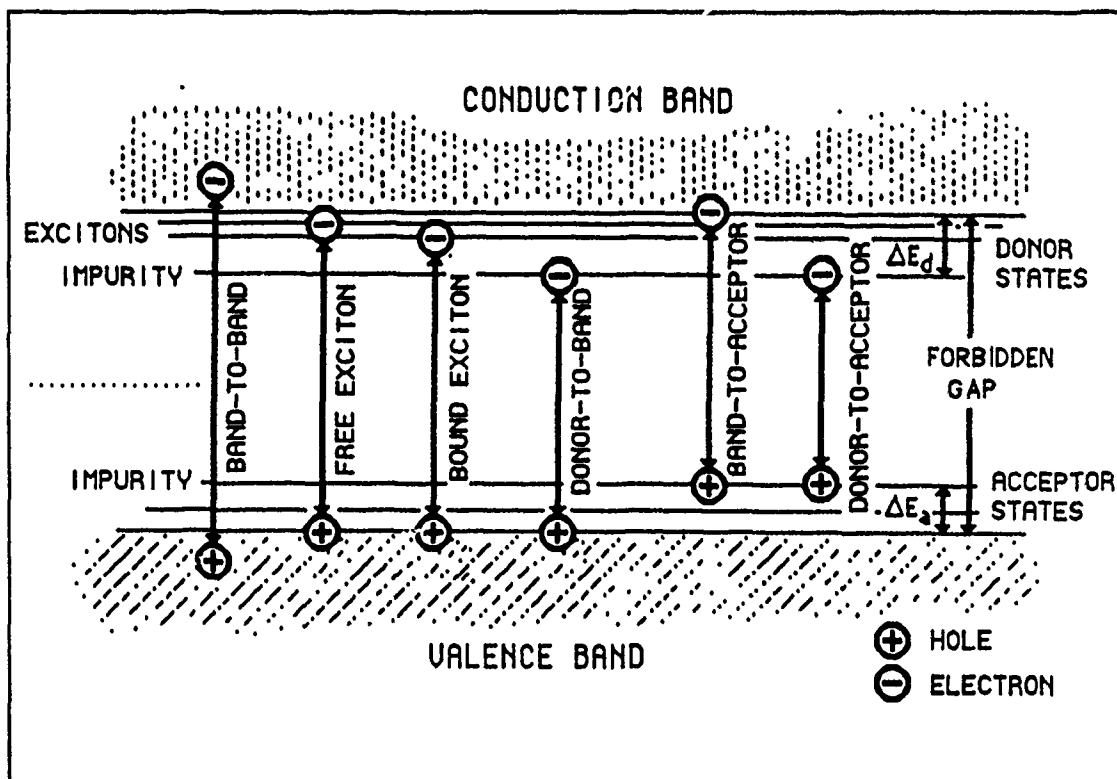


Figure 2. Radiative transitions (33:9)

In gallium arsenide (GaAs) semiconductors, impurities from the elements in Group II of the Periodic Table occupying Ga sites are acceptors, and those from Group VI occupying As sites are donors. Group IV elements produce donors if they

replace Group III elements, and acceptors if they replace Group V elements, hence they can produce both *p*-type and *n*-type activities (79:197).

The following definitions can be applied to both GaAs and CdSe conduction band and valence band transitions at temperatures only near liquid helium (4.2 degrees Kelvin), but the specific values quoted are applied to GaAs. The symbols ΔE_d and ΔE_a are the donor and acceptor ionization energies, respectively.

2.2.1.1 Band to Band. Conduction band to valence band radiative transitions have not been seen in GaAs produced by today's technology. This direct recombination process is highly improbable. For this transition to occur, both the electron and the hole must be moving and within absorption range of each other, which is on the order of 5.0×10^{-9} meters. For these conditions to be met with any probability, their lifetime in the transition state must be approximately one second. This is hundreds, if not thousands, of times greater than observed lifetimes, and, therefore highly improbable to occur (22:96).

2.2.1.2 Band to Excitons. An electron and a hole pair bound together by their electrostatic force is called an exciton. It transports energy through the lattice, but it does not transport charge because it is electrically neutral. Since it has no net charge, it does not react to electric fields (22:60-61) (41:296). Excitons can be either free or bound. Free excitons move throughout the lattice until they eventually recombine. Such recombinations will produce spectral radiation with energies of 1.5152 eV. Bound excitons must remain close to impurity atoms. Based on observed radiation energies, they are thought to exist in several different transition states: e.g., exciton bound to an ionized donor (1.5133 eV), and exciton bound to a neutral acceptor (1.5125 eV) (76:341-351). For a particular transition, small shifts in radiation energies can be attributed to different donor and acceptor types. High quality GaAs will produce strong exciton emission spectra (33:8).

2.2.1.3 *Band to Impurity Transitions.* The transition from the conduction band to the bound acceptor level occurs frequently. As the concentration of impurity atoms increases, the conduction band to acceptor transition spectrum broadens. In general, differences between acceptor ionization energy for different elements allow identification of the impurity species. It is important to note that in GaAs the donor impurity ionization energies lie so close together that individual identification is very difficult (33:8-10) (76:341-351).

2.2.1.4 *Donor-Acceptor Pair Combinations.* "Donor-acceptor pair combination involves an electron bound to a donor and a hole bound to an acceptor. Since energy levels associated with substitutional donor impurities are all very close to one another and just beneath the conduction band edge, every band to acceptor line can have a donor-acceptor pair transition (on the low energy side) if a donor is present." (33:10) Again, in the case of GaAs, the energies lie so close together that donor impurity species identification is extremely difficult.

For electrons to move from the valence band to the conduction band they must be excited by energies greater than the bandgap energy. In order for electrons to leave the impurity levels, they must acquire energy greater than the binding energy of that impurity. Excitation sources will be discussed in the remaining sections.

2.3 *Cathodoluminescence*

When keV electrons strike a semiconductor surface several interactions can occur: some of the electrons are backscattered, secondary electrons are produced within the material, and characteristic photons are produced in the x-ray, ultraviolet, visible, and infrared regions of the spectrum. Cathodoluminescent spectroscopy determines the characteristics of the semiconductor material by interpretation of the emitted photons (72:22).

2.3.1 *Electron Penetration* Cathodoluminescence involving electron energies of less than 1×10^4 eV must be performed in well-evacuated chambers. Otherwise, these low energy electrons will be absorbed in a centimeter or less of ordinary air. A low electron energy threshold exists where cathodoluminescence becomes ineffective in producing spectra of sufficient intensity. This occurs when either the electrons lack sufficient energy to penetrate the surface layer, or the energy is insufficient to overcome the repulsive force generated by secondary emissions, or both. Electron repulsion due to space charge along the electron beam will prevent high beam densities, and this will also decrease spectrum intensities. Low-voltage operation does present the advantage of better electron beam targeting (deflection and culmination) (45:427-428).

Several methods have been developed to determine the depth of penetration of energetic electrons. From Thomson's work at the end of the nineteenth century and, later, that of Widdington, there emerged the so-called Thomson-Widdington law which can be stated as:

$$x = a(V_0^2 - V^2) \quad (1)$$

where

V_0 = the incident electron potential

V = the potential at penetration depth x

a = a constant approximately proportional to the inverse of the density of the solid

This gives a maximum penetration x_0 proportional to the square of the initial electron energy (26:686-688).

In 1960, Feldman studied penetration depth of 1-10 keV electrons in solids at normal incidence (24:455-459). He was able to fit his data to an equation of the form:

$$R = bE^r \quad (2)$$

where

R = the depth of penetration

E = the energy of the electrons

b, r = constants related to the material being bombarded

Martinelli and Wang studied penetration of normally incident electrons with energies of 3-7 keV into GaAs. They also fitted their data to Feldman's equation and determined that for GaAs, $b = 270 \text{ \AA}$, and $r = 1.46$ (48:3350-3351).

Rosenstein found, in 1972, that a 45 degree variation of incident angle from normal resulted in only a 10% decrease in penetration depth. He was able to show that oblique electrons lose more energy at the surface than normal electrons. Maclin, in 1981, made the approximation that the penetration depths of the normal and 45 degree oblique electrons were the same, allowing him to substitute Martinelli and Wang's numbers into Feldman's equation. He was then able to calculate the 45 degree oblique electron penetration depth. He found that 1500 eV electrons penetrate approximately 490 \AA , and 900 eV electrons penetrate approximately 230 \AA (47:18-19). These results, and other calculations pertinent to this work are found in Table 1. It is also important to point out that 5, 50, and 100 μA beam currents

Table 1. Electron beam energies and penetration depths in GaAs

<i>Electron Beam Energy (V)</i>	<i>Penetration Depth (\AA)</i>
900	230
1000	270
1500	490
2000	740
3000	1340

focused to a 4 mm diameter circle will produce incident fluxes of 2.49×10^{14} , 2.49×10^{15} , and 5.0×10^{15} electrons/cm² respectively.

The penetration depth of electrons in CdSe is calculated to vary between 70 μm at 200 keV and 500 μm at 800 keV (63:159).

2.3.2 Specific Energy Losses Penetrating electrons will lose their energy through inelastic scattering and the production of secondary electrons. The specific energy loss takes the differential form of dE/dx , where E is the residual primary-electron energy at penetration depth x . Various studies of energy loss from particles in matter show that dE/dx as a function of electron energy is the same. This equation is:

$$-dE/dx = \frac{2\pi N Z e^4 \ln(E/E_i)}{E} \quad (3)$$

where

E = energy of electrons

N = the number of bound electrons per cubic centimeter of the solid

Z = the atomic number (or mean atom number) of the solid

e = the electronic charge

E_i = the ionization energy averaged over all the electrons

Over the range of 300 to 3000 eV, the effective electron range varies as $E^{1.4}$ (26:692-694).

A depth profile illustrating the effects of multiple scattering and subsequent diffusion of the electrons is found in Figure 3. It shows that the greater the electron beam energy, the deeper it penetrates into the material. By varying the beam energy, different regions within the material can be made to luminescence.

2.4 Photoluminescence

Photoluminescence in semiconductors occurs when upper energy levels are optically excited and subsequent recombinations of electrons and holes release photons. Emission lines associated with radiative combinations are most narrow and intense

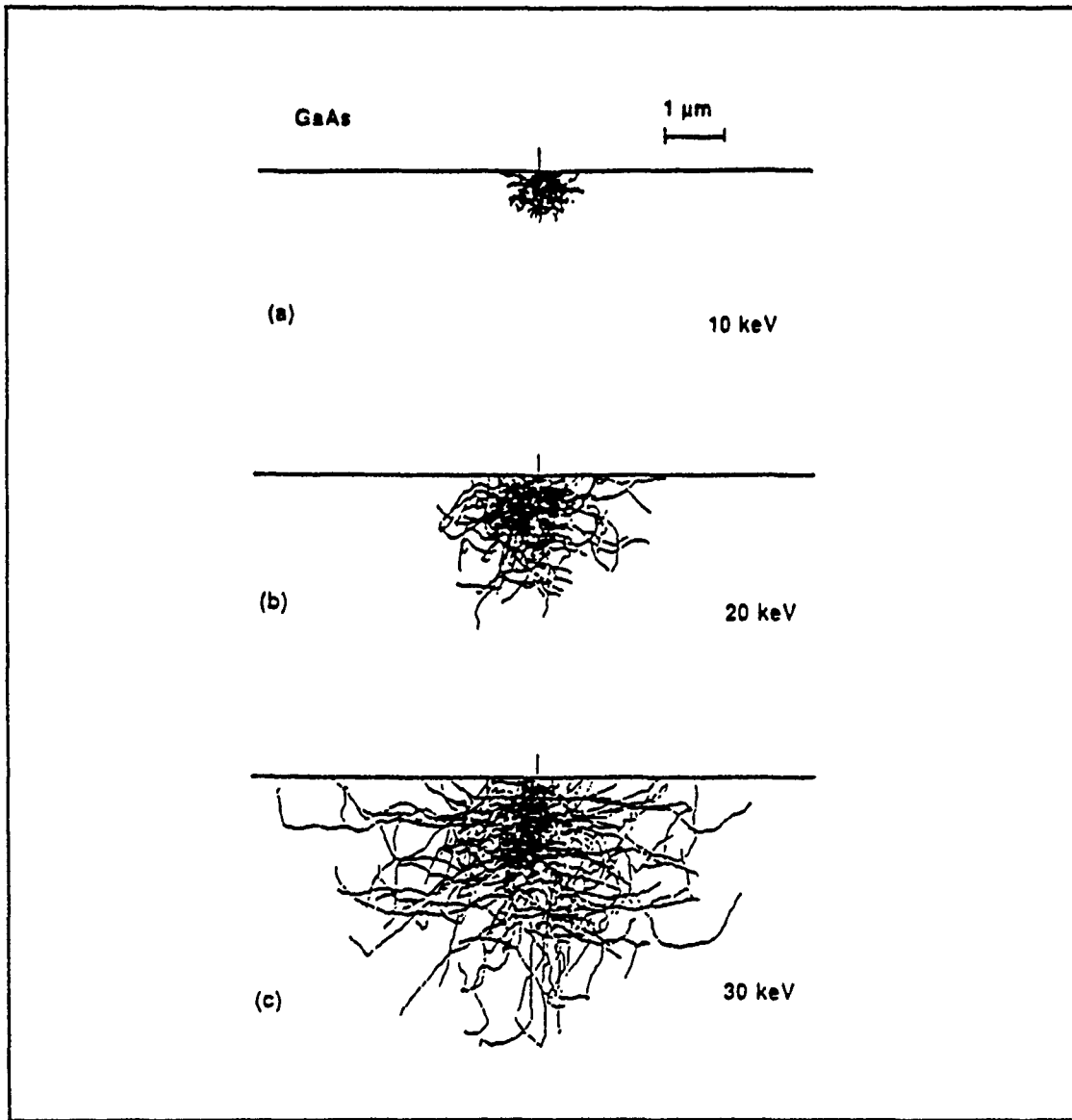


Figure 3. Trajectories of 100 electrons of (a) 10 keV, (b) 20 keV, and (c) 30 keV calculated by the Monte Carlo method for GaAs (78:64)

when sample thermal energy is reduced. This is usually accomplished by cooling the sample with liquid helium (4.2 degrees K) or liquid nitrogen (77 degrees K) (33:7).

Photons penetrating the semiconductor material will interact following the conventions of the energy band theory. Three interaction processes can be distinguished: creation of electron-hole pairs by absorption of the exciting light, radiative recombination of electron-hole pairs, and escape of the recombination radiation from the sample (76:182). Once the energy has been delivered and absorbed, there is no difference between cathodoluminescence and photoluminescence processes.

2.4.1 Penetration Depths Transmission of light through a medium is governed by Beer's law:

$$I(x) = I_0 e^{-\alpha x} \quad (4)$$

where

$I(x)$ = intensity of the light as a function of the distance into the medium

I_0 = intensity of the light at $x = 0$

e = base of the natural logarithm

α = the absorption coefficient of the material for the wavelength of interest

x = the distance into the medium

This calculation is dependent on the absorption coefficient of the material and the wavelength of the incident photon. Note that the penetration depth is expressed as a function of the relative intensity of light at a point inside the material. For example, consider the photoluminescence of GaAs. The absorption coefficient of GaAs is $3.7 \times 10^4 \text{ cm}^{-1}$ at a wavelength of 6328 Å. This is the wavelength of a helium-neon laser. The intensity of the He-Ne light at a depth of 2700 Å would be reduced to $1/e$ (36.8%) times its initial value, and this depth is usually referred to as a penetration depth.

2.5 Conclusion

Luminescence occurs when crystalline material absorbs energy and re-radiates it as photons. These photons are characteristic of the allowed energy levels within the crystal. Photons are produced by the return of electrons to their ground energy levels from one of many possible excited states. If the excitation energy is provided by a beam of energetic electrons, the emission is called cathodoluminescence, and if it is provided by a beam of photons (light) the luminescence is called photoluminescence. The luminescent light can be captured and luminescent intensity plotted as a function of wavelength. Because each photon emitted by the crystal will have a wavelength corresponding to the energy difference characteristic of the chemical element from which it came, it is possible to identify a particular species of impurity belonging to particular wavelengths.

In this review, general concepts of luminescence have been brought to light for use in the discussion and conclusion chapters. The following chapter is a literature review of current radiation effects on gallium arsenide and cadmium selenide.

III. Literature Review - Low Earth Orbit Space Environment and Radiation Effects on Semiconductors

3.1 Introduction

This chapter reviews the literature on the low earth orbit environment and the effects of radiation on semiconductors. It establishes the composition of the environment and the estimated energies of the particles found there. It also examines the interaction of laboratory induced radiation on semiconductors. The major topics discussed in this review are the low earth orbit radiation environment, atmospheric composition, radiation effects on semiconductors in general, and radiation effects on III-V compounds.

3.2 Low Earth Orbit Environment

The components of the space environment between 400 and 500 km that have a potential to alter the M0006 semiconductors are: galactic radiation, solar particulate radiation, geomagnetically trapped radiation, and atomic oxygen. This near earth space region varies in composition with solar activity, seasonal changes, longitude and latitude, and altitude. Sufficient data exists from research rockets and satellites, and from terrestrial radiation models, to establish a good estimate of the environmental conditions for this region.

Galactic radiation is probably the result of super novae. The products of their explosions are high energy electrons and various elemental nuclei. The electrons are bound to the magnetic field of the nova, while the nuclei escape into space with velocities very close to the speed of light. These extremely energetic particles cause substantial damage to materials they impact with. Fortunately, their flux is very small so that their overall contribution to radiative change in the material is minor (2:9).

Solar radiation is comprised of electromagnetic waves and charged particles. The electromagnetic radiation, most of which falls in the near ultraviolet, visible, and near infrared portions of the spectrum, is not of sufficient energy to cause damage in GaAs and CdSe semiconductors. The approximate amount of energy required to displace an atom in GaAs is 236 keV, and 250 keV in CdSe. Gamma rays with wavelengths shorter than 5.261×10^{-12} m would have sufficient energy to produce displacements. This range of gamma rays constitutes 0.0001 percent of the solar spectrum, and represents a spectral irradiance of 10^{-4} ergs/cm²-sec- μ m, therefore, it was highly unlikely that a sufficient dose of these particles existed to cause noticeable changes to the samples. Most of the gamma rays, x-rays, and ultraviolet rays emitted by the sun are absorbed in the atmosphere (19:1-5) (18:483) (52:500).

Protons and electrons emitted during large solar flares often have energies comparable to low-energy galactic cosmic radiation. These very energetic particles are usually accompanied by particles of a magnitude of lower energy. These solar flare products have sufficient energy to damage some spacecraft materials either by direct collision or by secondary particles produced by their interaction with the atmosphere (2:9) (3:623-639) (18:486-487).

The earth's magnetic field and atmosphere greatly reduce the amount of radiation that reach it's surface through attenuation. They also create two regions of high radiation flux between roughly 1.1 and 11.0 earth radii. Galactic and solar radiation directed into this region by magnetic field lines congregate based on their energy. The trapped charged protons and electrons constitute what is known as the Van Allen belt (2:9) (52:499-500).

3.2.1 Galactic Radiation Galactic cosmic radiation is composed of very energetic nuclei from nearly every chemical elements. They are distributed isotropically throughout the galaxy, and therefore enter the earth's atmosphere from all directions. They are often generally reported to consist of 85% protons, 13% helium (alpha par-

ticles), and the rest heavier nuclei (74:2) (14:14). Their relative abundances are shown in Table 2.

Table 2. Relative abundances of radiation nuclei based on oxygen (9:944)

Element	Solar-Flare Cosmic Rays	Sun	Universal Abundances	Galactic Cosmic Rays
1_1H	700	1000.000	1000.000	350.00
2_2He	107 ± 14	~ 100.000	~ 100.000	50.00
3_3Li	...	$\ll 0.001$	$\ll 0.001$	0.30
4_4Be ${}_5B$	≤ 0.02	$\ll 0.001$	$\ll 0.001$	0.80
6_6C	0.59 ± 0.07	0.600	0.300	1.80
7_7N	0.19 ± 0.100	0.200	≤ 0.80	≤ 0.80
8_8O	1.00	1.000	1.000	1.00
9_9F	≤ 0.03	$\ll 0.001$	$\ll 0.001$	≤ 0.10
${}^{10}_{10}Ne$	0.13 ± 0.02	?	0.400	0.30
${}^{11}_{11}Na$...	0.002	0.001	0.19
${}^{12}_{12}Mg$	0.043 ± 0.011	0.027	0.042	0.32
${}^{13}_{13}Al$...	0.002	0.002	0.06
${}^{14}_{14}Si$	0.033 ± 0.011	0.035	0.046	0.12
${}^{15}_{15}P$ – ${}_{21}Sc$	0.057 ± 0.017	0.032	0.027	0.13
${}^{22}_{22}Ti$ – ${}_{28}Ni$	≤ 0.02	0.006	0.030	0.28

By far, hydrogen nuclei are the most abundant of the radiation nuclei. These particles travel at near the speed of light, 3×10^8 m/sec, and have energies up to about 10^9 GeV with an average energy of about 4 GeV (2:11) (18:483) (74:2).

Estimates for the galactic cosmic ray flux near the earth's orbit are between 1 and 4 nuclei/cm²-sec (2:11) (14:14-16) (74:2). The earth's magnetic field will deflect weaker particles. "For a particular value of the magnetic field, the controlling quantity is the ratio of the particle momentum and the particle charge, since the momentum is a measure of the particle's resistance to change of direction and the charge is a measure of the deflecting force." (2:11) This ratio is called the "rigidity" and is expressed as

$$R = pc/Ze \quad (5)$$

where

R = "rigidity"

c = velocity of light

Z = atomic number of nucleus, number of protons

e = electronic charge per proton

p = momentum of particle = $M_0v \left(1 - \frac{v^2}{c^2}\right)^{-1/2}$

M_0 = rest mass of the particle

v = velocity of particle

Figure 4 shows the minimum momentum required of protons and alpha par-

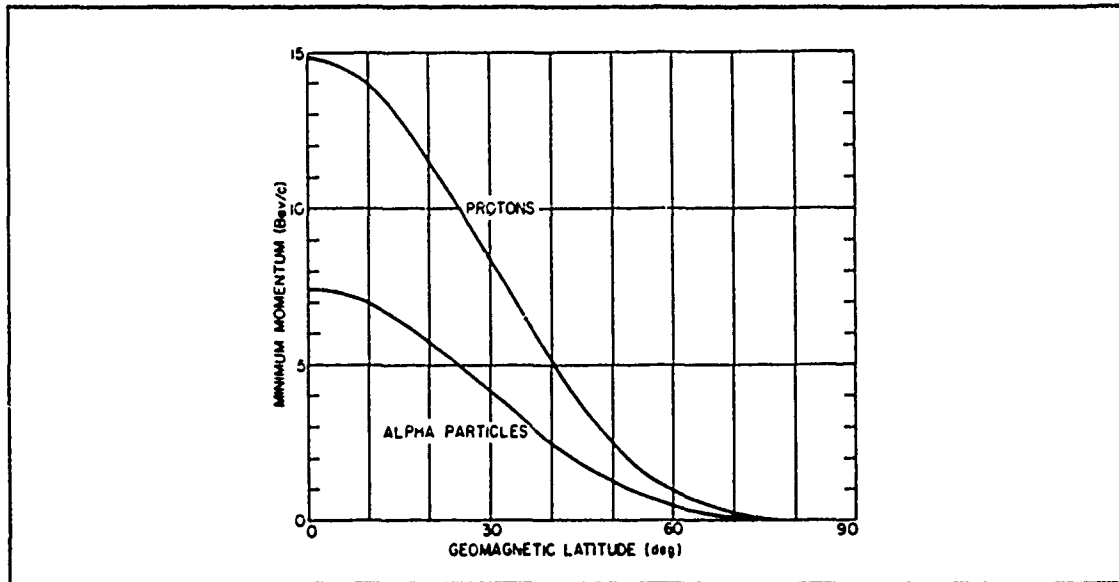


Figure 4. Geomagnetic cut-off momenta for vertically incident protons and alpha particles at the earth's surface for various geomagnetic latitudes (21:84)

ticles to penetrate the earth's magnetic field as a function of geomagnetic latitude. For purposes of illustration, a proton would need at least 4.5 GeVs of energy to penetrate the magnetic field at the equator (0 degrees latitude). It can be inferred from

this figure that a majority of the incident cosmic radiation will be deflected at the equator while at the poles the radiation will penetrate into the earth's atmosphere (2:13).

The minimum energy and flux of the galactic cosmic rays that arrived at the LDEF orbit can be determined from Figure 5 and Figure 6. These figures were

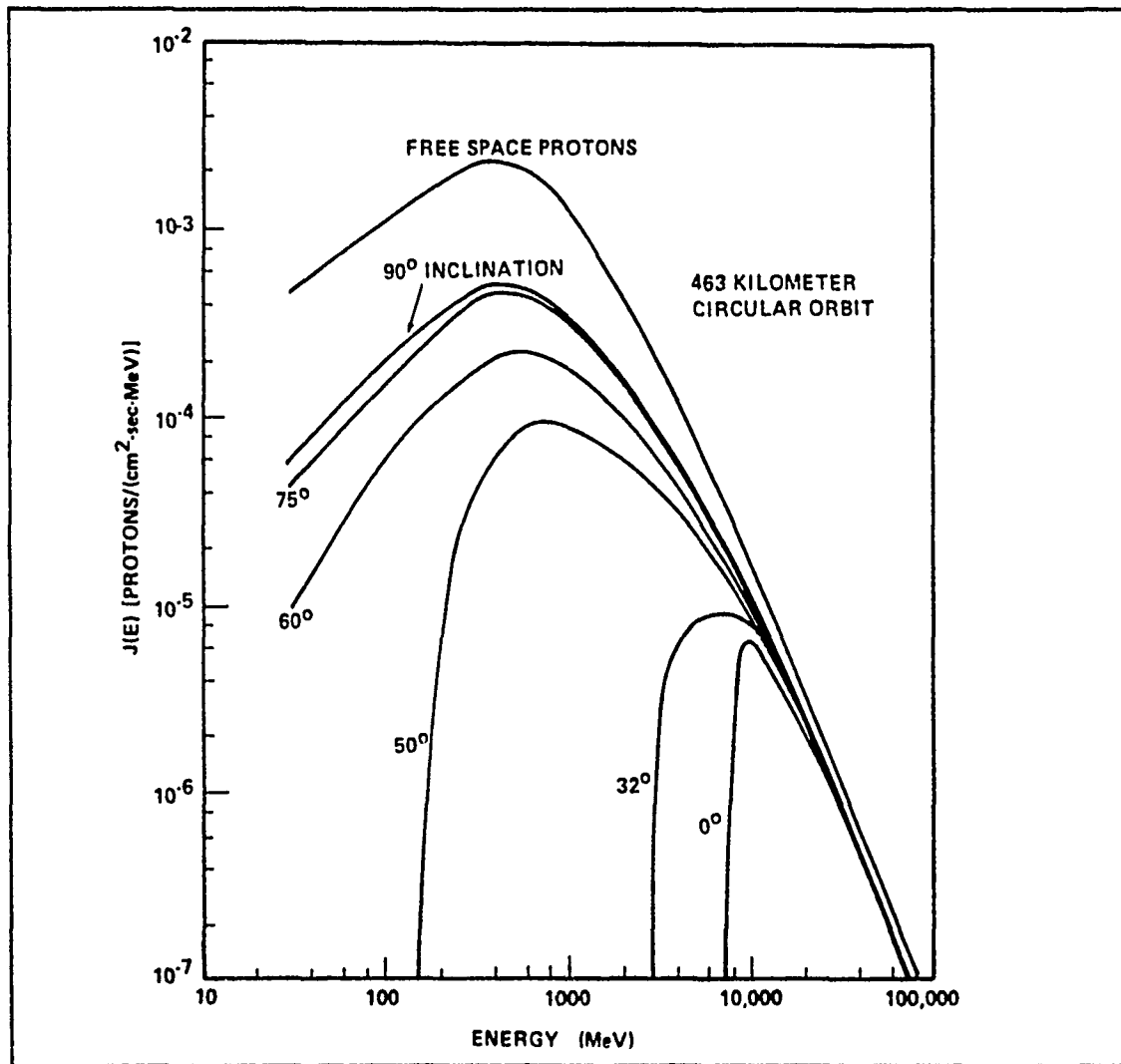


Figure 5. Differential energy spectra for protons in a 463-km orbit (14:30)

constructed by J. J. Wright in an attempt to arrive at useful methods for approx-

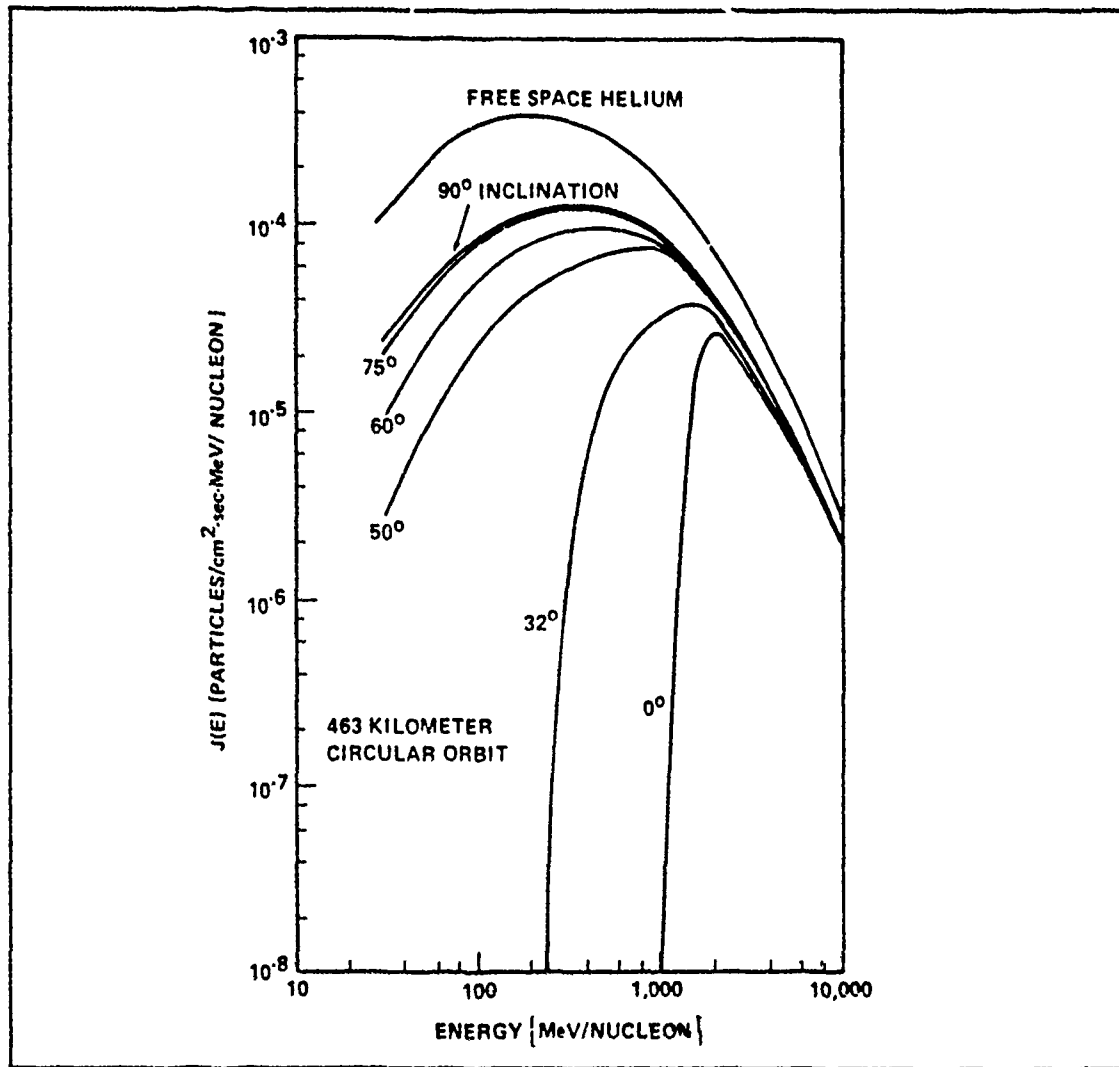


Figure 6. Differential energy spectra for helium nuclei in a 463-km orbit (14:30)

imating the cosmic ray spectrum in circular earth orbits where the spectrum will be averaged over several days (see (14:27-29)). The 32 degree inclination curve can be used as an approximation to the actual 28.5 degree LDEF orbit. Orbit inclination is the angle between the orbital plane and the earth's equatorial plane. The degree measurement, in this case 28.5 degrees, is also the greatest latitude, north or south, reached by the satellite while in orbit. His calculations yield that the LDEF probably encountered galactic protons of 3 GeV energy, and 10^{-5} protons/cm²-sec-MeV-str (3.77 protons/cm²-sec). Galactic alpha (helium nuclei) particles are calculated to be about 2.25 GeV energy and 4×10^{-5} particles/cm²-sec-MeV-str (1.13 particles/cm²-sec). These calculations are in agreement with observed particle densities and energies taken by Pioneer III and IV, and the Soviet space probe Cosmet II (2:11).

3.2.2 Solar Radiation Solar Radiation consists of both electromagnetic and particulate radiation. As previously mentioned, the majority of the electromagnetic flux incident upon the earth's atmosphere is in the visible and near visible region of the spectrum. The wavelength of radiation that would have sufficient energy to cause dislocation in the semiconductor material would be 5×10^{-12} m or smaller (236 keV or more). The amount of irradiance in that wavelength range emitted by a bright class 3 flare, one of the largest flares produced by the sun, would be 10^{-3} ergs/cm²-sec- μ m. This equates to approximately 50 photons/cm²-sec during a large solar flare, and 5 photons/cm²-sec during quite solar activity.

Large solar flares and eruptions often occur during the declining phase of the 11-year solar cycle. Solar cycle 21 began in 1976 and ran through 1987. The period during which the semiconductors were exposed directly to solar radiation was April 1984 through March 1985. The declining phase of this cycle started in 1982 and ended in 1987. Observed sunspot activity for the 11 month period of direct exposure was near the minimum of cycle 21, and there were no large flares during this time period (61:12). However, the last six months of 1989 provided some of the largest

flare eruptions since 1957. With fluences of about 10^{10} protons/cm²-sec, these flares may have had a pronounced impact on the amount of change in the samples.

High-energy protons and electrons accompany solar flares. Large flares accelerate protons to near galactic proton energy, and these protons arrive at the earth's atmosphere some 20 minutes after the occurrence. Electrons arrive approximately 24 hours later in a plasma cloud. The electrons arrive isotropically while the proton arrival is directionally dependent upon the earth-sun geometry.

Solar radiation is much more intense than galactic radiation due to the proximity of the earth to the sun. Solar proton fluxes can range from 1 particle to 10^6 particles/cm²-sec. Proton fluxes associated with large solar flares often reach 10^4 particles/cm²-sec at energies between 20 and 500 MeV, with a total flux of 10^{10} particles/cm²-sec for protons greater than 0.5 MeV. Minor flares normally produce 10^8 to 10^{12} particles/cm²-sec with energies ranging from 0.5 to 20 keV (2:16) (66:1-27).

Solar electrons fluxes are normally 1 to 40 times the accompanying proton flux. Average solar flares produce electron fluxes of 10^6 to 10^7 electrons/cm²-sec with energies of about 50 keV. Minor flares produce electrons with energies ranging from 0.25 eV to 10 eV (2:16).

3.2.3 Trapped Radiation Geomagnetically trapped protons, electrons, and perhaps other charged nuclei exist in two distinct zones, or belts, above the earth's atmosphere. Named after the person who discovered them, Dr. Van Allen, these belts are the result of charged particles forced to traverse north-to-south looping magnetic field lines (See Figure 7). The congregation of magnetic field lines at the poles force the particle to reflect (commonly referred to as "mirror points") back along the field line toward the opposite pole. Some particles precipitate from the belt after interaction with the atmosphere, while the rest continue to travel back and forth between the poles. As previously mentioned, galactic radiation and solar

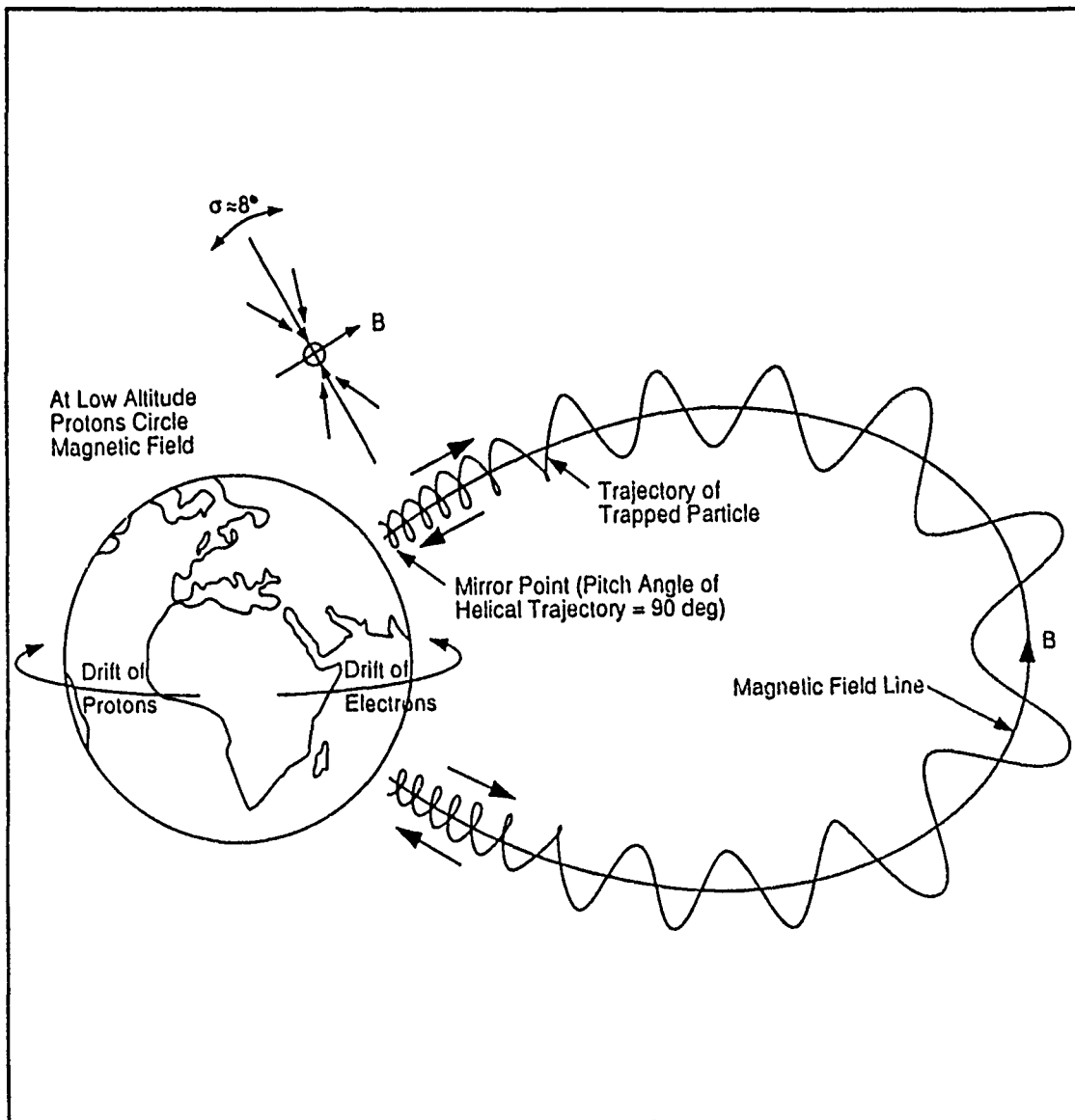


Figure 7. Charged particle movement along magnetic field lines (8:18)

radiation serve to constantly replace any losses in the belts.

In general, the inner belt starts from between 400 km and 1200 km, and extends to an altitude of 10,000 km. The starting point depends on the latitude. This belt is positioned between 45 degrees north and 45 degrees south latitude. The outer belt starts at approximately 10,000 km and extends to between 60,000 km and 84,000 km. Figure 8 shows the position of the inner and outer radiation belts in relation to the earth. Distances shown on the figure are in terms of earth radii, and are approximations. The actual belt limits change; solar activity level, for example, will change the limits of both belts.

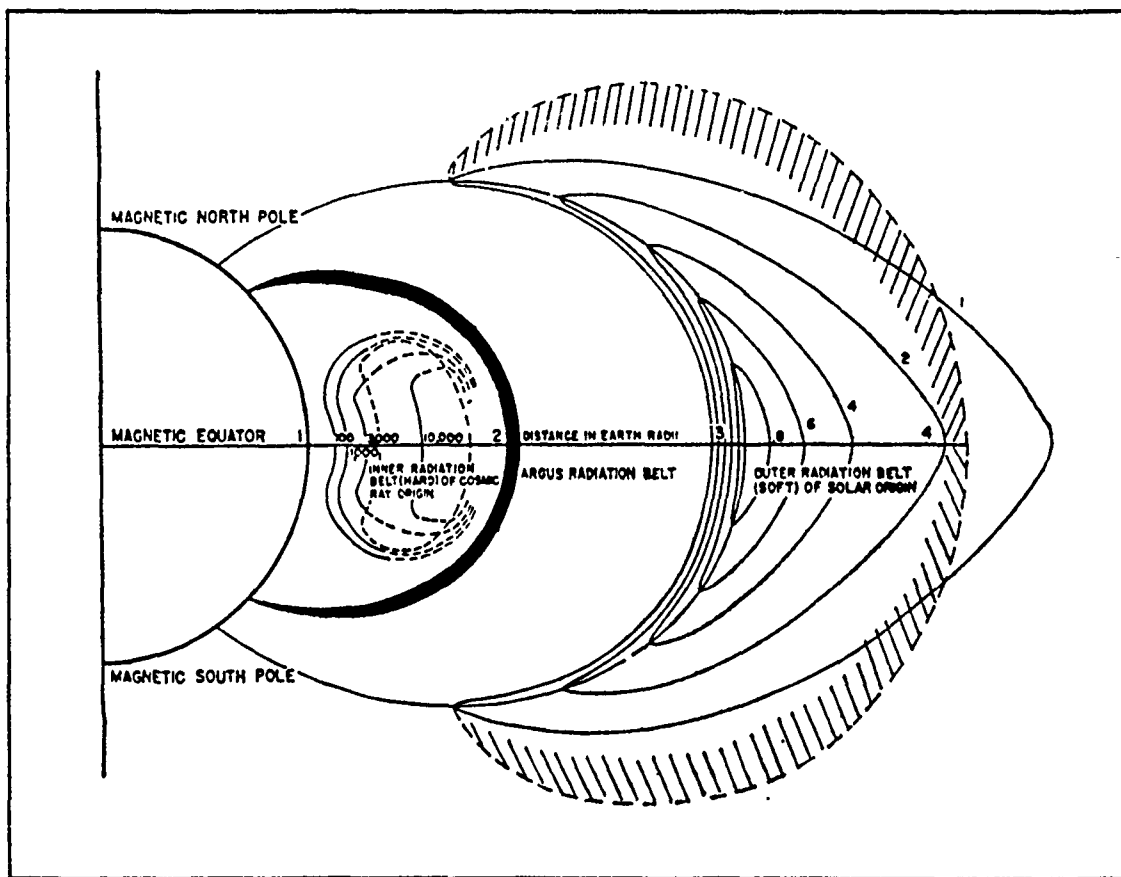


Figure 8. The inner and outer radiation belt as determined from Pioneer III and as calculated from theory (65:803)

The energies of the trapped particles range from 1 keV to hundreds of MeV. An example of electron intensity as a function of earth radii and latitude can be seen in Figure 9. Again, distances are in terms of earth radii. The greatest concentration of electrons occurs at about 1.3 earth radii, and is centered over the equator. Note the lack of particles between 1.0 and 1.15 earth radii due mainly to interaction with the atmosphere. In general, electrons can be found closer to the earth than protons due to their mean motions. Radiation belt electrons move very rapidly. A 500 keV electron will move at 85% the speed of light. A much heavier 500 keV proton will only move at about 3% the speed of light.

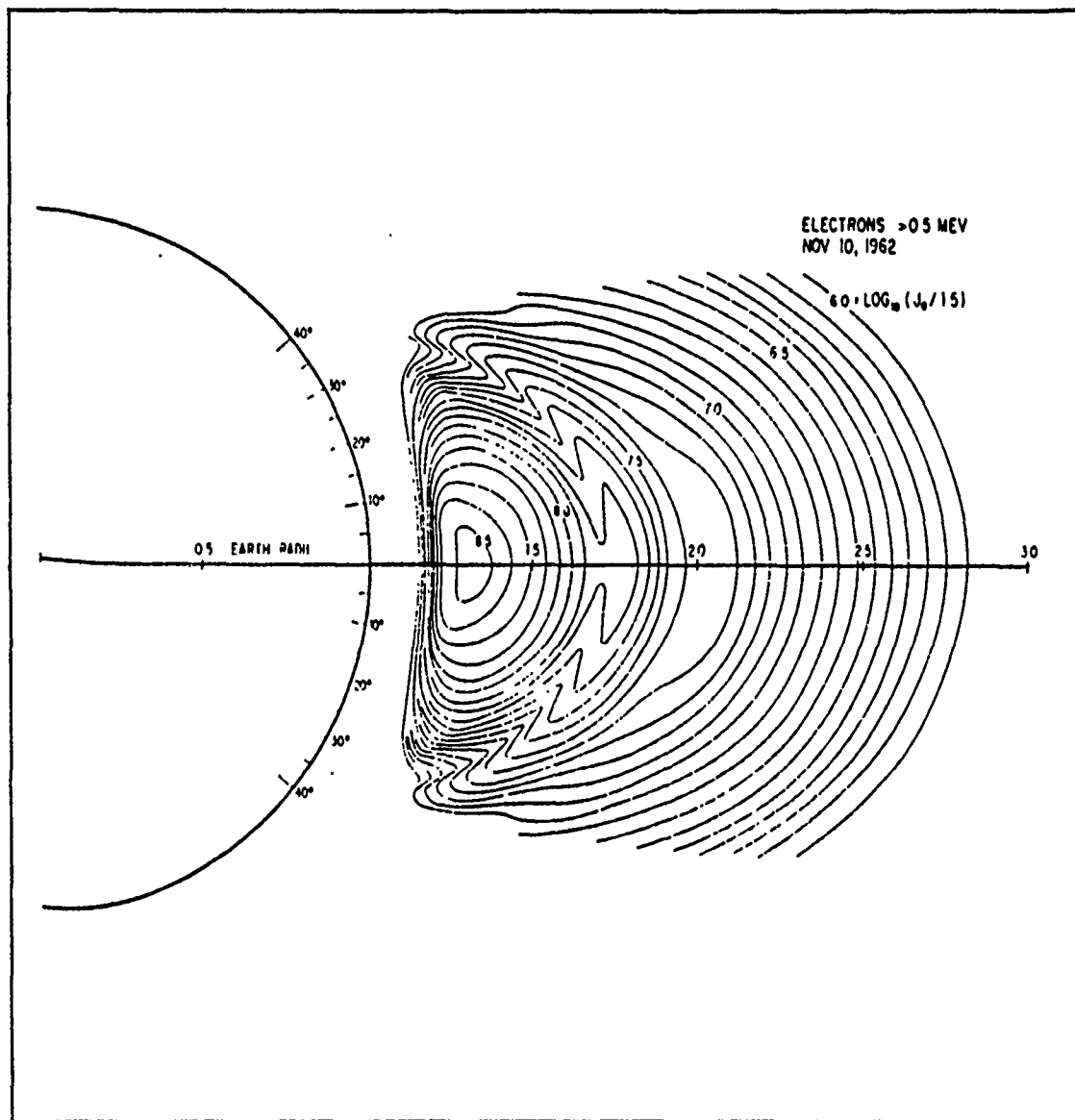


Figure 9. Contours of constant intensity of electrons with energies greater than 0.5 MeV (50:599)

The earth's geometric dipole does not sit on the north and south poles. A more accurate description is to place the dipole approximately 340 km off the geographic center of the earth and tilt the north magnetic pole towards Asia to 6.5 degrees N, 162 degrees E. This tilt causes magnetic field lines of a given dipole shell (a sphere of constant magnetic strength) to be "off-center" about the earth. The area in which these shells come closest to the earth is located over the east coast of South America and the South Atlantic Ocean at coordinates 30 degrees S, 45 degrees W (See Figure 10). Although other geomagnetic factors play a role in the creation of the magnetic anomaly in the South Atlantic, the dip of the magnetic pole is the main contributor (62:118-119).

The close proximity of the magnetic shells to the surface of the earth is responsible for two main effects. First, it is in the South Atlantic anomaly that the Van Allen radiation belt is the closest to the earth and the highest concentration of charged particles exists in near-equatorial latitudes. Figure 11 shows how the magnetic field lines (and trapped electrons and protons) "dip" down towards the earth's surface at about 45 degrees west longitude. In this figure, the "dip" is exaggerated by the compressed and straight horizontal axis. Second, the close proximity with the atmosphere results in this area having the highest precipitation of particles within the inner belt (62:124-126). The naturally occurring trapped radiation environment in the anomaly region remains fairly constant with time, although it does fluctuate with solar activity (74:4).

3.2.4 Atmospheric Considerations

3.2.4.1 Atomic Oxygen In low earth orbits a significant portion of the atmosphere is comprised of atomic oxygen (See Figure 12 and Figure 13). These figures show the extremes of the particle concentrations, and in general, the actual concentrations lie somewhere in between. The collision of the orbiting spacecraft with oxygen atoms results in an interaction energy of about 5 eV. If the incident

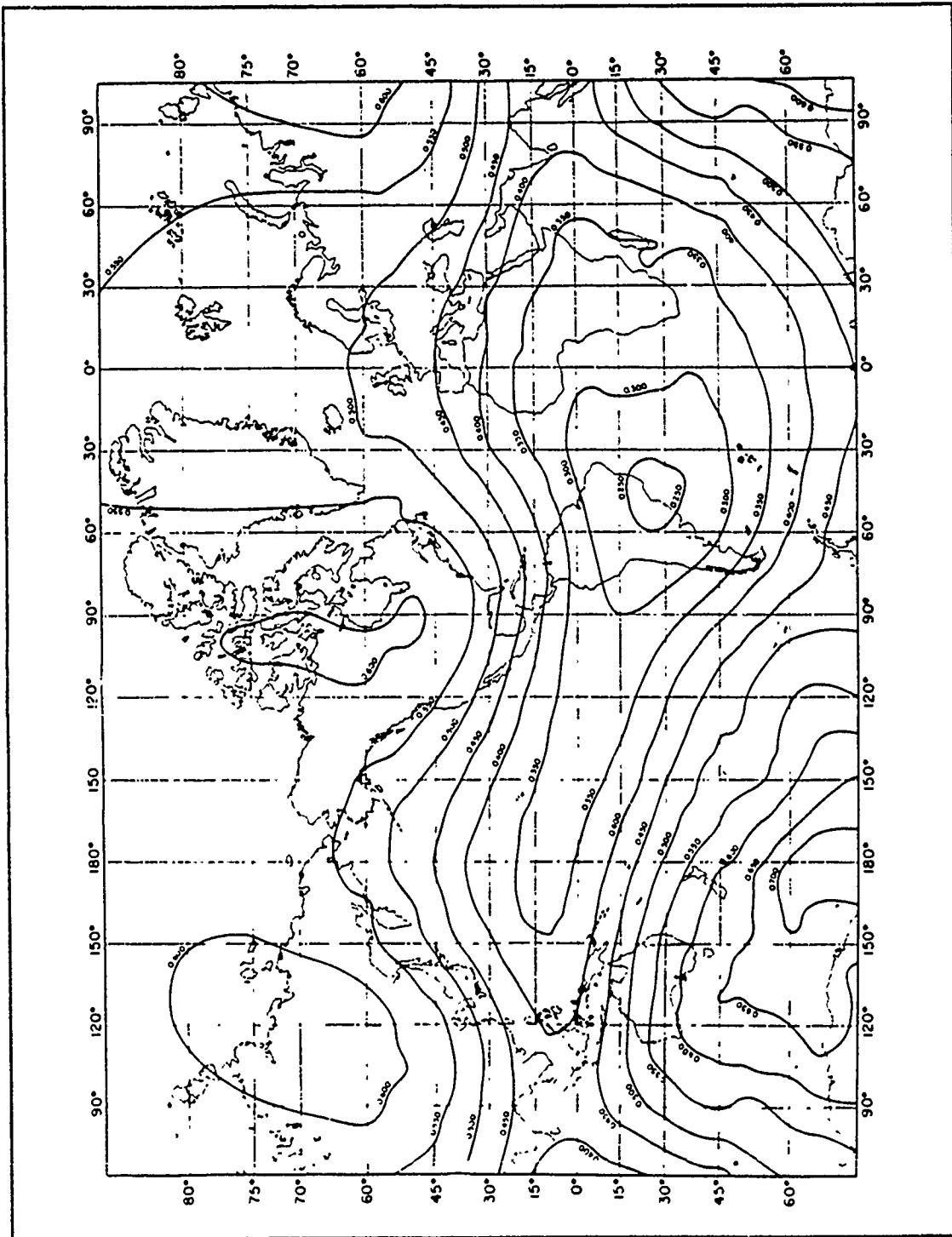


Figure 10. Total intensity F of the earth's magnetic field (in gauss) (21:155)

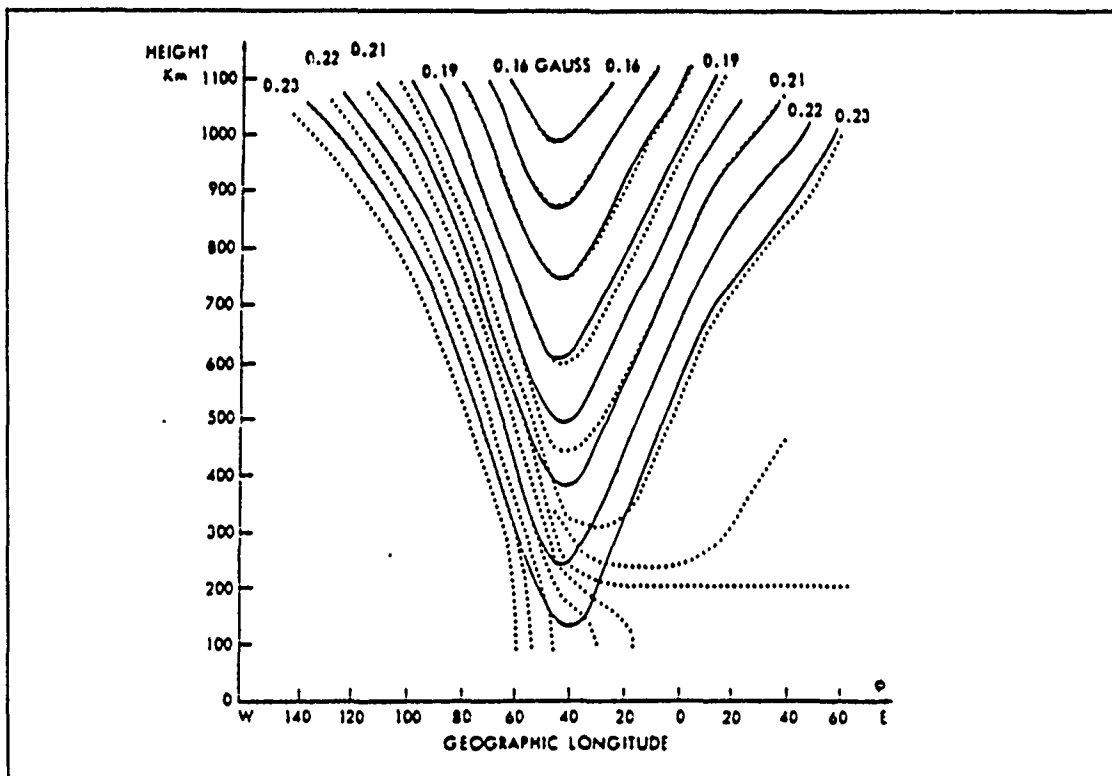


Figure 11. Altitude in km of constant B-L rings (*solid curves*) for $L=1.25$. *Dotted curves*: average mirror point "trajectories" of 300 keV electrons drifting through the anomaly, subject to coulomb scattering (62:125)

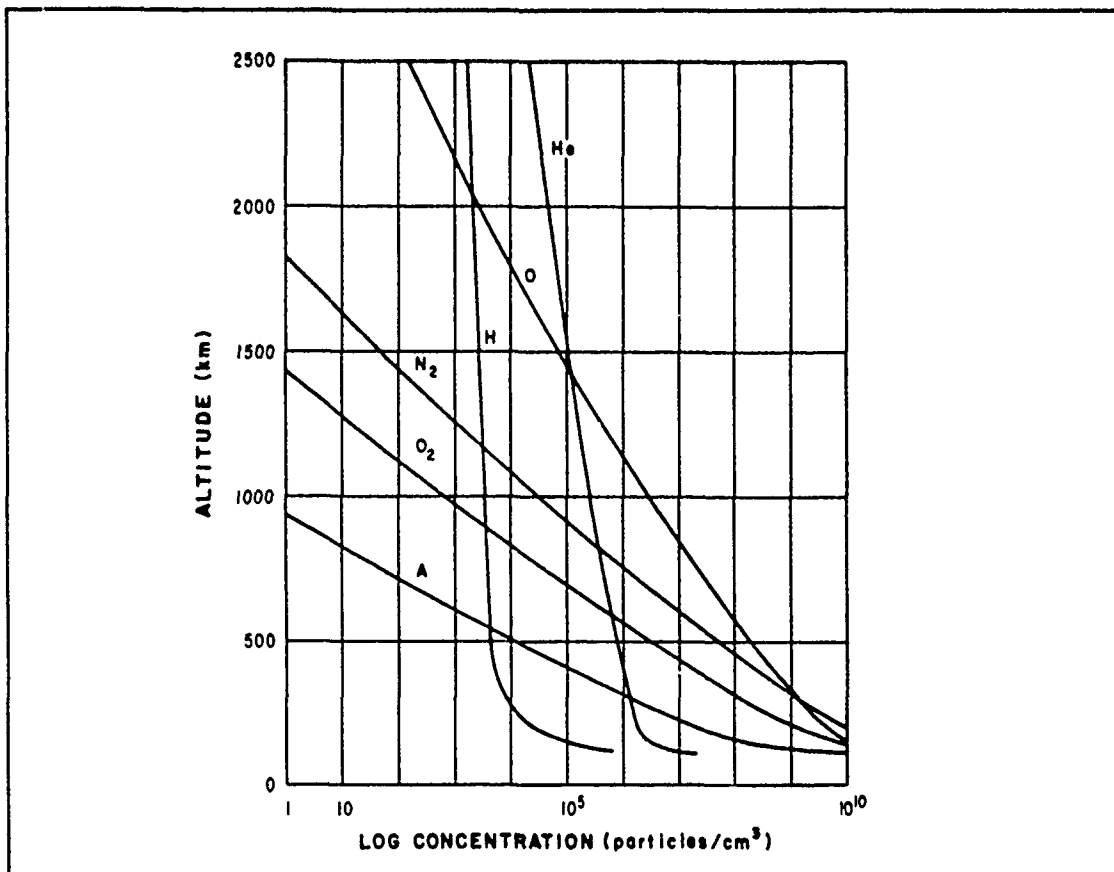


Figure 12. Daytime conditions near maximum of sunspot cycle (38:10)

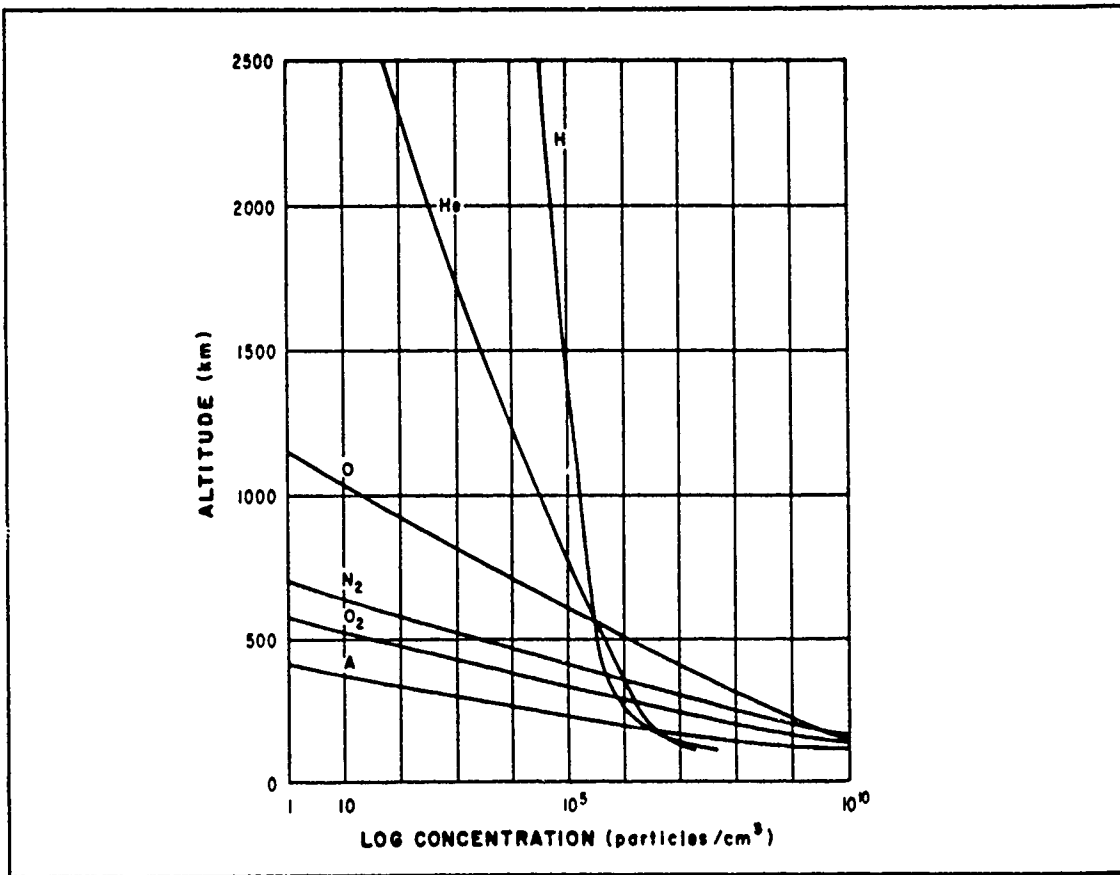


Figure 13. Nighttime conditions near minimum of sunspot cycle (38:10)

oxygen is captured on the surface for a period of a few lattice vibrations, it will then bond to a lattice atom and exit the surface with it. This event normally occurs with low, or thermal, energy particles. If the oxygen is not captured long enough, it will then be reflected almost specularly. In some instances, it may bond and remain with the lattice (29:645) (80:182). It has also been determined that the angle of incidence plays an important role in the interaction (36:3).

Atomic oxygen interaction with carbon has been studied in the laboratory. It was found that approximately 11.5% of the incident oxygen reacted with the carbon surface and formed an oxide. The remaining 88.5% should have left the carbon surface as unreacted atoms or molecules. Approximately 20% of these atoms recombined to form molecular oxygen (29:651) (30:6).

This region of low energy interactions has been sparsely studied until recently. Another experiment on the LDEF was to measure these interactions in greater detail. Data has not been found for GaAs or CdSe interactions with atomic oxygen. It is suspected that if oxidation did occur, its thickness would have been on the order of 10's of Å. Because both spectroscopic techniques used in this thesis examine the material far below this level, atomic oxygen will not be a factor in the analysis.

3.2.4.2 Thermal Environment The thermal temperature of the atmosphere at the LDEF orbit does change with time. The change is so small and gradual that it may be ignored. If we assume an average exospheric temperature of 1300 degrees K, Figure 14 shows the concentrations of atmospheric constituents.

The expected thermal environment for the 12 sides of the satellite was a maximum of 50 degrees C (122 degrees F), and a minimum of -10 degrees C (14 degrees F). This was due to the thermal coatings placed on the inside and outside of the satellite to minimize thermal fluxuations (16:306). Similar temperatures have been recorded on previous shuttle flights inside the bay with the bay oriented towards the sun (25:37). These LDEF temperatures are well below those required to initiate an-

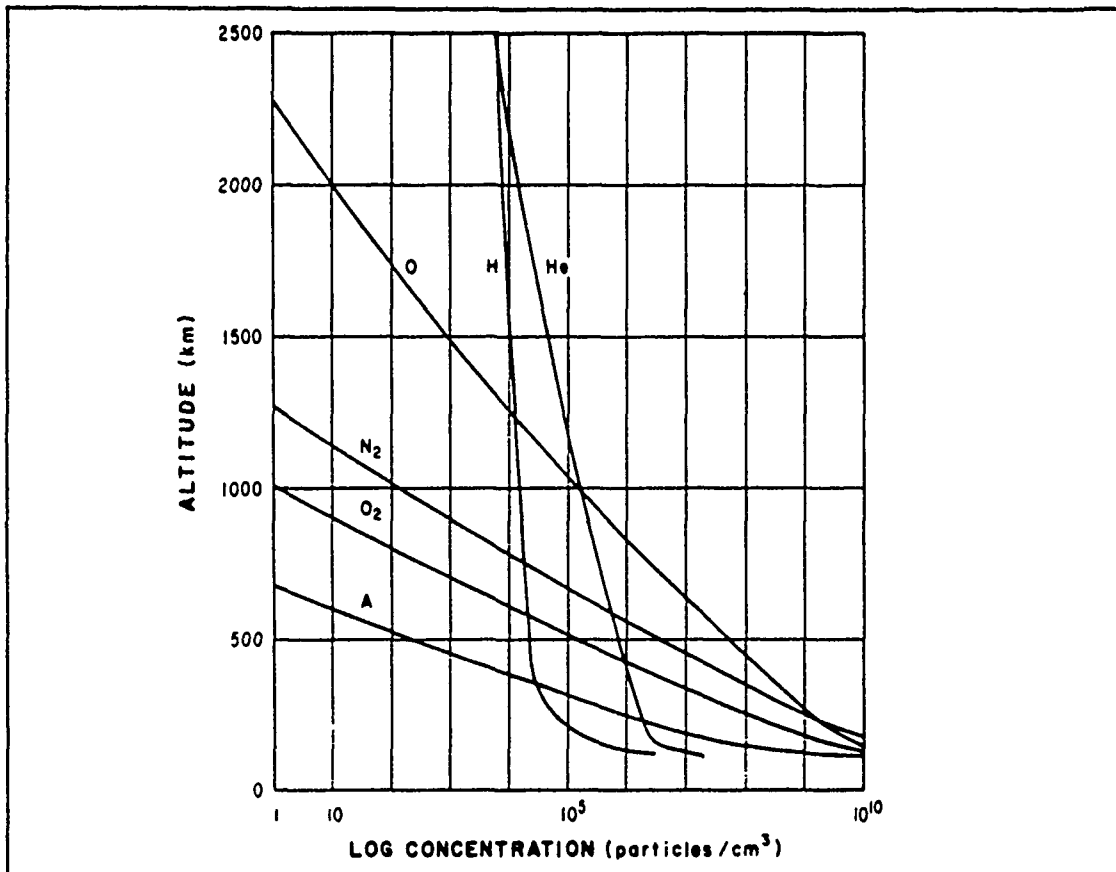


Figure 14. Concentrations of major atmospheric constituents for an exospheric temperature of 1300 degrees K (38:11)

nealing of damage in the samples ($\sim \geq 600$ degrees C (1112 degrees F)). Therefore, the thermal environment is not thought to have been a factor in the exposure of the samples.

3.2.4.3 LDEF Geometry It is no surprise that the highest concentration of trapped radiation within the LDEF orbital path would be in the South Atlantic Anomaly. Prior studies have calculated for a 400 km altitude and 28.5 degree inclination the shuttle would have an 85% radiation free orbit relative to the radiation within the anomaly. Although Figure 15 is for a satellite at 170 km altitude, the

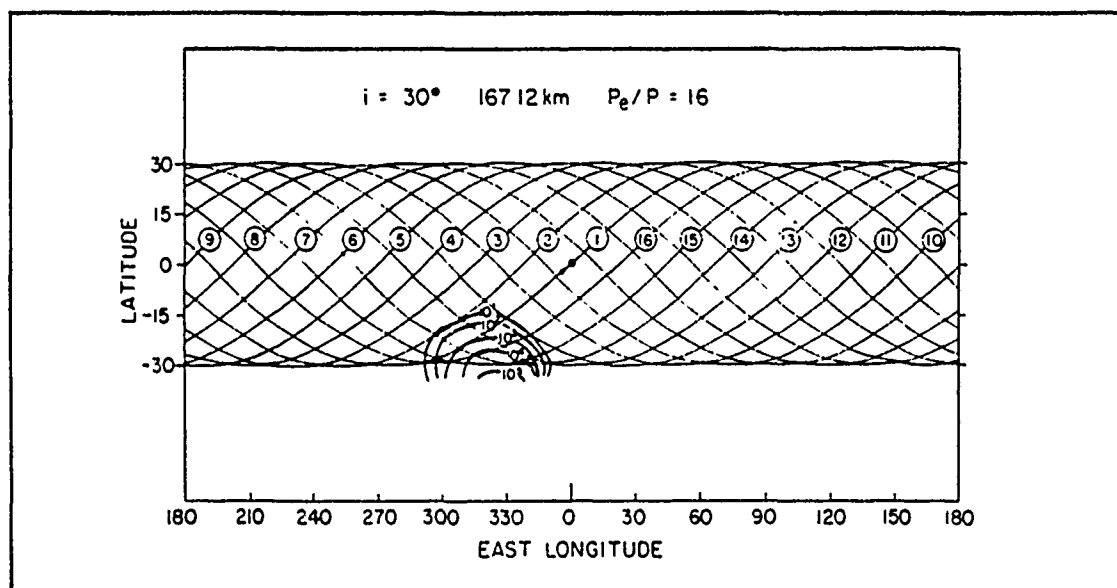


Figure 15. Omnidirectional flux contours for electrons with $E \geq 0.5$ MeV. Inclination 30 degrees, altitude 170 km, period 1.5 hours (67:809)

same anomaly encounter is depicted. The numbered curves represent ground traces for each of the 16 orbits made during a 24 hour period. For the electron flux contours shown, the satellite would enter the South Atlantic Anomaly 6 out of the 16 orbits. The maximum electron and proton fluxes ($E \geq 0.5$ MeV) for 400 km altitude were calculated to be approximately $1 \times 10^8/\text{cm}^2\text{-day}$ and $2 \times 10^7/\text{cm}^2\text{-day}$ respec-

tively (16:305). Similiar results were obtained by Benton (8:28) and Stassinopoulos (69:Table 242,243).

Because the LDEF was three-axis stabilized, the location of the sample tray on the satellite structure made a difference as to the amount of directional solar proton, cosmic ray, and gamma ray exposure it received (electron fluxes were considered isotropic). This geometry did not influence the amount of geomagnetically trapped protons, electrons, and nuclei the samples received because the LDEF passed through the particles which were moving thousands of times faster, resulting in an isotropic bombardment. In the same regard, galactic cosmic rays were considered isotropic, and thus their exposure was not effected by the sample tray orientation relative to the other 11 sides. Obviously, the space end of the satellite would receive more flux than the sides.

The attitude of the satellite with respect to the earth, and its velocity vector, is shown in Figure 16. The main geometric axis was aligned with the earth's radius vector, and the satellite did not rotate about any of its three axis. The M0006 samples were located on side 2, which is adjacent to the trailing surface (See Figure 17).

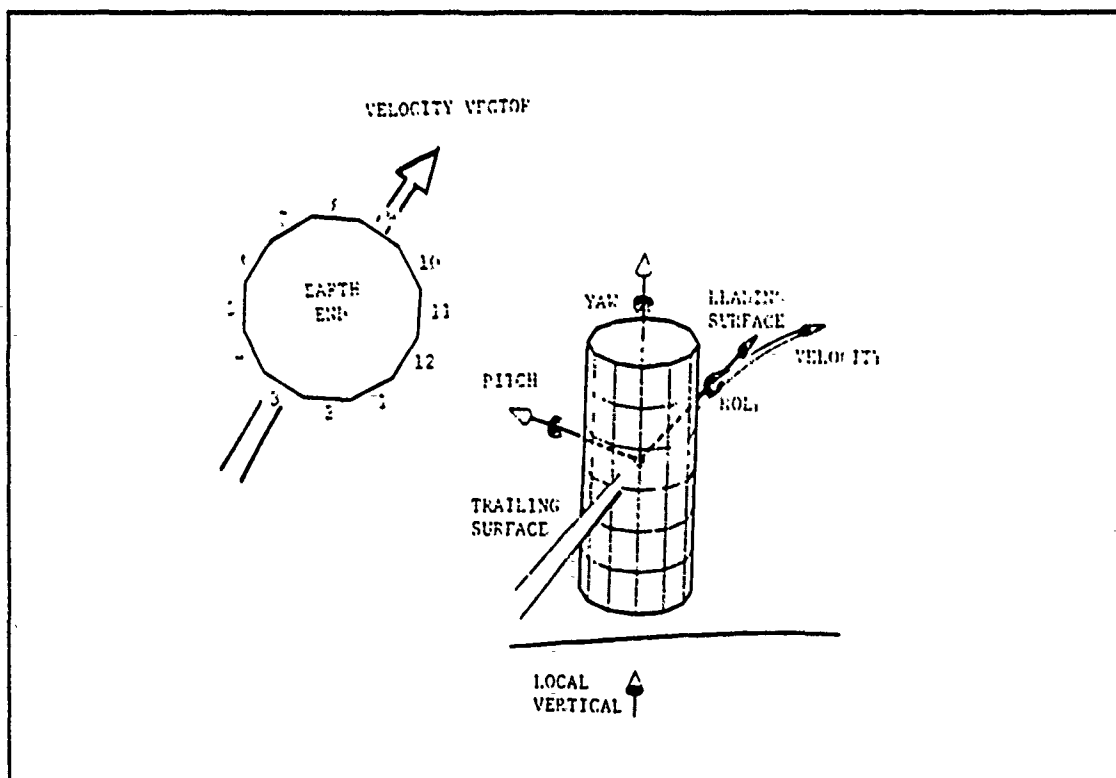


Figure 16. LDEF orientation in space (16:304)

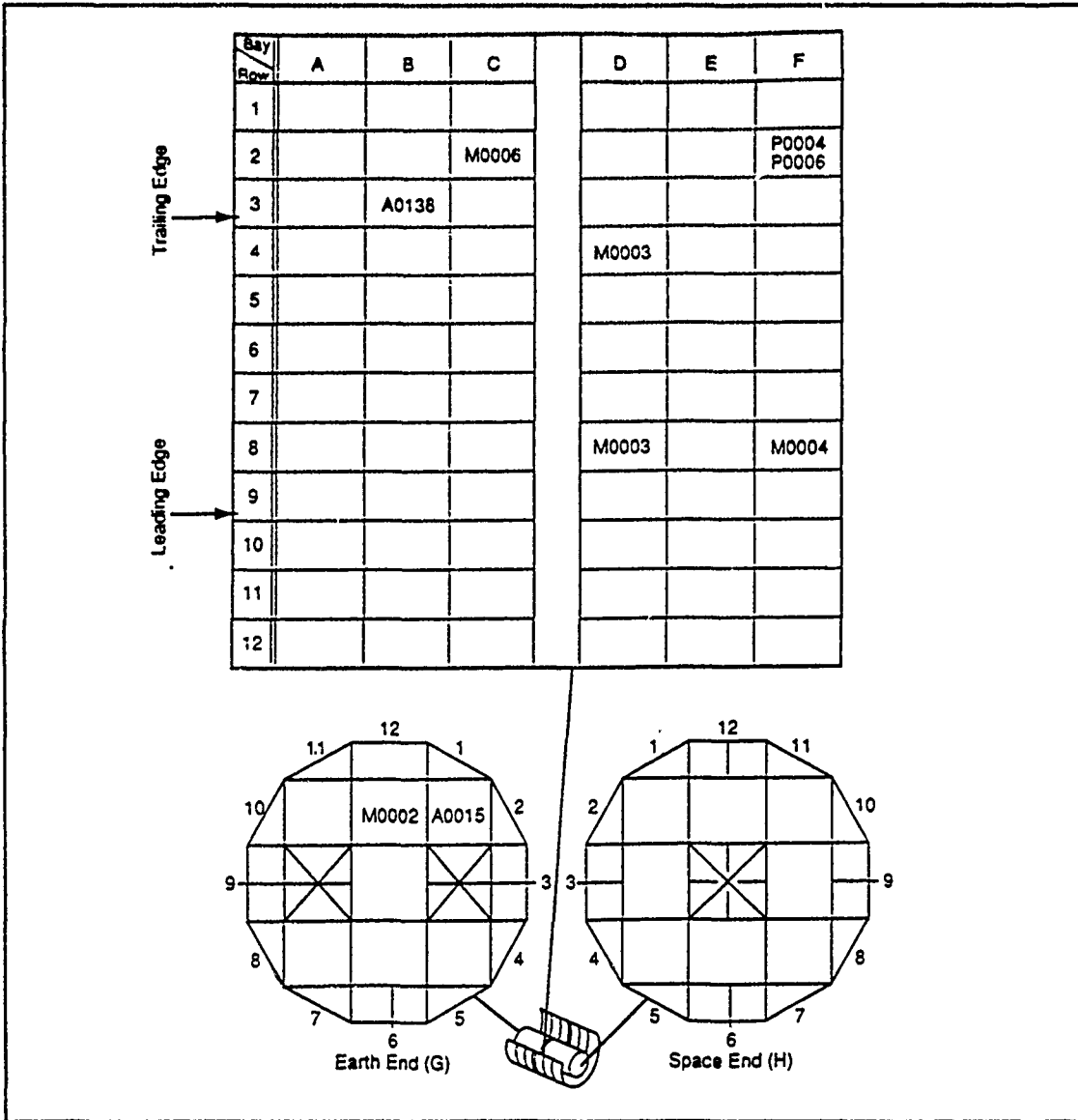


Figure 17. LDEF structure (8:9)

The amount of accumulated solar exposure is shown in Figure 18. It represents the contribution of directional solar radiation to the sample exposure. It is based upon LDEF/sun line-of-sight, and takes the encounter geometry and exposure time into account. Rows 2, 4, 8, and 10 would receive the same amounts of exposure due to symmetry. From the figure, it can be gleaned that the samples received approximately 70 days solar exposure (at normal incidence) during the 11 months of exposure.

3.2.4.4 Vacuum Environment The passage of the LDEF satellite through a predominantly atomic oxygen environment with a vacuum in the neighborhood of 10^{-10} torr created an ambient particle flux change between leading and trailing surfaces. The main reasons for the change are attributed to the deflection of the ambient particles by the leading surfaces, and the removal of atomic oxygen from the ambient flow due to accommodation by the satellite surfaces. Both of these mechanisms would result in a depleted zone, or wake, on the trailing surface of the satellite. Table 3 illustrates the ambient flux change.

Table 3. Ambient population at 550 km, 1000 degrees K; H $\sim 5 \times 10^4/\text{cm}^3$, He $\sim 2 \times 10^6/\text{cm}^3$, O $\sim 8 \times 10^6/\text{cm}^3$ (16:307)

<i>Location</i>	<i>Flux, particles/cm²-sec</i>		
	H	He	O
<i>Leading Surface</i>	6×10^{10}	7×10^{12}	10^{14}
<i>Trailing Surface</i>	10^6	3×10^1	4×10^{-19}

3.2.5 Summary Although galactic cosmic rays, solar flare cosmic rays and gamma rays have sufficient energy to cause changes in the semiconductor samples, their very small fluxes make detection of the changes very difficult with spectroscopic techniques. Solar flare protons also have sufficient energy and flux to cause change,

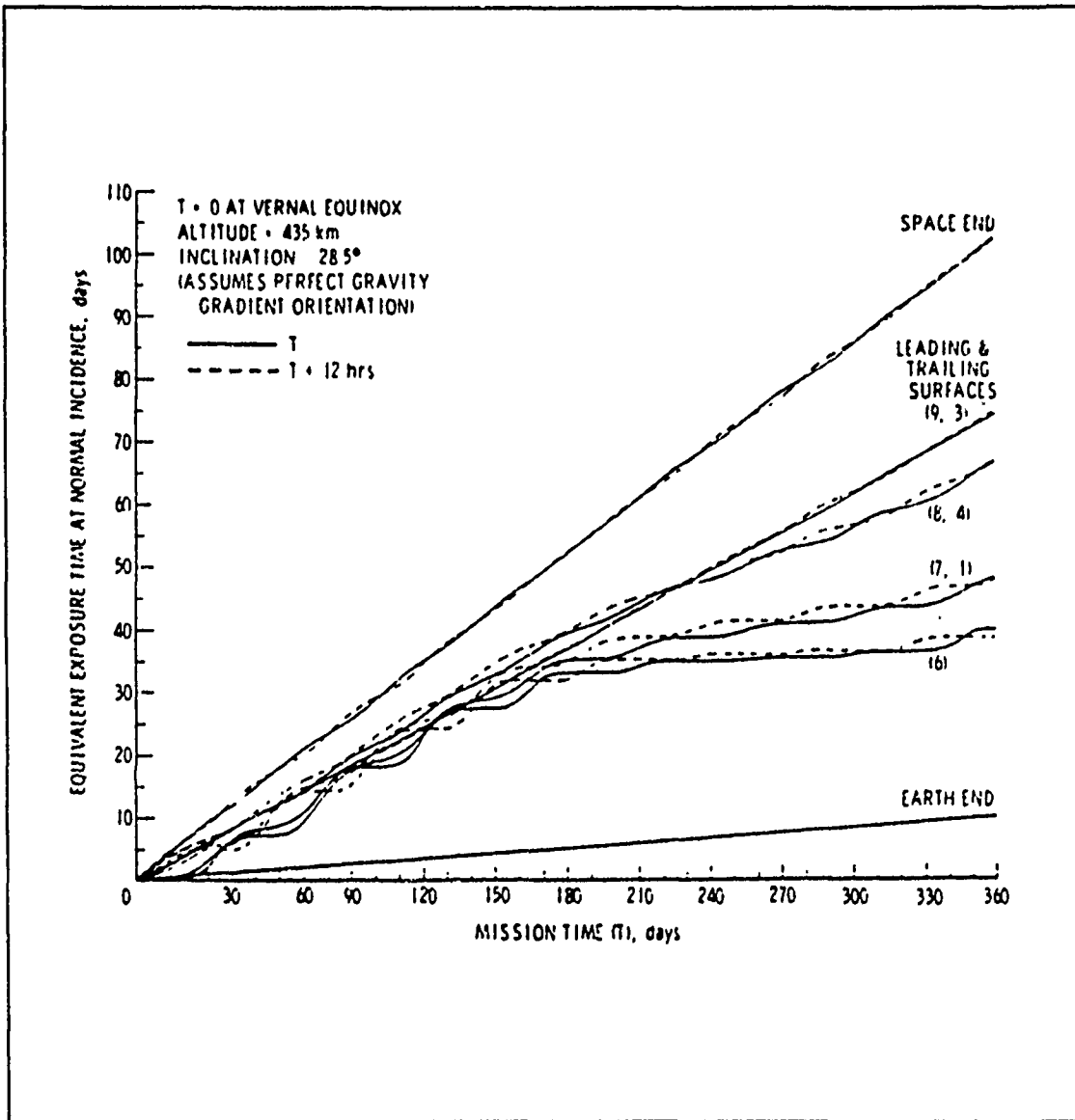


Figure 18. LDEF accumulated direct solar dose (16:304)

but due to the directional nature of their fluxes and hence the sample panel being in the proper orientation to receive these fluxes only 18% of the time, their contribution to any significant change can be considered only minimal. The high energy protons and electrons presiding in the South Atlantic Anomaly would present the best opportunity to inflict change in the samples. With a period of 90 minutes, the LDEF passed through the anomaly on the average of 6 times every 24 hours. Assuming the flux contour region shown in Figure 15 is 60% larger at 500 km altitude, the satellite would be exposed to particles with E greater than 0.5 MeV on the average of 17.5 minutes per day. Anticipated electron and proton fluxes would be 1.16×10^3 electrons/cm², and 2.3×10^2 protons/cm².

3.3 *Radiation Effects On Semiconductors*

3.3.1 *General Effects* Radiation effects in semiconductors are produced by three types of irradiating particles: photons (gamma rays), charged particles (protons, electrons, and cosmic rays), and neutrons. Gamma rays are photons with energies higher than x-rays. Photons have zero rest mass and neutral charge. Protons have a positive charge while neutrons are neutral in charge, and both have the same mass. The proton is most often seen as an ionized hydrogen atom. Electrons have a negative charge with an almost negligible mass. And cosmic rays are high-energy charged particles consisting mostly of hydrogen nuclei and helium nuclei (44:2) (68:6).

The extent of the radiation effects is dictated by the properties of the impinging particle and the bombarded material. For the particle, its mass, charge, and kinetic energy are the most influential properties. For the material, its mass, charge, and density are the most important properties (68:6).

Photon interaction with the target material produces energetic free electrons. The photoelectric effect is dependent on the energy of the incident photon and the atomic number Z of the material. The probability that a photon will excite an

electron from an orbit decreases with increasing photon energies because interaction durations are smaller for faster, more energetic photons. However, with the increase in atomic number, the binding energies decrease for electrons in outer orbits and the probability of photoelectric interaction increases. During the interaction, the photon is completely absorbed by the electron which then escapes from the electron cloud. An adjacent outer orbital shell may then give up an electron to fill the vacancy.

Compton scattering involves highly energetic photons which give up a portion of their energy during interactions with bound electrons. The energy of the photon is greater than the binding energy of the K shell electrons (closest electron orbit to the nucleus and possess the largest binding energy). After transferring sufficient energy to free an electron, the photon continues on through the material. As photon energy increases, Compton scattering dominates over the photoelectric effect (68:10).

Photon pair production requires at least 1.02 MeV of energy. It occurs when a photon is absorbed by a high-Z nucleus, which then emits a positron-electron pair (a positron has a positive charge and has the same rest mass as an electron).

Rutherford scattering (Coulomb scattering) occurs when charged particles interact with the material. Cosmic rays, electrons, and protons can cause lattice displacements, and cosmic rays can create secondary radiations as they are stopped. Displacement energies for gallium and arsenide atoms are 8.8 and 10.1 eV, respectively, and defect production thresholds are 228 and 273 keV, respectively (73:36). These charged particles are stopped by electric fields surrounding the lattice atoms. Sufficient energy for ionization will be transferred to the lattice atom during glancing encounters. Collisions with a lattice atom nucleus can cause lattice displacements. The numerous electric field interactions will cause the most energetic cosmic rays and protons to have a very short range, hence, they do most of their damage near the surface of the material (2:34).

The secondary radiations from cosmic rays in the form of neutrons and gamma rays may penetrate deeply into the material. Since the absorption of gamma rays pro-

duces electron emissions, gamma rays can indirectly produce displacements. Gamma rays are emitted when neutrons are captured. Additionally, the capturing atom will recoil (displace) itself out of the lattice. Energetic electrons are also capable of producing displacements by the Compton scattering process. This cascading of potentially damaging emissions explains why neutrons are so damaging to semiconductors.

Neutrons can interact with target materials in three ways: elastic scattering, inelastic scattering, and transmutation. In elastic scattering, the neutron gives part of its energy to a lattice atom, which may be displaced by the transfer. A 1 MeV particle can cause many displacements before stopping or exiting a material. The struck atom will receive on the order of hundreds of eVs of kinetic energy. Because a typical atom requires only 25 eV to become free of the lattice, it will have sufficient remaining energy to cause additional displacements of neighboring atoms. In this manner, a region of damage can result from the passage of one energetic particle (2:32) (68:19). An electron will be emitted because of ionization. Inelastic collision occurs when the incident neutron is absorbed by the target atom, and a neutron of lesser energy is emitted. Additionally, a gamma ray will be emitted with an energy equal to the difference in neutron energies. This inelastic collision may also cause displacement. Transmutation occurs when the neutron is absorbed in the nucleus which then emits a proton or alpha particle. The nucleus is then converted to that of another element. Because the fluxes of thermal neutrons in space is very low, the target material would have to be extremely pure and undoped in order for transmutations to become significant compared to dislocations (2:40) (68:12).

The penetration range for radiation particles can be found in Figure 19. The range is expressed in grams/cm². As an example, the M0006 sample tray cover and thermal shield was made from aluminum approximately 0.313 inches or 0.795 cm thick. Aluminum has a density of 2.70 grams/cm³. The range of the radiation particles required to penetrate the cover and shield can be determined to be 2.146 grams/cm². This corresponds to 40 keV photons, 4 MeV electrons, 40 MeV protons,

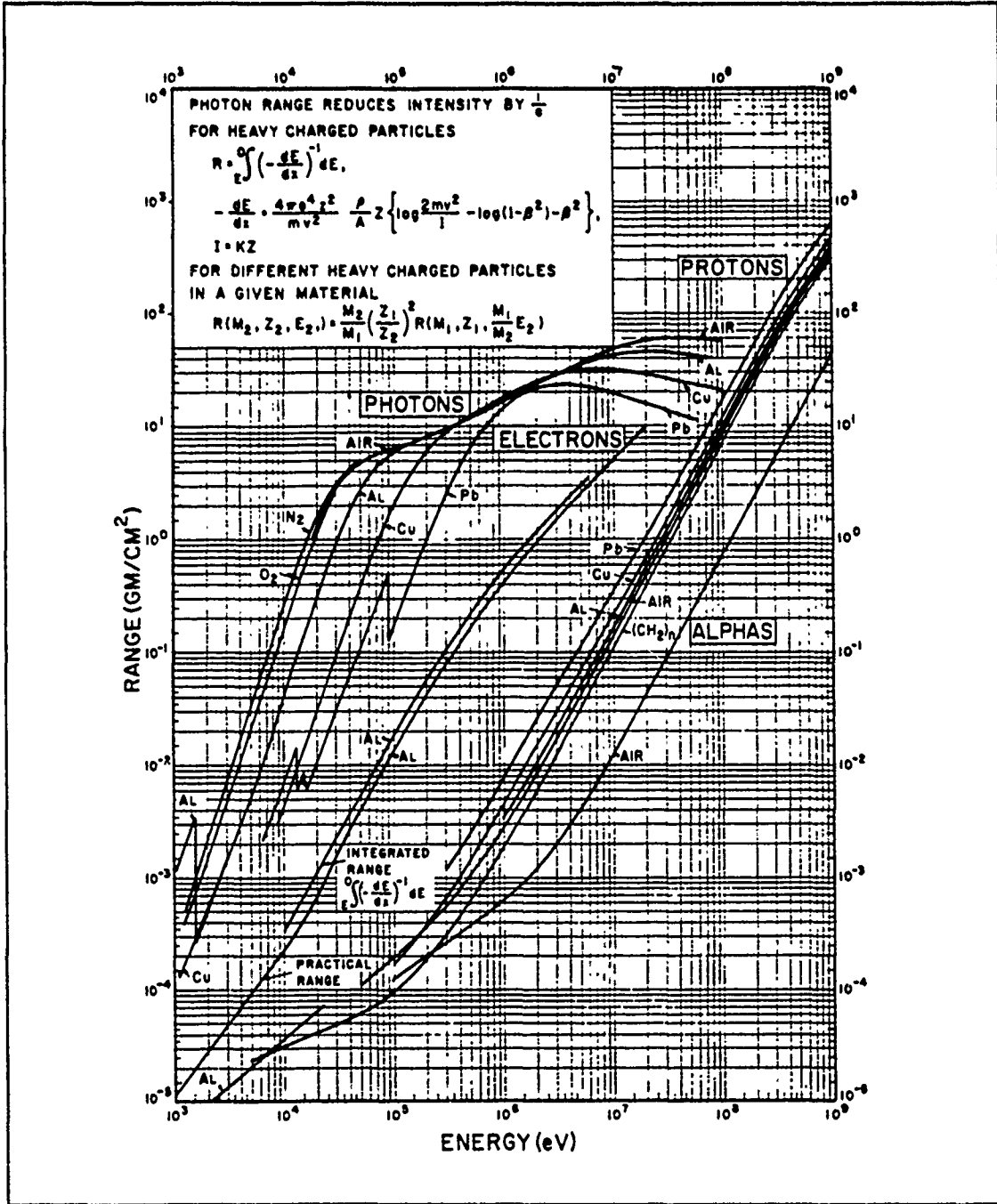


Figure 19. Range-energy curves for penetrating radiations (21:86)

or 180 MeV alpha particles. Particles of lesser energy would not penetrate through the cover to the semiconductor samples below, while those with just the required energy would penetrate through but not have sufficient energy left to effect the samples.

Two basic interaction outcomes dominate the radiation effects possibilities: displacement of atoms from their lattice sites (displacement damage) and generation of electron-hole pairs (ionization). For the average particle, a portion of its total energy is deposited in the lattice in the form of ionization damage, and the remainder results in dislocation damage. Fast neutrons are known to primarily produce displacement damage, and low energy electrons produce ionization damage (44:3) (68:13). The absence of an atom from its normal lattice site is called a vacancy. If it moves into a non-lattice location, it is referred to as an interstitial defect. When vacancies and interstitials are adjacent, they are referred to as close pairs, or Frenkel pairs. Two adjacent vacancies or interstitials are called divacancies or di-interstitials.

Another type of defect due to radiation damage is the simple defect, or point defect. Defect clusters are regions of closely spaced defects. Vacancies and interstitials can also form additional types of simple defects when they are adjacent to impurity atoms which are referred to as defect-impurity complexes (68:18).

Just as impurity atoms have discrete energy levels in the bandgap between the conduction band and the valence band, radiation-induced defects can be associated with similar energy levels in the bandgap. Therefore, the basic scenario for radiation changes in semiconductors is: atoms are displaced by incident radiation particles, additional energy levels are formed in the bandgap, the spectrum of the material is altered (2:41) (68:19).

3.3.2 *Gallium Arsenide* Irradiation effects in GaAs can be placed into three distinct groups: (a) quenching or generation of luminescence peaks, (b) decreases or increases in peak intensity, and (c) shifts of peak locations to higher or lower energies. A particular change may be the same for the entire spectrum, or may even have an opposite change in a separate spectral region. In order to better identify specific changes, the spectrum will be divided into three separate emission regions: (1) exciton emission, (2) free-to-bound emission, and (3) donor-acceptor pair emission.

In general, peak quenching and decreases in luminescence intensity are most often observed in GaAs. Peak shifts are sometimes seen as a result of irradiation, and usually shift towards longer wavelengths (70:826). The reappearance of quenched peaks or the generation of new peaks sometimes occurs after annealing the sample at temperatures near or greater than 500 degrees K (5:679) (37:113). Since, however, this annealing phenomena did not occur since the flight samples were exposed, these types of peaks will not be considered.

3.3.2.1 *Peak Quenching and Generation* Bombardment with particles whose energies are greater than the damage threshold energy will most probably create non-radiative recombination centers. It has been found that electrons possessing threshold energy (1.0 ~ 1.5 MeV) and fluxes greater than 10^{18} particles/cm², and protons and neutrons of 4 MeV energy and fluxes of 10^{13} particles/cm², will produce a quenched, featureless spectrum (5:679). On the other hand, energies less than threshold will usually produce degradation of luminescence. Displacement energies for gallium and arsenide atoms are 8.8 and 10.1 eV, respectively, and defect production thresholds are 228 and 273 keV, respectively (73:36).

Electrons with energies of 1 MeV and 8×10^{15} particles/cm² flux have generated, in *n*-type GaAs, several electron traps. These electron traps were located as follows: E2, 0.18 eV; E3, 0.41 eV; E4, 0.71 eV; and E5, 0.90 eV. The P1, P2, and P3

electron traps were located at 0.36, 0.50, and 0.72 eV, respectively, for the irradiated and annealed sample (60:355).

Thermal neutron irradiation with a flux of around $10^{11}/\text{cm}^2\text{-sec}$ is responsible for the generation of three peaks located at 1.30, 1.40, and 1.46 eV for Te doped (*n*-type) GaAs. The first peak is generally assumed to be associated with Cu contaminants, the second with an As vacancy, and the last with a Te occupying an As vacancy. The peaks associated with edge emission and Te donor - Ga vacancy transition are sensitive to prolonged fluxes of the neutrons and become totally quenched after 24 hours of irradiation (27:103). Another neutron (or gamma-ray) generated line at 1.35 eV was reported for *n*-type material, and the luminescence intensity was sensitive to irradiated flux change (70:827). In Sn doped material bombarded with 1.25 MeV gamma-rays, two lines appeared at 0.70 eV and 0.60 eV (10:573).

3.3.2.2 Peak Intensity Changes The 1.40 eV line of *n*-type GaAs decreases with electron irradiation, but the 1.15 eV line in the same sample increases (46:215). The 1.486 and 1.37 eV lines in Cd doped GaAs show a significant decrease with increasing electron fluences (4:779). Neutron irradiation causes a decrease in intensity of the 1.42 and 1.14 eV lines in Te-doped material (27:104), and protons of 200 keV energies will induce a broad 1.46 eV peak (46:216).

Neutron and gamma-rays will cause an increase in luminescence intensity of the 1.508, 1.35, and 0.96 eV lines of *n*-type material, until the flux is raised up to about $10^{13}/\text{cm}^2$ for neutrons, and $2 \times 10^{17}/\text{cm}^2$ for gammas. Then the luminescence will decrease sharply with increasing flux until the peaks are quenched (70:826).

3.3.2.3 Peak Shifts In *n*-type GaAs bombarded with neutrons or γ -quanta, the edge emission peak located at 1.508 eV has been observed to shift to 1.494 eV (longer wavelengths) (70:826). Electron irradiation produces a similar shift toward lower energy in the 1.37 eV peak, but the 1.489 eV peak shifts toward higher energy (shorter wavelength) with increasing fluence of electrons (4:783)

3.3.3 *Cadmium Selenide* In general, radiation effects manifest in this material mainly by a decrease of the intensity of exciton lines with an increase in luminescence intensity of other lines, and may shift in some peak positions towards longer wavelength (lower energy). Additionally, new emission lines may be formed, but this radiation effect is much more sample dependent than the other two effects.

3.3.3.1 *Peak Quenching and Generation* Bombardment with electrons with energies greater than damage threshold for cadmium or selenium will cause the generation of new luminescence bands (63:603). Electrons with energies less than threshold have less significant effect on the spectrum. Above an energy threshold of 320 keV at 5 degrees K a new emission band at about 1.1 eV is produced, whereas a threshold at 250 keV at 77 degrees K produces a band at 0.99 eV. The generation of centers for the 1.1 eV luminescence accompanied by a decrease in the intensity of the 1.74 eV have been reported for CdSe with electron irradiation (63:606). Remember, the thermal environment for the LDEF was expected to be between 283 degrees K and 323 degrees K.

It was reported that the 1.73 eV line was produced for samples whose temperatures are greater than 100 degrees K at irradiation (42:406). It has been identified as an optically active center formed by a cadmium vacancy and donor complex.

A band attributed to the luminescence of excitons localized at surface potential fluctuations identified only as "band X," appears between 6380-6850 Å in the edge emission region in CdSe. When the sample is irradiated with beam energies of 2 keV at liquid helium temperature, this band slowly quenches with higher electron fluxes, or with increasing sample temperatures (15:1946).

Neutron bombardment of CdSe at 373 degrees K produced a new luminescence band at 7047 Å. This peak was interpreted as an electron transition from a Cl⁻ donor to an acceptor formed by a cadmium vacancy (6:4499).

3.3.3.2 Peak Intensity Changes Irradiation normally produces a decrease in edge luminescence, specifically for excitons (42:406). It also produces an increase in the 7153 Å (1.73 eV) line proportional to the increase in beam energy. The "band X" line displays a reverse correlation to the exciton lines. It will decrease in luminescence intensity as the bound exciton line increases considerably after the electron bombardment with a dose of $\sim 10^6$ electrons/cm² at 2 keV.

3.3.3.3 Peak Shifts Electron irradiation with sufficient energy produces a peak shift towards higher energies for the CdS donor-acceptor pair with enhanced luminescent intensity. Generally speaking, the edge emission will incur a small peak shift while the donor-acceptor pair will incur a much larger shift (13:1265-69) (63:605). CdS edge emissions tend to shift towards lower energy with increasing electron fluence (23:17).

3.3.4 Summary Radiation damage in GaAs most often results in decreases in luminescence intensity or quenching of peaks. Peak shifts are not as common, but do occur. Generation of new peaks is a rare event if the samples are not annealed. Radiation effects in CdSe appear sometimes as increases in luminescence intensity of certain peaks and shifts in peak positions. Additionally, new emission lines may be formed in irradiated CdSe samples.

3.4 Conclusion

The radiation environment in LDEF's orbital regime consists of galactic radiation, solar particulate radiation, geomagnetically trapped radiation, and atomic oxygen. The radiation most likely to have fluxes and energies sufficient to change the semiconductor samples was trapped radiation, which consisted of protons, electrons, and anomalous radiation nuclei.

Incident radiation with sufficient energy will cause permanent changes in the crystalline material. These changes, when viewed by luminescent spectroscopy, man-

ifest themselves as changes in peak intensities, locations, and the generation or disappearance of a peak altogether.

In this review, the nature of the low earth space environment was investigated, and the influence of the environment on the samples to be examined was determined. The next chapter will explain the apparatus and procedure used to examine the semiconductor samples.

IV. Apparatus and Procedures

4.1 The System

4.1.1 Sample Information The LDEF samples were bonded into circular one-half inch diameter, one-eighth inch deep recesses on a tray made of one-quarter inch thick aluminum. The bonding material was a Varian product called Torrseal, which has a reported temperature operating range of 228 K to 393 K. Two recommended removal techniques were given by the manufacturer. One method involved heating the Torrseal to 793 K, the other involved dissolving the Torrseal in dichloromethane (CH_2Cl_2). Both methods would alter the samples; heating would anneal the semiconductors, and dichloromethane would alter their surfaces (56:Section II). Ultimately, the samples were removed from the tray by boring in from the back side of the tray to within one five-thousandth of an inch, and final cutting with a razor knife. This process resulted in the LDEF samples remaining bonded to a circular one-half inch diameter, one five-thousandth inch thick piece of aluminum. Unfortunately, the boring and cutting process fractured six of the eight GaAs samples into many smaller pieces. With the exception of some shards from sample #21, the samples remained intact . . . held together by the Torrseal.

It became very important to determine the ability of the epoxy to hold the sample together at temperatures near 10 K and vacuums of 5×10^{-9} torr. In order to test the interactions of the different coefficients of expansion, similar test samples were constructed with close attention paid to the GaAs sample dimensions, Torrseal thickness, and aluminum size. Medium and large GaAs samples slowly dipped directly into liquid nitrogen and helium suffered fractures and shearing off part of the material, but the Torrseal held the entire sample bottom in place. Small and large GaAs samples placed in a vacuum chamber and cooled to 4.2 K over an one-half hour period suffered no adverse effects, and again the Torrseal held.

4.1.2 *System Overview* Figure 20 is a schematic of the experimental system. The samples were mounted to the end of a Helitran cold finger to facilitate lowering their temperature to about 16 degrees K in order to reduce thermal noise. A copper mask held the samples against the cold finger. Once mounted, the cold finger and samples were located in the approximate center of a very-high-vacuum chamber capable of 10^{-9} torr. Vacuum was achieved through a three stage process involving two sorption pumps, a Vaclon pump, and a titanium sublimation pump. A VG Microtech LEG 32 electron gun was the excitation source. Electron beam current was changed and monitored by the VG Microtech 326A power supply. Two lenses focused the luminescence onto the entrance slit of a grating spectrometer. A photomultiplier and signal amplifier provided data to a X-Y recorder which produced spectral graphs. An Argon laser was used to align the optics and as a secondary excitation source.

4.1.3 *Vacuum System* The vacuum system consisted of three different types of pump/control units: two Varian VacSorb sorbtion pumps; one Varian model 921-0041, 110 liter/second Noble Vaclon pump with model 921-0043 Pump Control Unit; and one Varian model 916-0017 Titanium Sublimation Filament Cartridge with model 922-0052 Pump Control Unit (See Figure 21). This system could obtain vacuums of 5×10^{-9} torr.

The 0.3 meter diameter and 0.67 meter high cylindrical vacuum chamber consisted of two main components. The upper chamber fit into a lip on the lower chamber to form a tight seal with the aid of a rubber o-ring. Samples are lowered into the chamber on a coldfinger through a hole located in the center of the top. The upper chamber had four large (8-inch) and four small (2.75-inch) ports which permitted access to the samples (See Figure 22). These ports were used either as windows or equipment mounts. One small port housed a Faraday cup on an extensible arm which could be used to monitor the electron beam current from the Superior electron gun. One large port contained a Brewster window through which the Argon laser was fired to excite the samples or align the optics.

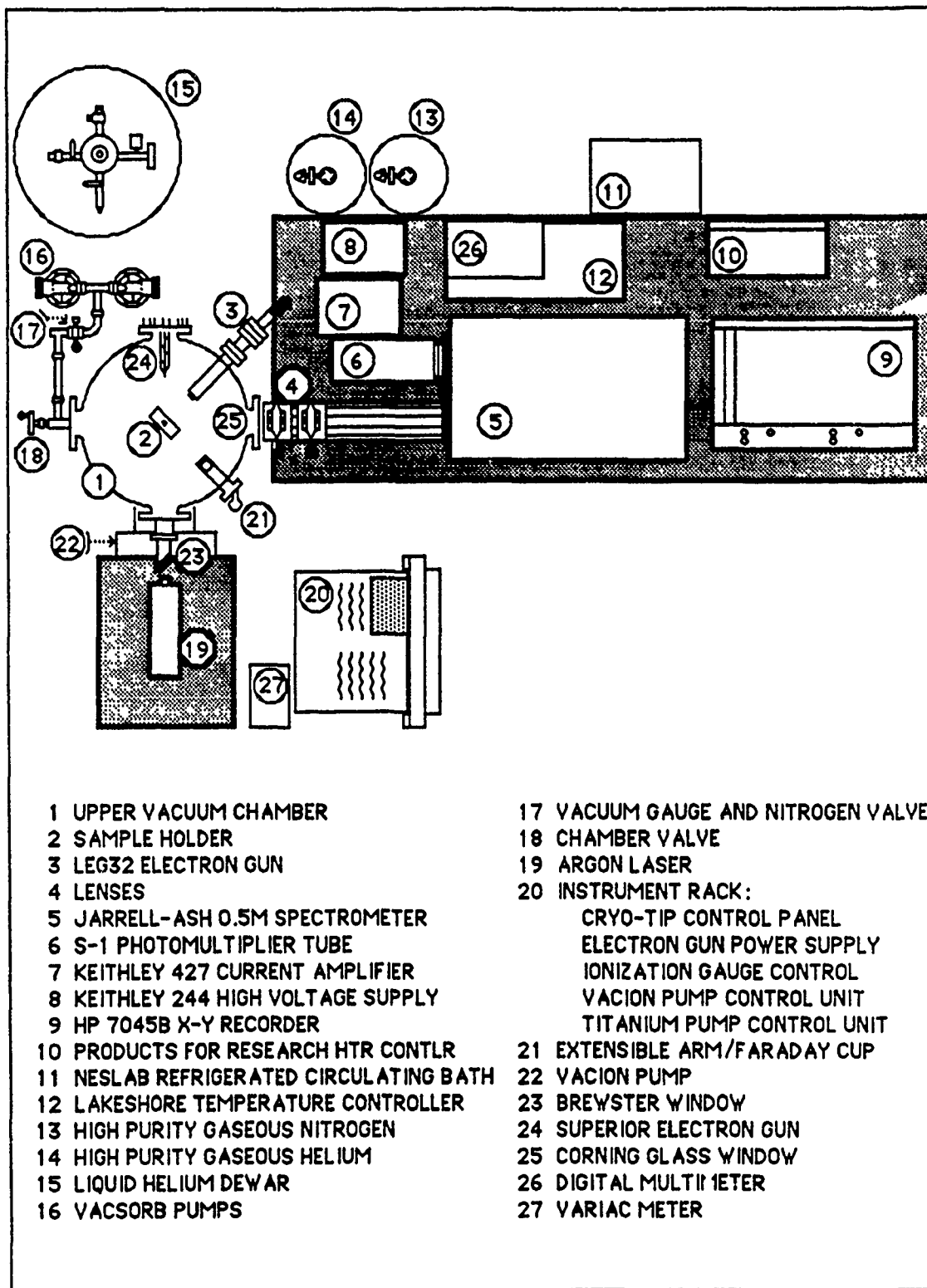


Figure 20. Schematic of the experimental system

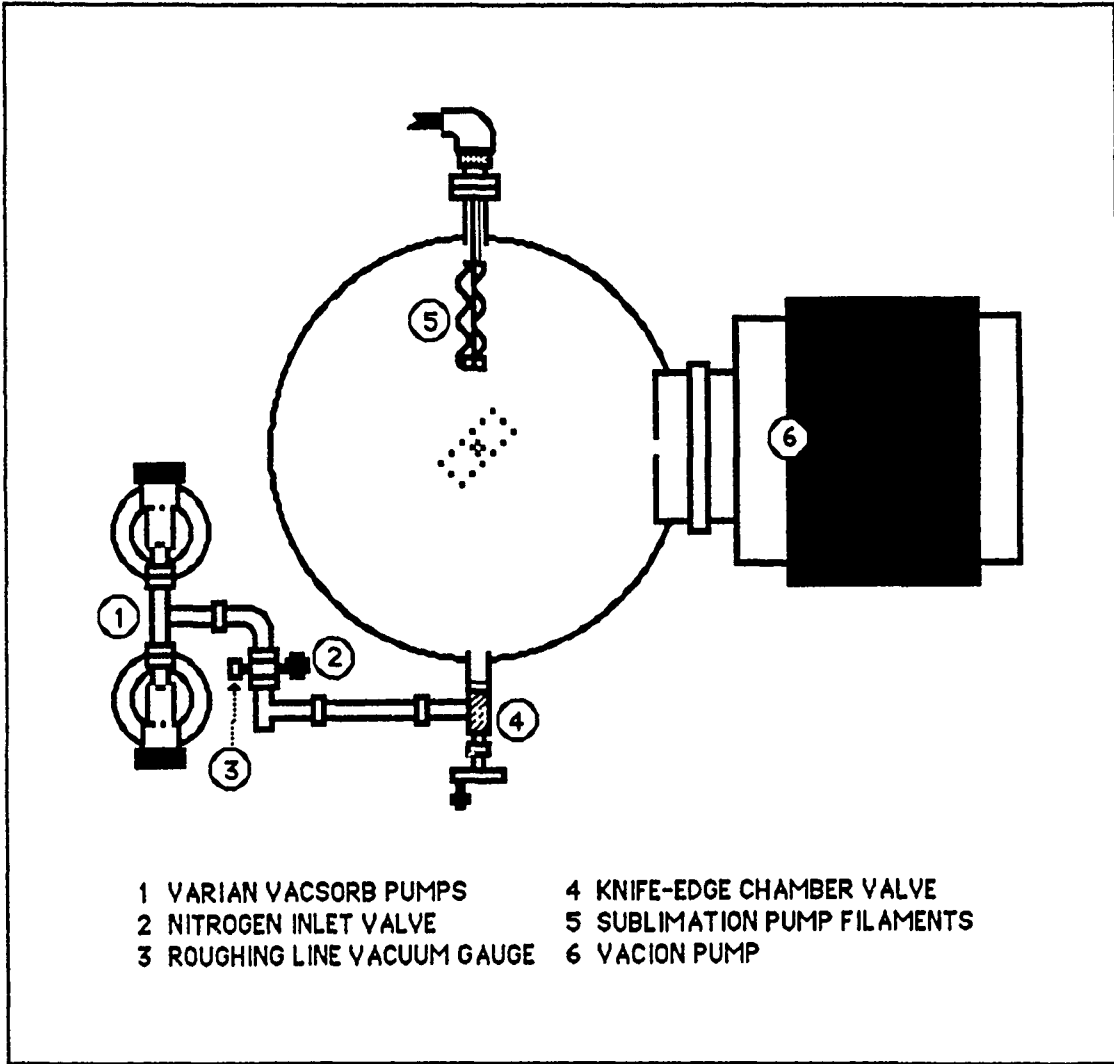


Figure 21. Vacuum pumps and locations

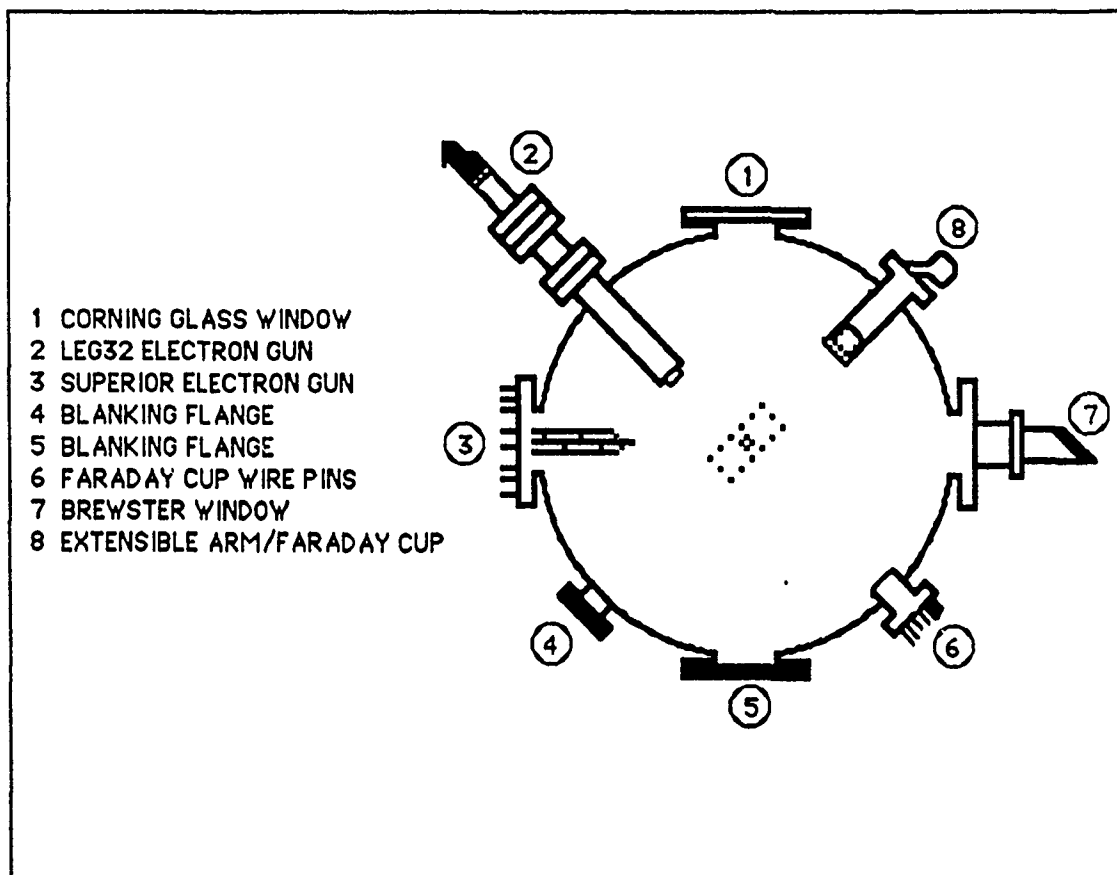


Figure 22. Construction of the upper chamber housing

The lower chamber contained ten small ports located around its mid-section, and three pump ports around its base, which were used to house pressure monitoring and pumping equipment (See Figure 23). Of the ten small ports, only the ionization

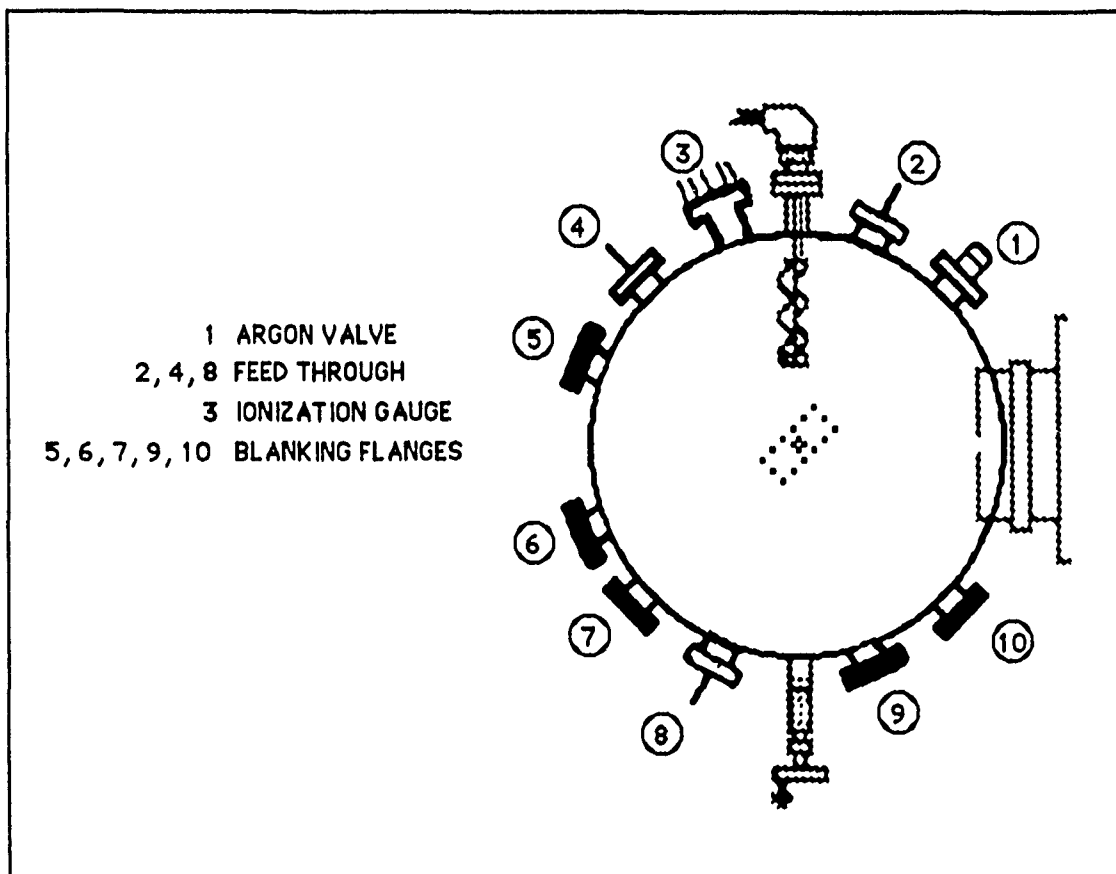


Figure 23. Construction of the lower chamber housing

gauge was used. A large port for the VacIon pump was located 90 degrees clockwise from the titanium pump. The port 180 degrees clockwise housed the chamber flow valve through which gaseous nitrogen was let in to back-fill the chamber to atmospheric pressure, or, through which the chamber was initially depressurized by two VacSorb pumps.

4.1.4 *Cryogenic Transfer System* Samples were mounted on a coldfinger (also referred to as a refrigerator) and cooled by an Air Products model LT 3-110 Helitran System. Major components of the system were the transfer line with coldfinger bayonet and dewar bayonet with extension, and the coldfinger with radiation shield and sample holder. The transfer line was comprised of two capillary-sized tubes. The center tube (cryo-tip line) transferred liquid helium from the dewar to the sample holder on the coldfinger. The second tube in the transfer line held the gaseous helium return of the center tube jacket produced during the pre-cooling process and by the coldfinger heater. The heater served to prevent damage to the coldfinger by warming the center tube jacket helium to above 200 K. In order to insulate the capillary tubes, the transfer line and coldfinger were evacuated to 1×10^{-5} torr. Exhaust gasses from the transfer line and coldfinger were routed to a control panel used to control the liquid helium flow through the system. This system was capable of cooling the sample finger to 10.0 K.

4.1.5 *Sample Finger* The sample finger attached to the Helitran cryo-tip cooling line was made completely of copper and held three resistive heaters, a GaAs temperature sensing diode (on the back of the holder), a Faraday cup, and a Au-Chromel thermocouple (also on the back). The sample finger was heated to 300 K before removal from the chamber. The heating was accomplished with a Lakeshore Crytronics temperature controller linked to the GaAs diode and the three resistive heaters. A microprocessor sensed the difference between a pre-set temperature and the actual sample finger temperature and applied current for heating if required. The Au-Chromel thermocouple linked to a Systron-Donner model 7000A digital multimeter provided an additional check on the temperature of the sample finger. This system served to control the temperature to better than 0.1 K. The sample finger was lowered into the chamber through a hole in the top of the chamber. Its length ensured the sample would be positioned in the same plane of the electron gun, Brewster window and Corning window. Two rubber o-rings on the coldfinger

ensured a vacuum could be accomplished while permitting the sample to be rotated for alignment.

4.1.6 Sample Handling All samples were kept in individual plastic containers and sealed in plastic bags. Samples were transferred to and from the container with rubber gloves and tweezers. The samples were occasionally cleaned with methonal and blown with dry nitrogen gas. These precautions were taken with all samples.

Samples were mounted to the coldfinger with a thin copper mask which was held in place with four small screws. To ensure a good thermal contact, a small amount of GE Varnish was placed on the back corner of the sample. The surface temperatures of the samples could not be directly determined even though the temperature of the coldfinger could be determined to within 0.1 K. It was believed the GE Varnish would enable the temperature of the sample to become very close to the temperature of the coldfinger even with localized heating from the electron beam.

4.1.7 Electron Gun A VG Microtech LEG32 electron gun provided the means for exciting the samples. The LEG32 gun is an electrostatically focussed, medium-spot electron source, capable of providing beam energies in the range 0.1 to 5 KeV. It has a current capability of up to 0.4 mA. The gun benefited from totally enclosed optics which significantly reduced the large amount of white light generated during its operation. It's shield measured eleven inches long, and one and one-quarter inches in diameter from the tip to within one-half inch of the base where it widened to one and three-eighths inches. This last half inch meant that the gun would not fit into standard one and three-eighths ports or nipples. Furthermore, its extra long length required a six and one-half inch nipple be constructed to position the tip of the gun a reasonable distance from the sample holder to permit aiming without sacrificing the ability to focus the beam. The gun can be operated as close as 15 mm, and has quadrupole scanning elements which ensure uniform beam scanning. The filament is thoria-coated rhenium, and is mounted on a replaceable ceramic

button. Additionally, the filament can be operated on either current, voltage, or power stabilized mode. For this research the gun was operated in current stabilized mode.

The power supply was the VG Microtech Model 326A. The model 326A supply is designed for the operation of a range of electron sources. This is possible by having common circuitry for beam energy, filament, Wehnelt, and deflector supplies, and a switchable section for focus and extractor voltage supplies to suit specific source requirements. Fully floating, the supply uses close tolerance components to provide high voltage stability, low drift and high setting accuracy for critical applications. Provision is made within the supply for three alternative filament operating modes, set by means of internal switches. Normal operating is in the current stabilized mode. The Wehnelt or grid acts as the control electrode to vary the emission current. Wehnelt voltage is controlled automatically by a feedback circuit to stabilize emission current at the preselected value. The focus voltage can be set by a rear panel switch as a fixed fraction of the final anode voltage (unipotential lens configuration) or as an independently variable voltage. Each pair of deflector electrodes is provided with a variable voltage balanced about the positive terminal of the beam energy supply, normally the potential of the final lens electrode.

4.1.8 Optical System The luminescence from the samples was focused on the entrance slit of a one-half meter spectrometer by an optical system consisting of two bi-convex lenses (See Figure 24). The lens closest to the sample measured 75.0 mm in diameter and had a focal length of 250 mm. The second lens measured 80.0 mm in diameter and had a focal length of 500 mm.

The focal length of the first lens was dictated by the need to place it outside the chamber, which would require at least a 230 mm focal length lens. A second lens with a diameter as large as the first lens would not lose the parallel luminescence light rays. The focal length and diameter of the second lens was chosen to minimize

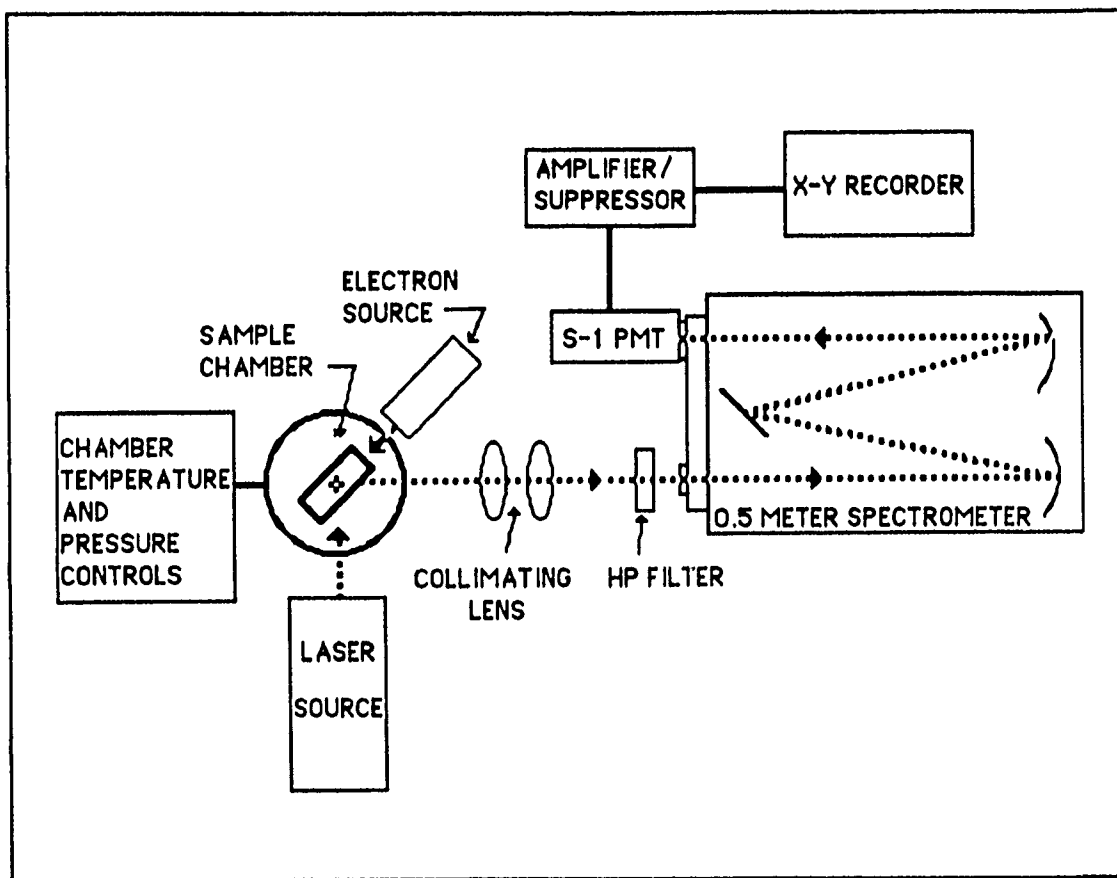


Figure 24. Layout of the optical system

luminescence loss and to closely match the F number of the spectrometer. The F number is the optimum angle at which light passes through the entrance slit of the spectrometer and strikes the first mirror. The F number describes this angle as the resultant of the lens focal length divided by its diameter

$$F = \frac{f}{D} \quad (6)$$

By closely matching the second lens to the spectrometer F number, one can optimize the amount of luminescent light that passes through the slit. The spectrometer F number is 8.6 and the second lens F number is 6.25. It should be noted that in order to match the spectrometer F number the second lens would have to be 58.1 mm in diameter, and so would the first lens in order to minimize light loss. If we consider the luminescence to be lambertian, and the collective power of the two lenses as a function of their solid angles

$$\Omega = \frac{A}{r^2} \quad (7)$$

(80 mm dia lens)

$$\begin{aligned} \Omega &= \frac{\pi(80\text{mm}/2)^2}{(230\text{mm})^2} \\ &= 9.5 \times 10^{-2} \end{aligned}$$

(58.1 mm dia lens)

$$\begin{aligned} \Omega &= \frac{\pi(58.1\text{mm}/2)^2}{(230\text{mm})^2} \\ &= 5.0 \times 10^{-2} \end{aligned}$$

The 80 mm lens would collect about twice as much light as the 58.1 mm lens. There exists a trade-off between light collection at the chamber window and optimization of focused light in the spectrometer. The second lens was positioned at

480 mm to slightly overfill the spectrometer grating and reduce alignment sensitivity.

4.1.9 Signal detection and Processing system The signal was passed through a Jarrell Ash 0.5 meter spectrometer which had a 1200 groove/mm, 2 inch square, blazed grating at 5000 Å. It was collected in one of two different photomultiplier tubes: RCA C31034 GaAs, and S-1. The C31034 provided signal detection in the 0.33 to 0.88 microns. The water cooled S-1 provided signal detection from approximately 0.6 to 0.98 microns. For the C31034 and S-1 PMTs, the exit signal was amplified and noise suppressed by a Keithley 427 current amplifier. It was then sent directly to a HP 7045B X-Y recorder where it was plotted on 14 inch by 17 inch sheets of graph paper.

The grating and PMT were switched towards the end of the thesis to permit examination of the samples around the 1 micron range. The grating was replaced with a 590 groove/mm, 2 inch square, blazed grating at 1.3 μm. A nitrogen cooled germanium detector provided signal detection from about 0.78 to 1.8 microns. For the germanium detector, the entering signal was passed through an optical chopper connected to a Scitec lock-in amplifier. Upon exiting the spectrometer and detector, the signal was passed through a Northcoast Model 823A noise suppressor. Again, the final signal was plotted on the HP X-Y recorder.

Data sheets were later reduced to 50% actual size and arranged onto Latexed template graphs by hand.

4.2 Procedure

4.2.1 Chamber Evacuation The chamber must always be backfilled with gaseous nitrogen. Since nitrogen has the highest pumping rate for both the VacSorb and Vac-Ion pumps, the chamber will be returned to a high vacuum pressure in the shortest amount of time.

Evacuation begins by closing the VacSorb, nitrogen inlet, and chamber valves.

The VacSorbs were cooled with liquid nitrogen after making sure the rubber outgassing covers normally raised during bakeout were down and closed. One VacSorb was opened and allowed to pump the roughing line down to 10 millitorr. This also served as a function check of the Hastings Model 461 thermocouple vacuum gauge attached to the roughing line between the VacSorbs. The chamber valve was opened and the first VacSorb allowed to pump until it became saturated (until the pressure no longer dropped). This usually occurred around 1 torr of pressure. The first VacSorb was then closed and the second opened. It pumped the chamber pressure down to between one and five millitorr. If it failed to do so, it was an indication that the VacSorbs need to be cleaned by baking for a period of 24 hours .

Once the chamber pressure was below 5 millitorr, the VacIon pump was started. The main chamber valve and one VacSorb should be left open during the initial VacIon pump operation. As the pump warmed, it outgassed and slowed down the pumping process. This was minimized by monitoring the pump voltage gauge and turning off the pump when it started to decrease in voltage. Any outgassing was removed by the VacSorb. The on/off procedure was followed until the pump could operate on its own, which normally occurred around fifty μ torr. The main chamber valve and VacSorb were closed when no voltage gain was obtained between on/off cycles, otherwise the VacIon pump would pump out the VacSorb. The VacIon pump remained on continuously until a switch in samples occurred, during which the chamber was backfilled with high-grade nitrogen.

The sublimation pump, or Ti-pump for short, was started at 1.0 μ torr with a 50% duty cycle. When the pressure reached 0.1 μ torr, the duty cycle was reduced to 25%. At 0.01 μ torr the pump was reduced to and maintained at 10% unless sample runs were being accomplished. Because the filaments created enough heat to increase the chamber pressure, starting the Ti-pump any earlier than 1.0 μ torr negated any gains the VacIon pump made in reducing chamber pressure.

4.2.2 *Sample Cooling* With the dewar bayonet end located approximately one-eighth inch from the bottom of the dewar, and the coldfinger bayonet screwed down one-half of the exposed thread on the coldfinger, the cooling procedure began by pressurizing the helium dewar to seven psi with high grade gaseous helium. The bayonets were always configured in the manner until a helium dewar change was needed. During a dewar change, gaseous helium was blown through the transfer system from the coldfinger side to the dewar side for a period of ten minutes. This procedure was followed each time the dewar bayonet was removed and prevented blockages in the system due to trapped water which would be turned instantly to ice after immersion into the liquid helium.

The shield and cryotip flow needle valves were fully opened to begin the flow of liquid helium from the dewar through the helitrans transfer tube. Initially, the ceramic flow balls hovered below one cubic centimeter/minute, but, as the helium made its way into the coldfinger, they rapidly rose to around seven or more cubic centimeters/minute.

The voltage across the thermocouple located in the sample holder was monitored during the cool down process. When the temperature reached approximately 273 degrees K (-0.50 mV), the coldfinger heater unit was plugged in. And when the temperature reached about 20 degrees K (-4.50 mV), the dewar pressure was bled-off to 4.0 psi. It was found that dewar pressures above 4.0 psi induced temperature, pressure, and signal noise fluctuations which almost appeared harmonic in nature. It is believed that thermodynamic problems brought about by the limited helium flow through the cryotip and dominating back-pressure of the dewar caused these sometimes disastrous fluctuations, which should be avoided at all costs. Next, the flow needle valves were closed until the cryotip flow was about 3.5 cc/min and the shield flow was about 2.0 cc/min. With these settings, the sample could be maintained at approximately 13 degrees Kelvin for a period of one hour.

To stop the flow and warm-up the sample, the flow valves were closed and the

dewar pressure reduced to below 2 psi. The Lakeshore temperature controller was pre-set to room temperature so that its microchip monitor would add current to heat the sample holder until it was at room temperature. The coldfinger heater was unplugged when the coldfinger temperature reached approximately 273 degrees K (-0.50 mV). The coldfinger was kept in the vacuum chamber and allowed to return to room temperature before removal in order to prevent condensation.

4.2.3 Electron Beam Alignment The electron beam was initially centered onto the sample surface by visual means. The beam would cause a blue luminescence if it struck stainless steel as found in the four mount screws or the coldfinger, or if it struck the copper mask or copper sample mount. With few exceptions, GaAs would not emit a visible glow, so the beam was aligned using the surrounding material luminescence. Additionally, the electron gun sheath had a small hole in its end which permitted white light generated by the gun's operation to strike the sample holder in the upper right corner. The luminescence from the beam was lost in this white light, so that area was avoided during the alignment procedure.

Gun current was measured using a meter on the Microtech 326A power supply. The beam current could be altered by changing the filament current. The gun current did tend to wander with increasing filament current, probably due to the 326A power supply being designed for 50 hertz, but used with the American standard 60 hertz, which may induce a phase sync problem. The Faraday cup mounted on the transversing arm was used initially to determine the Superior electron gun current, but was not used for the LEG32 electron gun because of the 326A current meter, and because the Faraday cup would need to be remounted to accommodate the 90 degree LEG32 beam entrance angle as opposed to the 135 degree Superior beam entrance angle.

The manufacturer's optimum operating distance for the LEG32 was reported to be 15 millimeters. Due to the availability of Varian extension nipples, the closest

the LEG32 could be brought to the sample was two and one-half inches, or 62.5 millimeters. This imposed a slight focusing problem resulting in a spot approximately four millimeters in diameter.

4.2.4 Spectrometer Alignment The 0.5 meter Ebert spectrometer was mounted on three lab jacks to a built-up laboratory desk. Alignment was accomplished by first adjusting the height of the entrance slit to the laser using the lab jacks and a hand level. Next, the spectrometer was shifted side-to-side on the stands and taped securely in place. With the cover removed, the HeNe laser beam was routed through the spectrometer so as to strike the grating, two mirrors, and the exit slit in their centers. The photomultiplier tube was not in place during this operation. Final adjustments were made after the coldfinger was rotated 180 degrees and the sample struck with electrons. The initial sample was ZnS because it provided bright blue luminescence which allowed the same alignment procedure. This later proved very important because the laser beam strike and the electron luminescence strike on the entrance slit were approximately one-half inch apart. This discrepancy was reproducible with other samples, and the cause is believed to be a slight slant in the coldfinger verticle axis.

4.2.5 Optics Alignment A 24 inch optical bench with two translating mounts served to place the two lenses into the luminescence path. The optical bench was initially aligned with the top center of the chamber exit window and spectrometer entrance slit using a He-Ne laser. The translating mounts were selected to have both vertical and horizontal adjusting micrometers. The first lens was placed about four millimeters from the exit window. With the PMT, amplifier, and recorder in place and working, the lense position was adjusted to provide the maximum signal. The second lens was added and placed approximately 48 cm from the entrance slit. It too was adjusted to provide the maximum signal. A 6300 Å long-pass filter was taped in front of the entrance slit to filter out white light and reduce noise in the signal.

4.2.6 *Luminescence Measurements* The cathodoluminescence data was taken from GaAs and CdSe samples in the 8000 Å to 9750 Å wavelength range. The Hewlett Packard X-Y recorder was calibrated along the X axis to provide the exact same wavelength for each spectrum. The internal drive of the spectrometer was tested against a clock to measure the exact speed in units of Å/min. The spectrometer was then calibrated against an Argon lamp at the 8424.6 Å line. The calibration was found to be within two-tenths of an Å. Initial spectra were taken with spectrometer and recorder drive settings of 250 Å/min and 50 sec/in respectively. This resulted in 208.333 Å/in on the graph paper. Spectral lines could be read accurately from the graph paper to within 1/100th of an inch, which resulted in an accuracy of ± 2.08 Å.

Spectra was taken by starting the spectrometer drive at 7962 Å with the entrance slit set at 400 microns. The argon lamp was placed in the beam path to acquire a 8115.3 Å and 8424.6 Å line for reference purposes. The run took approximately seven and one-half minutes to complete. Three runs of 5, 50 and 100 microamp gun current settings were made at 1000, 2000, and 3000 gun voltage settings. For each run, one additional run was made with variable recorder vertical settings to maximize resolution. This meant that at least 18 runs were made on each sample. Additional runs were made if interesting spectral lines appeared, and usually involved narrowing the entrance slits and maximizing gain in an attempt to better resolve the lines.

V. Results and Discussion

In this research project, cathodoluminescence and photoluminescence data were taken from seven pairs of GaAs and two pairs of CdSe samples. One sample from each pair, referred to as the "control samples," was kept on the earth's surface as references. The other sample pairs, referred to as the "exposed samples," were exposed to a 480 km low earth orbit radiation environment. In this chapter, luminescence data from each individual sample will be discussed, and then comparisons of sample pair spectra will be made to locate changes. Luminescence features and changes will be identified using data gathered in previous chapters. Correlations will be drawn between known radiation effects in artificially irradiated semiconductors, and the observed changes in the exposed samples.

The purpose of this research project was to provide the first-cut analysis of the samples in order to provide sufficient information to plan future analysis efforts. Consequently, analysis will focus more on looking for radiation-like effects, than in identifying every change with an irradiating particle or mechanism.

A description of the samples can be found in Table below. Sample 21 was not examined because during the removal process from the LDEF sample tray it's surface was damaged beyond usefulness.

5.1 Results

5.1.1 LEC, undoped, semi-insulating, GaAs (Cominco) An undoped GaAs crystal (referred to as Cominco) was chosen as the calibration sample for the apparatus because of its simple structure and ample documentation. The results of the initial spectra generated by the apparatus were compared to previously published spectra, and adjustments were made to the apparatus to correct deficiencies. In this manner, the apparatus was tested and fine-tuned during a two week period with

Table 4. LDEF sample descriptions

<i>Semiconductor Type</i>	<i>Sample</i>	<i>Description</i>
CdSe	12	R111A, high resistance, sulfur contaminated, C axis 111-surface
CdSe	13	M111A, low resistance, sulfur contaminated, C axis 111-surface
p-GaAs	14	6.42×10^{18} Zn/cm ³ , sample #9-16, $\mu=103$, $\rho=0.0106$
n-GaAs	15	1.42×10^{16} /cm ³ , sample #249
GaAs	16	compensated, epitaxial, defective density 10^5 , high resistance
n-GaAs	17	$2-4 \times 10^{18}$ Si/cm ³ , (100) +5 degrees, $\rho=0.001$, density less than 100/cm ²
GaAs	18	Si doped (100), #7189p, EPD = 5200/cm ² , $\rho=0.0013$ Ohm-cm, $\mu=1662$ cm ² /volt-sec, $N = 2.9 \times 10^{18}$ /cm ³
GaAs	19	Si doped (100), #7476p, EPD = 1500/cm ² , $\rho=0.0015$ Ohm-cm, $\mu=1995$ cm ² /volt-sec, $N = 2.1 \times 10^{18}$ /cm ³
GaAs	20	Si doped (100), #4018p, EPD = 4900/cm ² , $\rho=0.0028$ Ohm-cm, $\mu=2411$ cm ² /volt-sec, $N = 0.92 \times 10^{18}$ /cm ³
GaAs	21	Si doped (100), #6744p, EPD = 5300/cm ² , $\rho=0.0037$ Ohm-cm, $\mu=2534$ cm ² /volt-sec, $N = 0.66 \times 10^{18}$ /cm ³

the result of producing spectra with signal-to-noise and resolution very near that achieved with a 100 mW laser.

The Cominco sample produced three distinct peaks at various electron energies and fluxes. The weak peak at 1.514 eV is probably due to excitons bound to a neutral donor. Williams reports three distinct exciton lines in this region for GaAs:Si, and that the peaks are the result of exciton annihilations (76:342). The largest peak consists of two lines at 1.494 and 1.491 eV which can be attributed to C and Mg impurities respectively. They result from transitions of free electrons in the conduction band to holes bound to C or Mg acceptor (free-to-bound transition) (51:12.4). The spread-out weak peak at 1.458 - 1.454 eV is believed to be phonon replicas of the lines in the main peak (phonon energy of 36.4 mV).

The two lines comprising the main peak were sensitive to electron beam voltage and flux. At 1.5 keV and 5 μ A flux, the Mg free-to-bound transition peak (1.491 eV) is stronger than the C free-to-bound transition (1.494 eV) peak. Increasing the beam voltage to 2.0 keV results in an increase in C transition activity to equal Mg's. At 3.0 keV, the C transition dominates over the Mg (See Figure 25). If the beam voltage is held constant at 2.0 keV and the flux increased from 5 to 20 μ A, the C line can again be seen to dominate.

5.1.2 Sample #12; CdSe:S, high resistance The luminescence spectra of CdSe varies from sample to sample. For example, the impurity-related edge luminescence may or may not be seen, and the relative intensities of the luminescence bands associated with free and bound excitons are also sample dependent (11:865). This high-resistance, sulfur contaminated CdSe semiconductor spectrum shows near edge emissions and its phonon replica of five lines at 1.737, 1.714, 1.692, and 1.667 eV, located approximately 400 Å from the absorption line (approximately 1.84 eV) (54:20) (63:308). The 1.737 eV line was believed to be a donor-cadmium vacancy acceptor transition (42:412). The origin of the 1.714 eV peak is unidentified at this point.

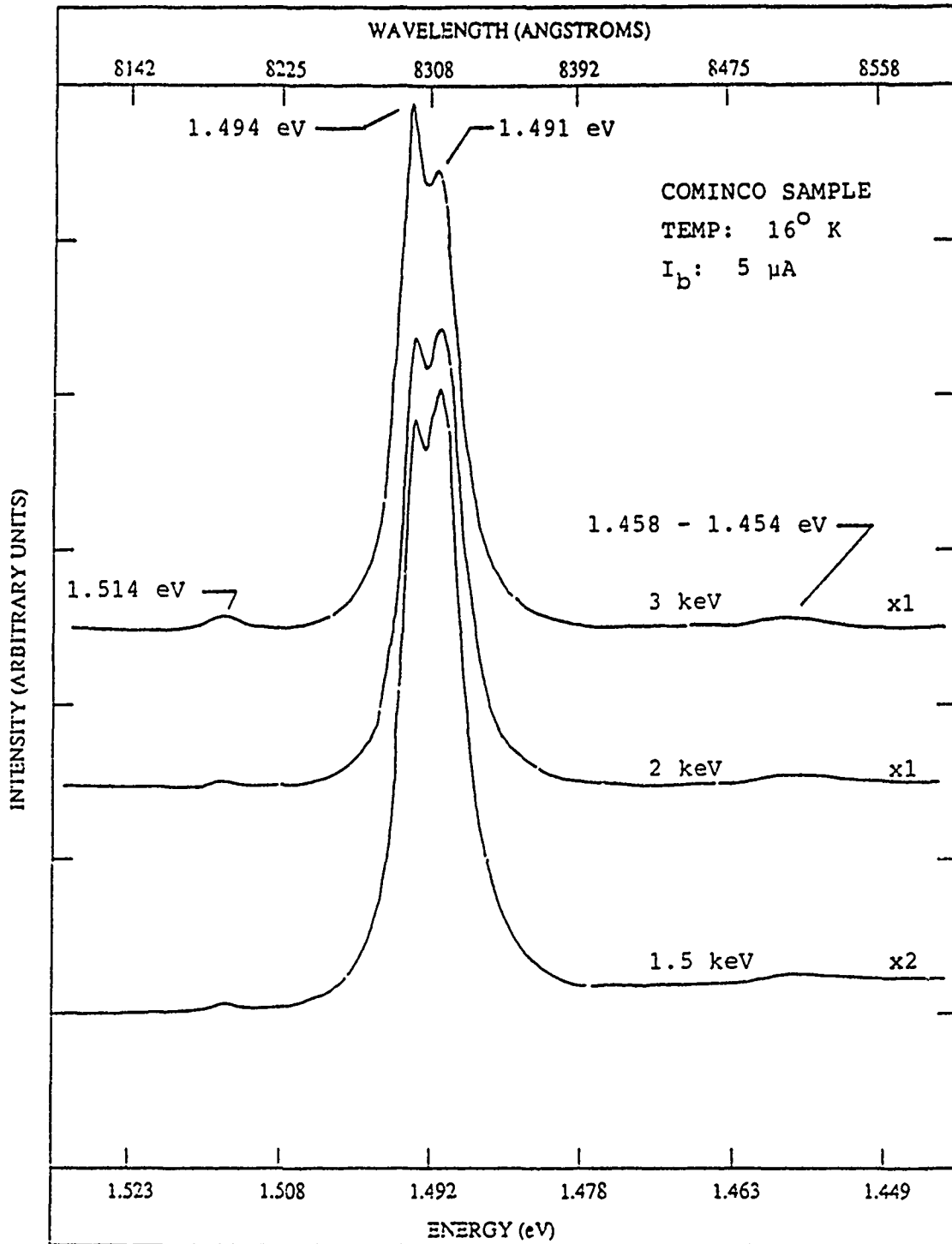


Figure 25. Cathodoluminescence spectra of sample Cominco; LEC, undoped, semi-insulating GaAs

The remaining peaks were separated by 0.026 eV; the exact energy for CdSe phonon replicas (7:334) (58:42).

It has been found from the control sample that the relative luminescent intensity of the 1.714 eV line increased much faster than that of the 1.737 eV line as beam energies and fluxes increased. The sample did not show peak shifts, but the luminescent intensities of the spectra increased with decreasing beam energy or flux. Additionally, decreases in flux with constant beam energy resulted in peak shifts toward longer wavelengths.

The exposed sample displayed the same structure as the control sample, except the 1.737 eV transition was the dominant peak regardless of beam energy or flux. Peak locations were: 1.739, 1.715, 1.693, and 1.665 eV. Similar to the control sample, it also revealed an increase in luminescence with a decrease in beam energy or flux, and the peak shifts toward longer wavelengths with a reduction in beam flux.

The exposed sample had about five times more intense luminescence than the control, which was the result of radiative centers formed after radiation bombardment. At lower beam voltages, the peaks of the exposed sample located at approximately 1.73 eV, when compared to the same peaks on the control sample, shifted towards shorter wavelengths (See Figure 26).

5.1.3 Sample #13; CdSe:S, low resistance The observed emission for the low-resistance, sulfur contaminated CdSe control sample can be separated into three parts: (a) four lines, 1.822, 1.818, 1.808, and 1.792 eV, closely spaced, occur near the band edge. Of these, the 1.818 line is the most intense. The 1.822 eV line is believed to be the result of free excitons, the 1.818 eV line was attributed to excitons bound to neutral donors, and the 1.808 eV line is believed due to excitons bound to neutral acceptors (15:1946). The 1.792 eV line was the result of a phonon replica of the 1.818 eV line. (b) Several very small peaks on the high-energy side of the strong 1.729 eV line were observed, although they are not clearly shown in the figure. However,

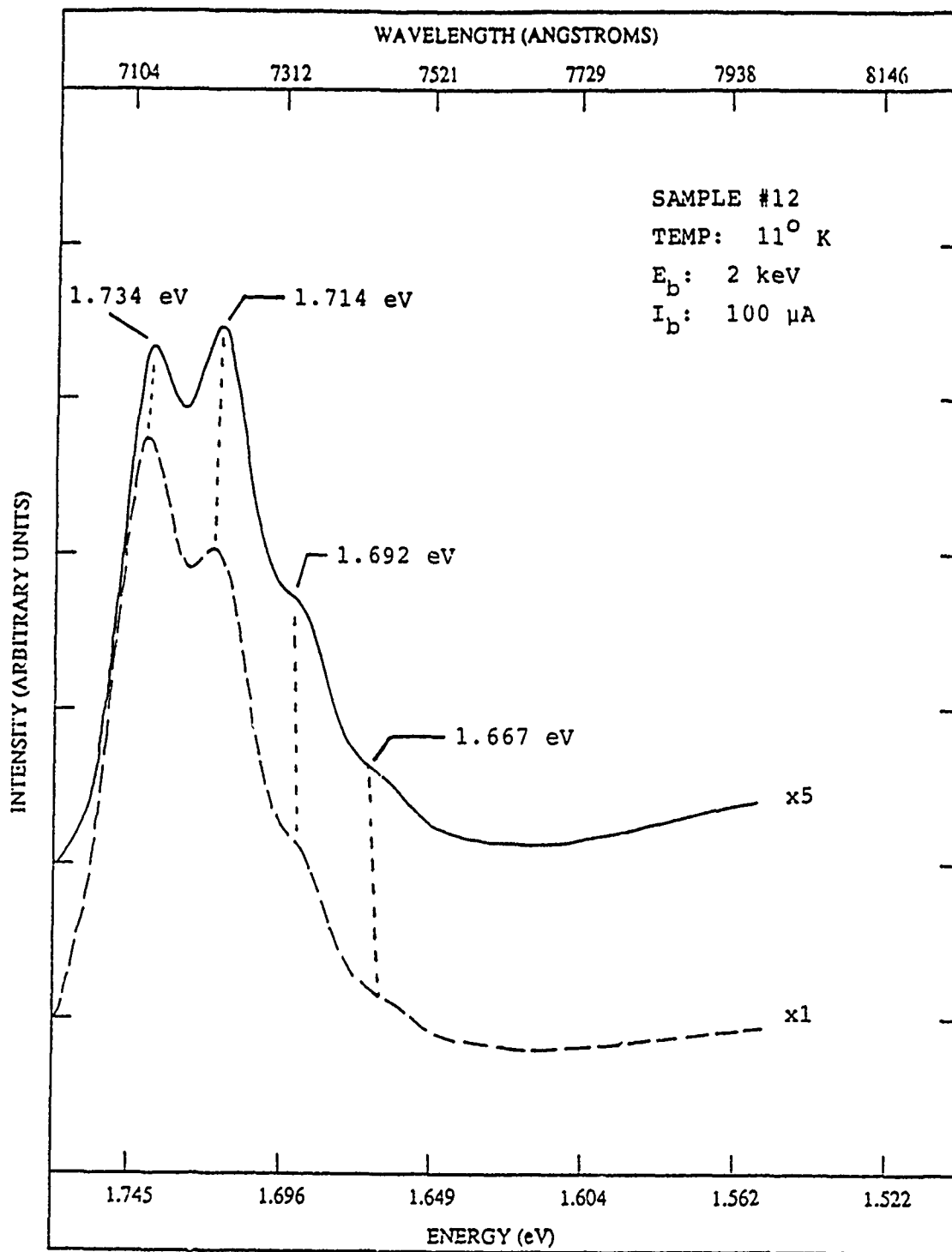


Figure 26. Cathodoluminescence spectra of sample #12; high-resistance, sulfur contaminated CdSe. Dashed line represents exposed (irradiated) sample; solid line represents control (unirradiated) sample

photoluminescence clearly revealed four weak lines from our sample, although as many as six similar lines had been reported in the region before (58:41). These lines are of unknown origin. (c) A peak at 1.729 eV and its phonon series of five lines were observed in the lower energy region. The first line appeared at 1.729 eV, and is attributed to a donor-cadmium vacancy acceptor pair transition. The remaining peaks were evenly spread and decreased in intensity towards longer wavelengths. They appeared at 1.703, 1.677, 1.652, 1.626, and 1.600 eV. Their spacing equalled 0.026 eV, which corresponds in energy to the optical phonon absorbed by the lattice (7:344) (58:42).

The control sample did not show significant variation in peak location due to changes in electron beam energy contrary to the control sample #12, but did show a slight peak shift toward longer wavelengths with a decrease in electron flux. The intensity of the luminescence was found to decrease with a corresponding decrease in electron beam energy.

The exposed samples had the same peak structure as the control samples, with the exception that the 1.822 eV line did not appear, and the surface emission line at 1.818 eV became very intense. The exposed sample did not change intensity due to electron beam energy or flux changes contrary to the sample #12. It did, however, experience a small shift towards longer wavelengths for decreasing electron fluxes.

In comparison to the control sample, the third group of peaks shifted to longer wavelengths for the exposed sample for all beam energies and fluxes (See Figure 27). Another change is that for low electron fluxes of 2.5×10^{14} electrons/cm² the exposed samples showed a stronger luminescence intensity than that of the control sample, whereas, at higher fluxes of 5×10^{15} electrons/cm², both samples displayed the same luminescent intensity. This may be the result of radiation induced defect centers near the surface dominating low flux excitation. At higher fluxes, the defect centers compete with pre-existing luminescent centers. In contrast, photoluminescence showed that the control sample gave stronger luminescence signal than that

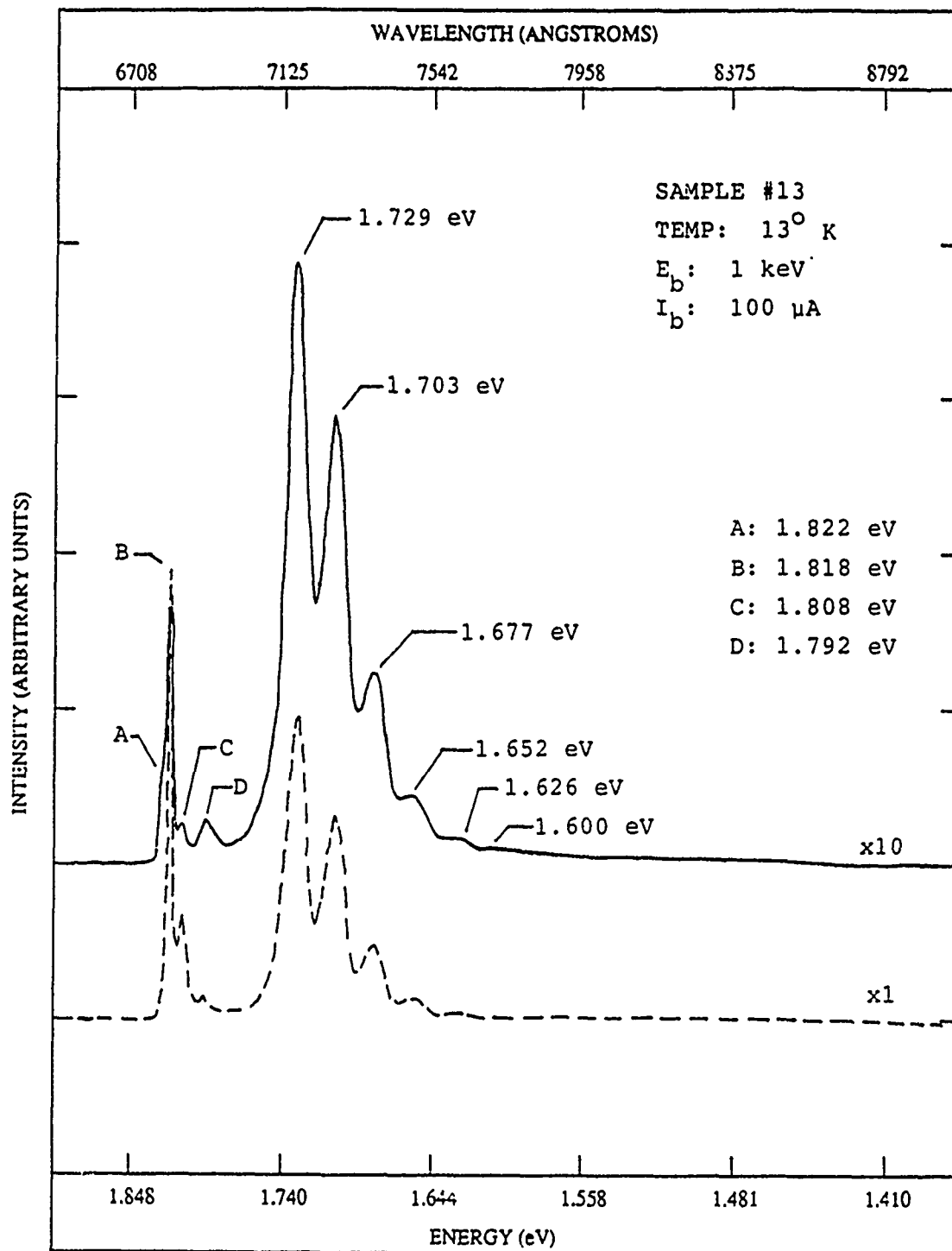


Figure 27. Cathodoluminescence spectra of sample #13; low-resistance, sulfur contaminated CdSe. Dashed line represents exposed (irradiated) sample; solid line represents control (unirradiated) sample

of the exposed. With photoluminescence, the photons are generated deeper within the material, perhaps beyond the range of dominating radiation defect centers.

Another change is the exposed sample displayed an increase in exciton edge emission luminescent intensity and a decrease in the 1.729 line series luminescent intensity when compared to the control sample. This type of change has been seen in CdS, a similar II-VI semiconducting material, and was the result of electron bombardment (13:1266).

5.1.4 Sample #14; p-GaAs:Zn, 6.42×10^{18} Zn/cm³ This heavily Zn-doped p-GaAs did not show any change in peak locations nor luminescence intensity between control and exposed samples. Both samples exhibited a broad peak at 1.476 eV with a shoulder at around 1.494 eV. They also displayed a long tail that probably led to a broad emission located at 1.39 eV (not shown in the figure) (5:679). Figure 28 shows typical spectra for this sample.

The weak peak located on the shoulder (1.494 eV) is believed to be the result of conduction band electron to C acceptor transitions. The broad peak (1.476 eV) may be due to a combined effect of free-to-bound and/or donor-acceptor pair transitions of various acceptors such as Zn, Si, and Ge.

5.1.5 Sample #15; n-GaAs, 1.42×10^{16} /cm³ The unintentionally-doped n-type GaAs did show a slight luminescence change between control and exposed samples. Three distinct peaks were found in both samples: 1.520 eV, probably consists of band-to-band recombination by means of excitons (10:572); 1.491-1.494 eV, dominant peak believed to result from free-to-bound and/or donor-acceptor pair transitions of carbon acceptor and also possibly Mg acceptor; 1.457 eV, weak peak generated by phonon emission of the 1.494 eV line. The peak positions remained about the same before and after irradiation.

The S-1 detector broke between examining the control and exposed sample and

a replacement was not available. Therefore, the exposed sample was not examined in full region that the control was, nor was it kept to the same scale in order to take advantage of the resolution offered by the C31034 detector's reduced scanning region. Thus, unfortunately, the relative intensity of luminescence obtained from both control and exposed samples can not be made. Although the spectra could not be overlaid, the peak positions were compared during analysis. It is worth noting that both samples displayed small peak shifts with varying electron voltages and constant current. There were no shifts with constant voltage and varying currents (See Figure 29 and Figure 30).

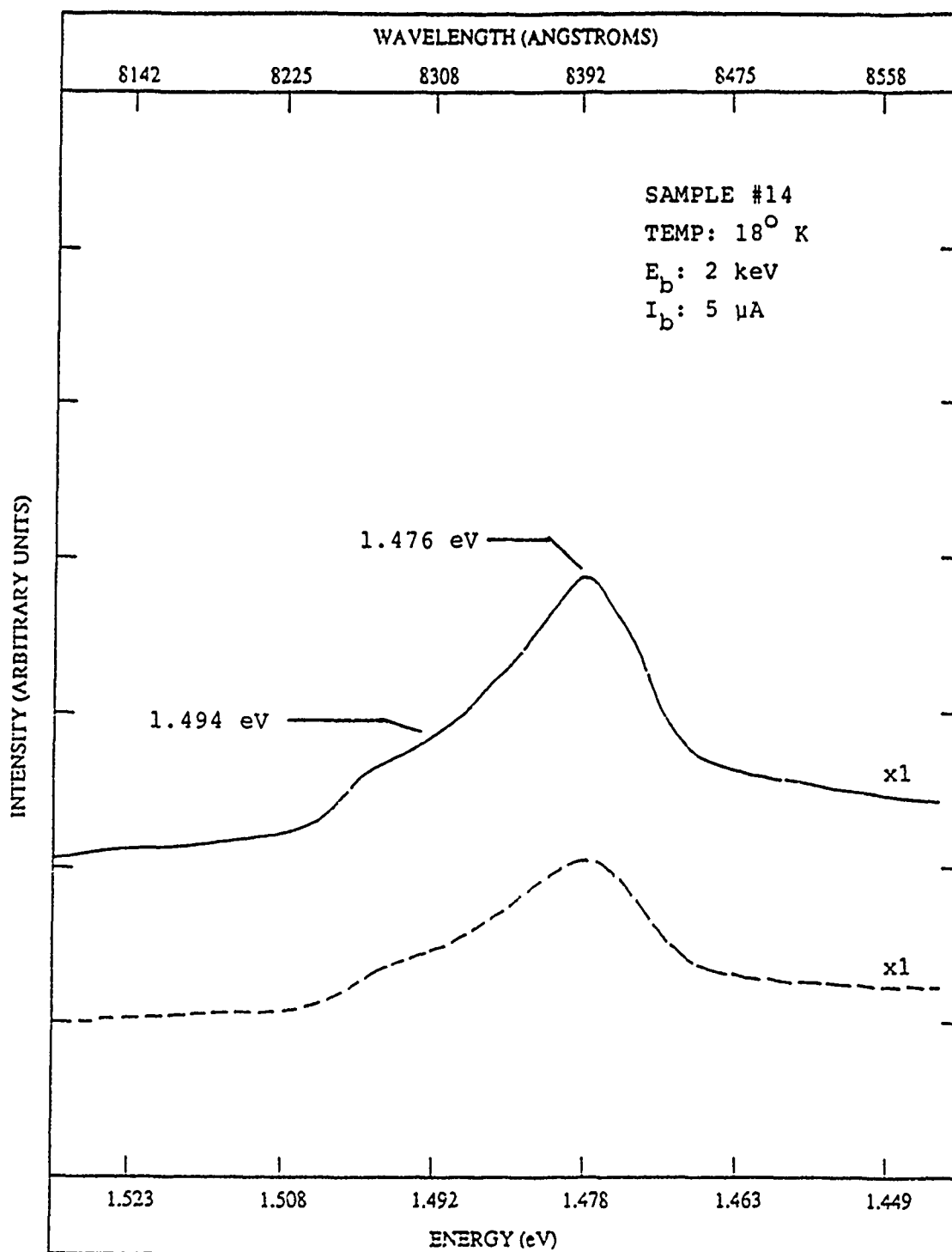


Figure 28. Cathodoluminescence spectra of sample #14; Zn-doped (*p*-type) GaAs (6.42×10^{18} Zn/cm³). Dashed line represents exposed (irradiated) sample; solid line represents control sample (unirradiated)

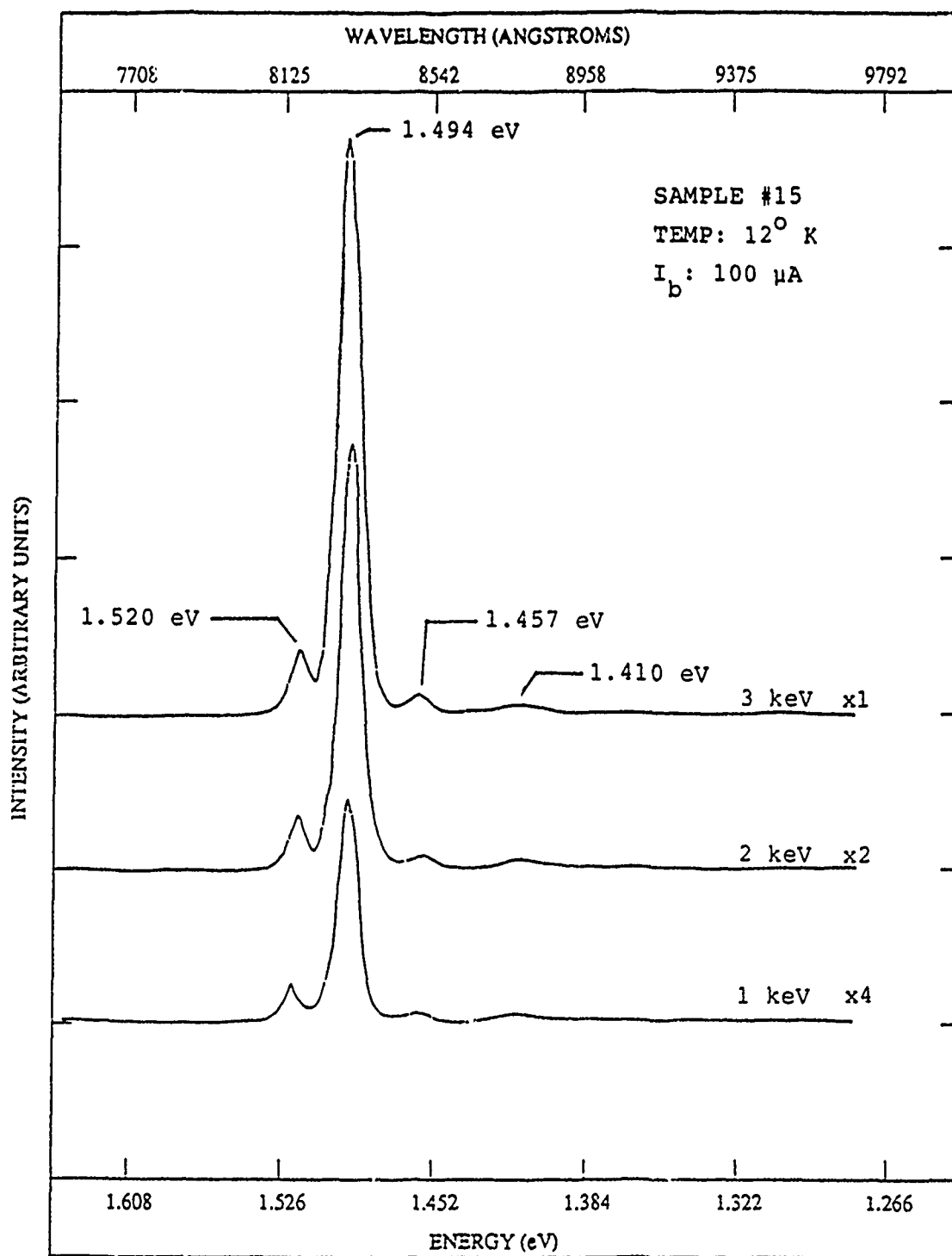


Figure 29. Cathodoluminescence spectra of sample #15; undoped (n -type) GaAs ($1.42 \times 10^{16}/\text{cm}^3$) control (unirradiated) sample at $100 \mu\text{A}$ and varying beam energy

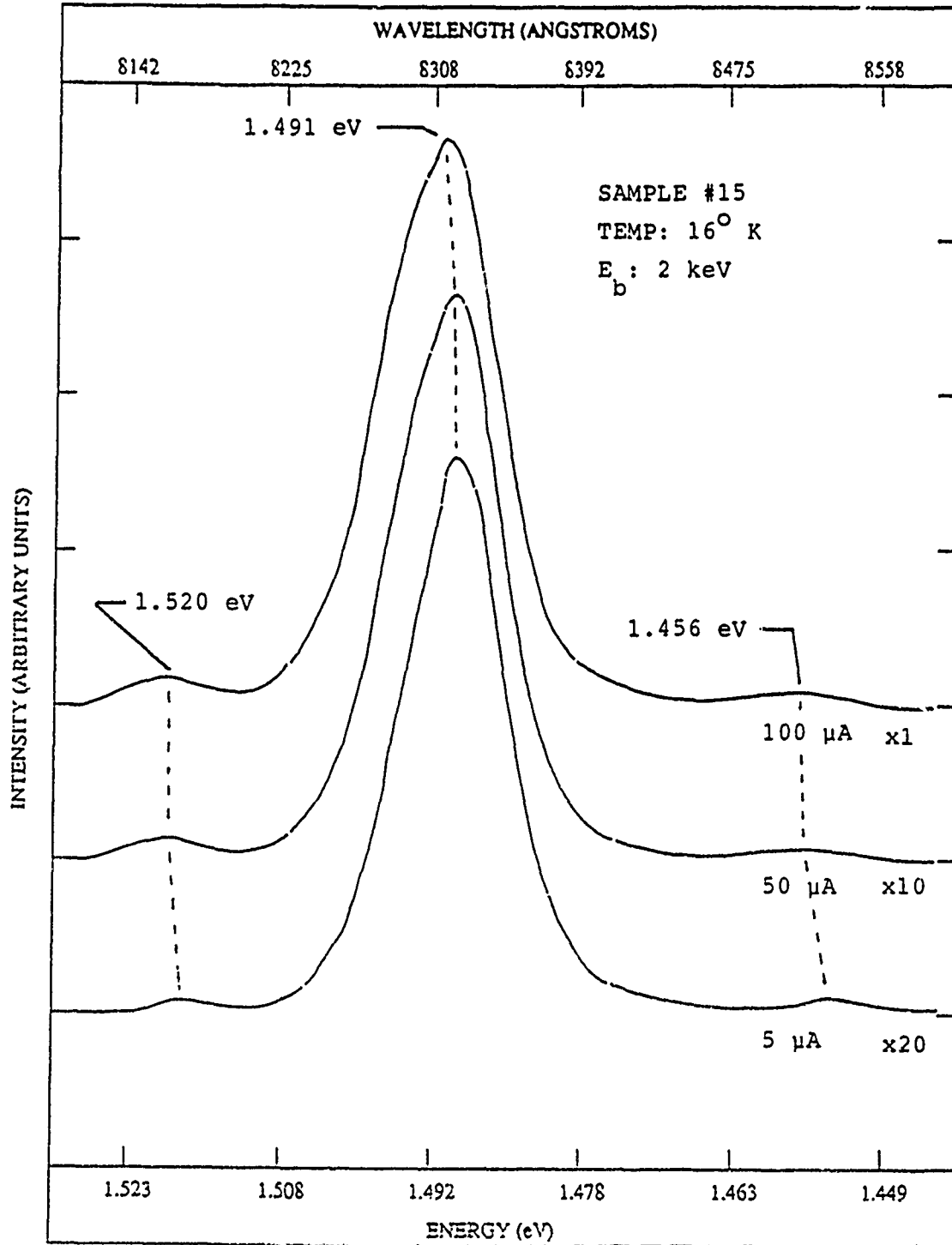


Figure 30. Cathodoluminescence spectra of sample #15; undoped (*n*-type) GaAs ($1.42 \times 10^{16}/\text{cm}^3$) exposed (irradiated) sample at 2 keV and varying beam current

5.1.6 *Sample #16; compensated GaAs, epitaxial, high resistance* All spectra taken on both samples of the compensated, epitaxial GaAs were void of any features and consisted of only flat noise lines. Consequently, these samples could not be analyzed for changes due to radiation.

5.1.7 *Sample #17; n-GaAs:Si, $2-4 \times 10^{18}$ Si/cm³* This heavily Si-doped, *n*-type, GaAs did show changes to the spectra after exposure to space radiation, mainly in the formation of radiationless recombination centers. Both the samples both showed a simple spectra for 100 μ A current, and similar results were obtained from photoluminescence measurement. However, at 5 μ A current, the spectra became complex as numerous additional peaks were introduced.

The 100 μ A control sample displayed the following peaks as shown in Figure 31: 1.476 eV, conduction band electrons to Ge acceptor transition and donor to Si acceptor transitions; 1.182 eV, (1.22 eV) complex of a donor associated with a Ga vacancy found in heavily doped *n*-type GaAs (51:12.5) (37:114-117); 0.760 eV, believed to be due to an arsenic antisite As(Ga) associated with EL2 (12:13.2). The 5 μ A control sample displayed numerous additional peaks in the region 1.0 eV to 0.745 eV believed to be electrons and hole trap deep levels generated by defects, including 0.828 eV, related to the Cr acceptor (57:13.7);

The 100 μ A exposed sample displayed a broad peak at 1.166 eV, believed to be the shifted 1.179 eV peak. At 5 μ A the following additional peaks were observed: 1.429, 0.938, 0.84 and 0.774 eV. The origins of these luminescence peaks were given above. See Figure 32.

The most significant change that occurred due to space radiation exposure was the quenching of the 1.479 eV and 0.77 eV lines (See Figure 33). The 1.479 eV line reappears only in the low beam voltage and current spectra as a very faint peak (See Figure 34. One explanation for their disappearance could be that the donors and acceptors formed complexes with the generated non-radiative centers.

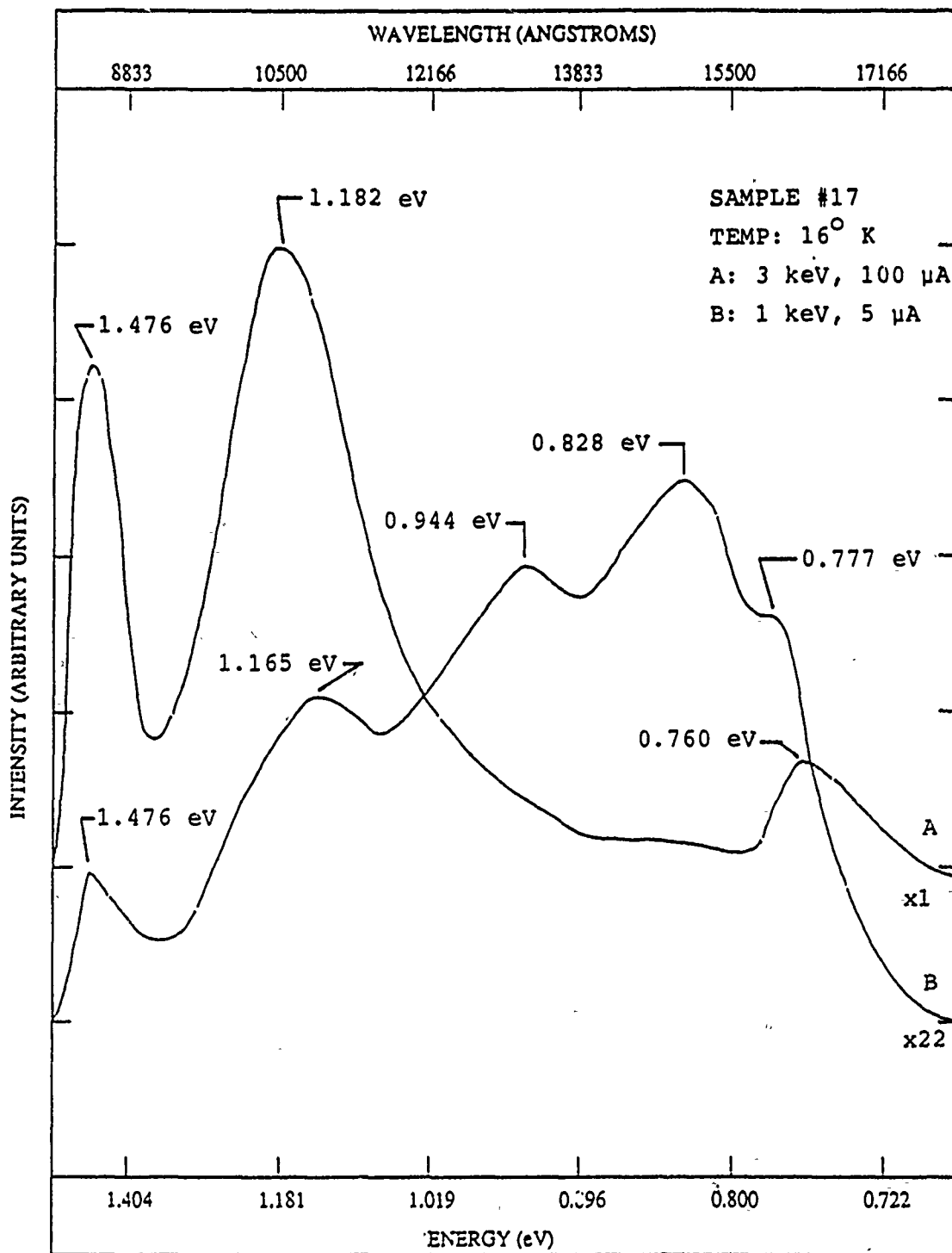


Figure 31. Cathodoluminescence spectra of sample #17; Si-doped (*n*-type) GaAs ($2-4 \times 10^{18}/\text{cm}^3$) control (unirradiated) sample at 3 keV - 100 μA , and 1 keV - 5 μA

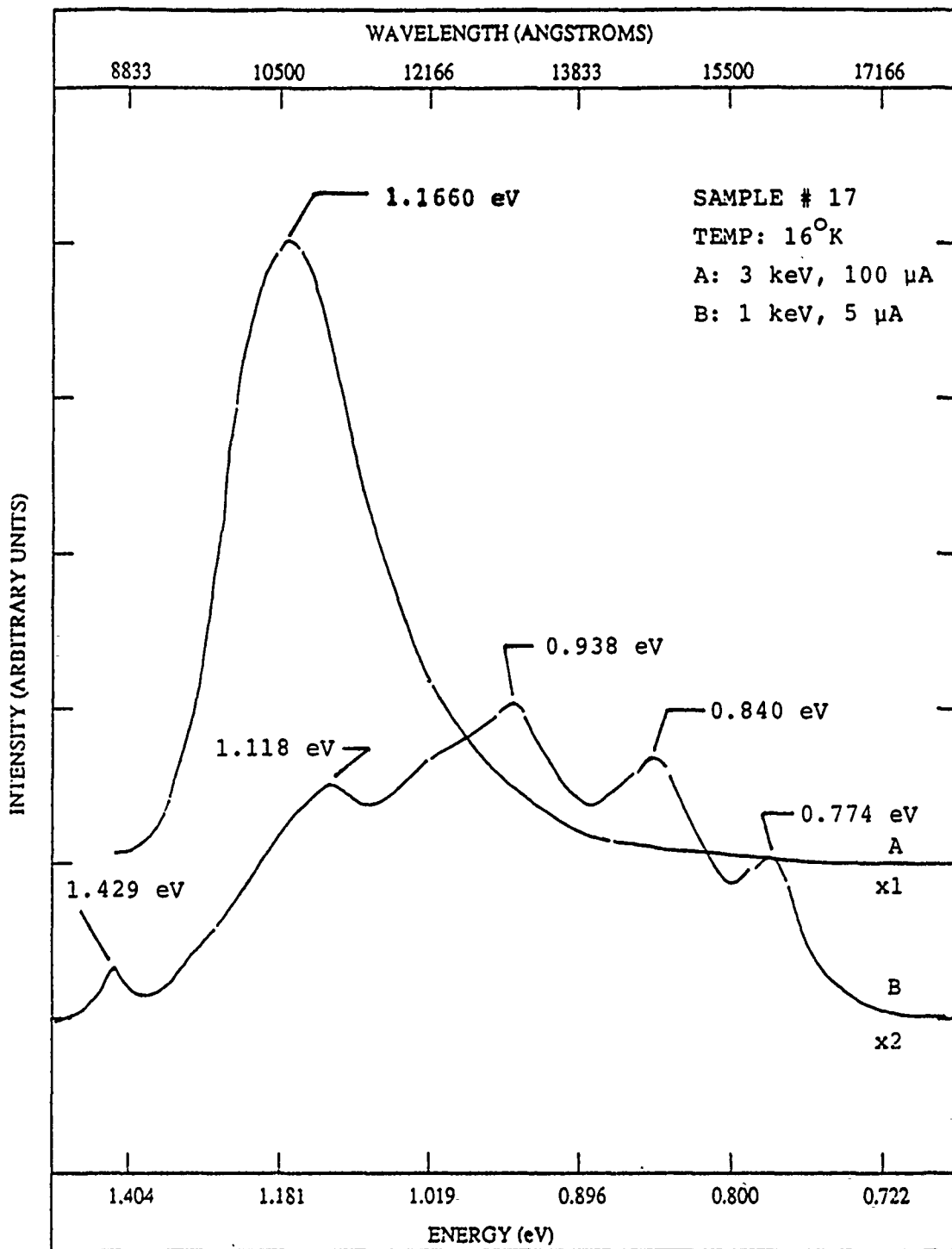


Figure 32. Cathodoluminescence spectra of sample #17; Si-doped (*n*-type) GaAs ($2-4 \times 10^{18}/\text{cm}^3$) exposed (irradiated) sample at 3 keV - 100 μA , and 1 keV - 5 μA

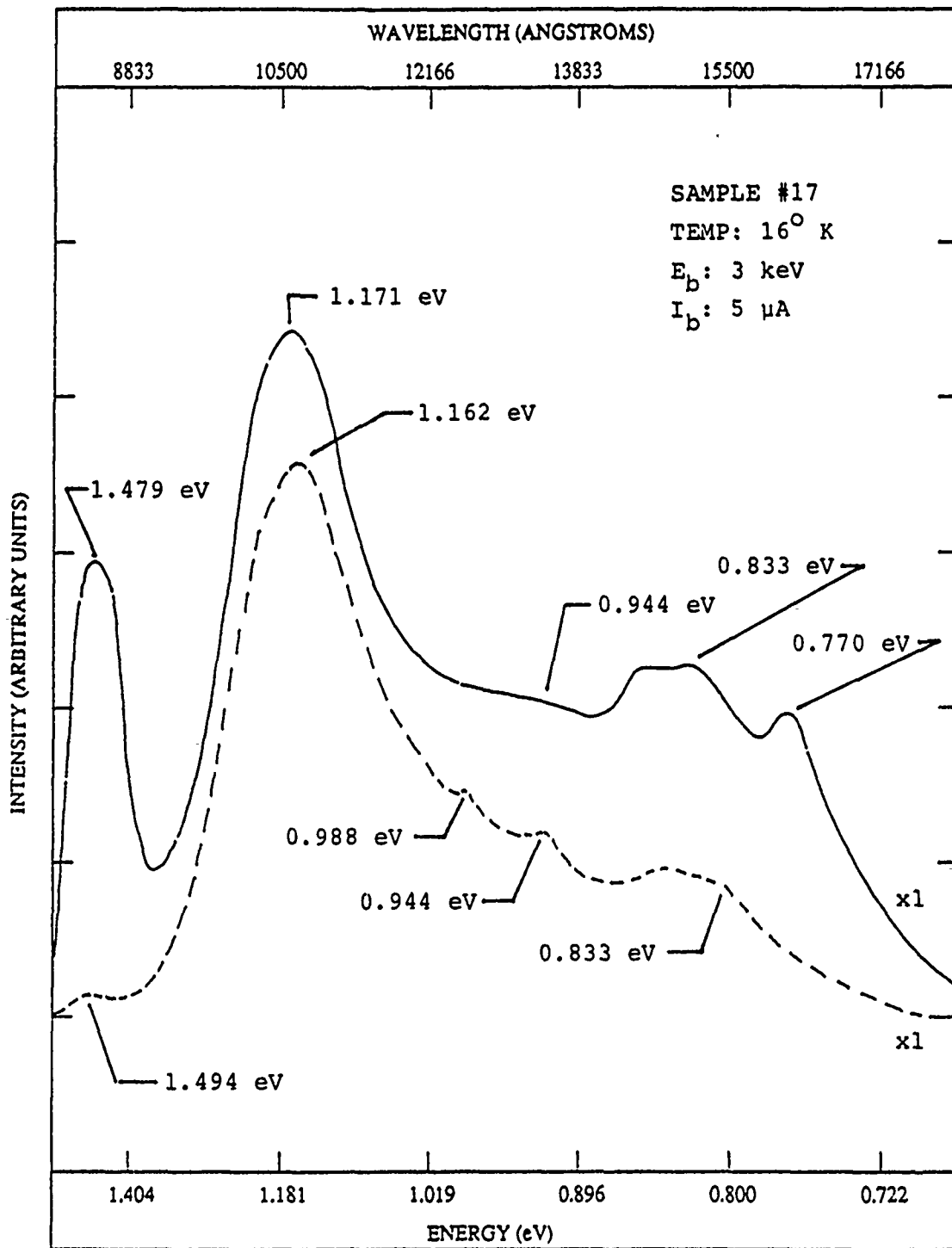


Figure 33. Cathodoluminescence spectra of sample #17; Si-doped (*n*-type) GaAs ($2-4 \times 10^{18}/\text{cm}^3$) control and exposed samples at 3 keV beam energy. Dashed line represents exposed (irradiated) sample; solid line represents control (unirradiated) sample

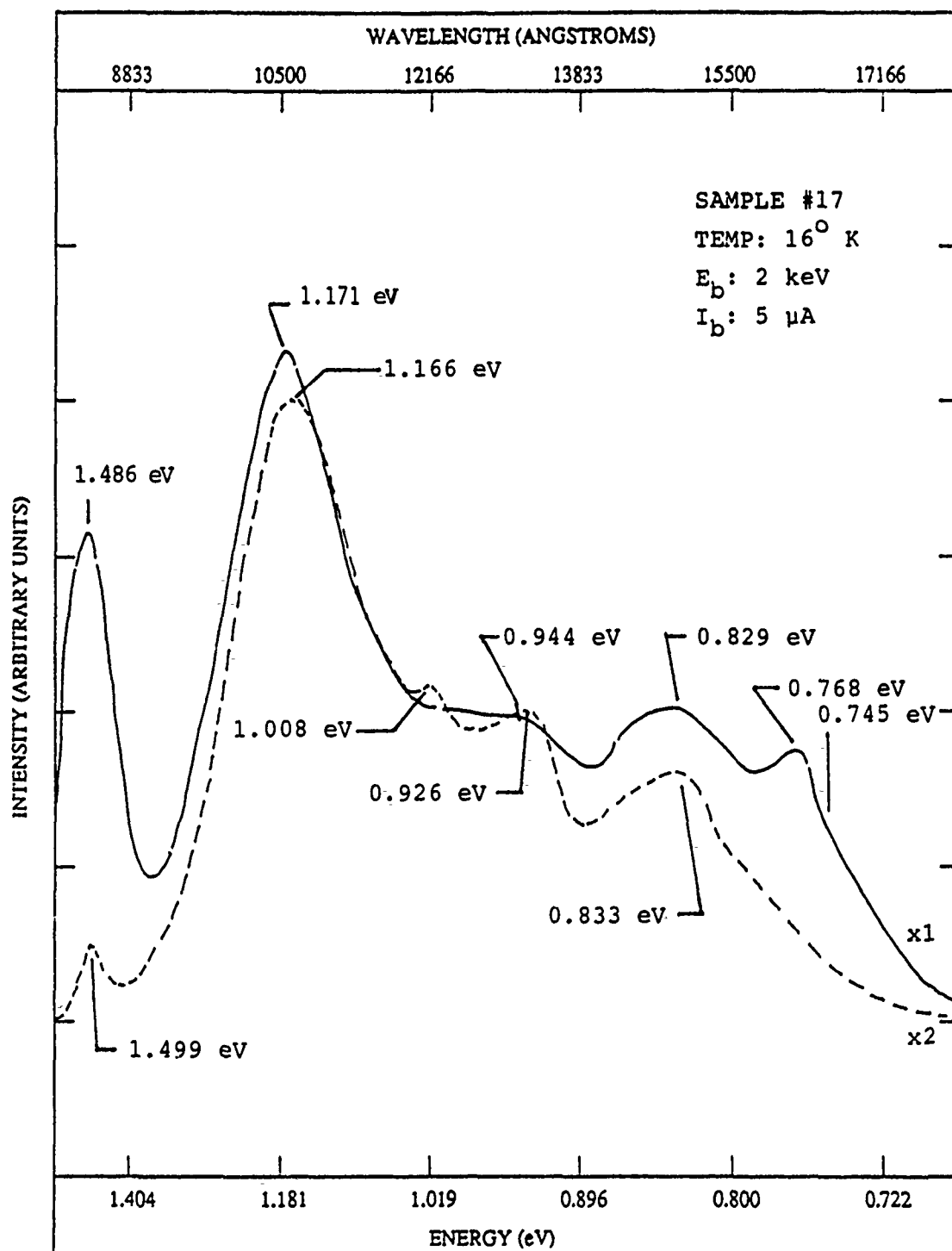


Figure 34. Cathodoluminescence spectra of sample #17; Si-doped (*n*-type) GaAs ($2-4 \times 10^{18}/\text{cm}^3$) control and exposed samples at 2 keV beam energy. Dashed line represents exposed (irradiated) sample; solid line represents control (unirradiated) sample

5.1.8 *Sample #18; GaAs:Si, $N = 2.9 \times 10^{18}/\text{cm}^3$* Both samples heavily doped with Si displayed a single broad peak; the control sample peak at 1.504 eV was believed to be the result of mainly exciton, silicon free-to-bound, and carbon free-to-bound transitions, and the exposed sample 1.489 eV peak was believed to be the result of mainly silicon and carbon, free-to-bound and donor-acceptor pair transitions.

The control sample peak is thought to result from 1.494 and 1.51 eV lines, which form a symmetric curve at 3.0 keV and 100 μA . But it has been found that at 2.0 keV, the 1.494 eV line dominates over a 1.51 eV line, and at 1.0 keV the opposite occurs. This domination results in a lop-sided curve. The exposed sample does not exhibit the same behavior. It displays the same uniform curve at about the same peak location.

The exposed (irradiated) sample does show a general peak shift towards longer wavelengths (See Figure 35), and decreases dramatically in luminescence intensity.

5.1.9 *Sample #19; GaAs:Si, $N = 2.1 \times 10^{18}/\text{cm}^3$* This heavily Si-doped *n*-type GaAs sample resembles #17 in spectral structure, although the 1.479 eV peak does not disappear after irradiation in this sample. The significant change was the decrease in overall luminescence intensity of the exposed sample.

Major peaks found in the 100 μA control sample are: 1.473 eV, probably belongs to donor-to-acceptor pair transition of a Si occupied in As site; 1.148 eV, a complex of a donor associated with a Ga vacancy; 0.904 eV, related to Cr acceptor. See Figure 36.

Peaks found in the exposed sample are: 1.479 eV, DAP Si(As); 1.146 eV, a complex of a donor associated with a Ga vacancy; 0.902 eV, related to Cr acceptor; 0.745 eV, believed to be related to an arsenic antisite defect.

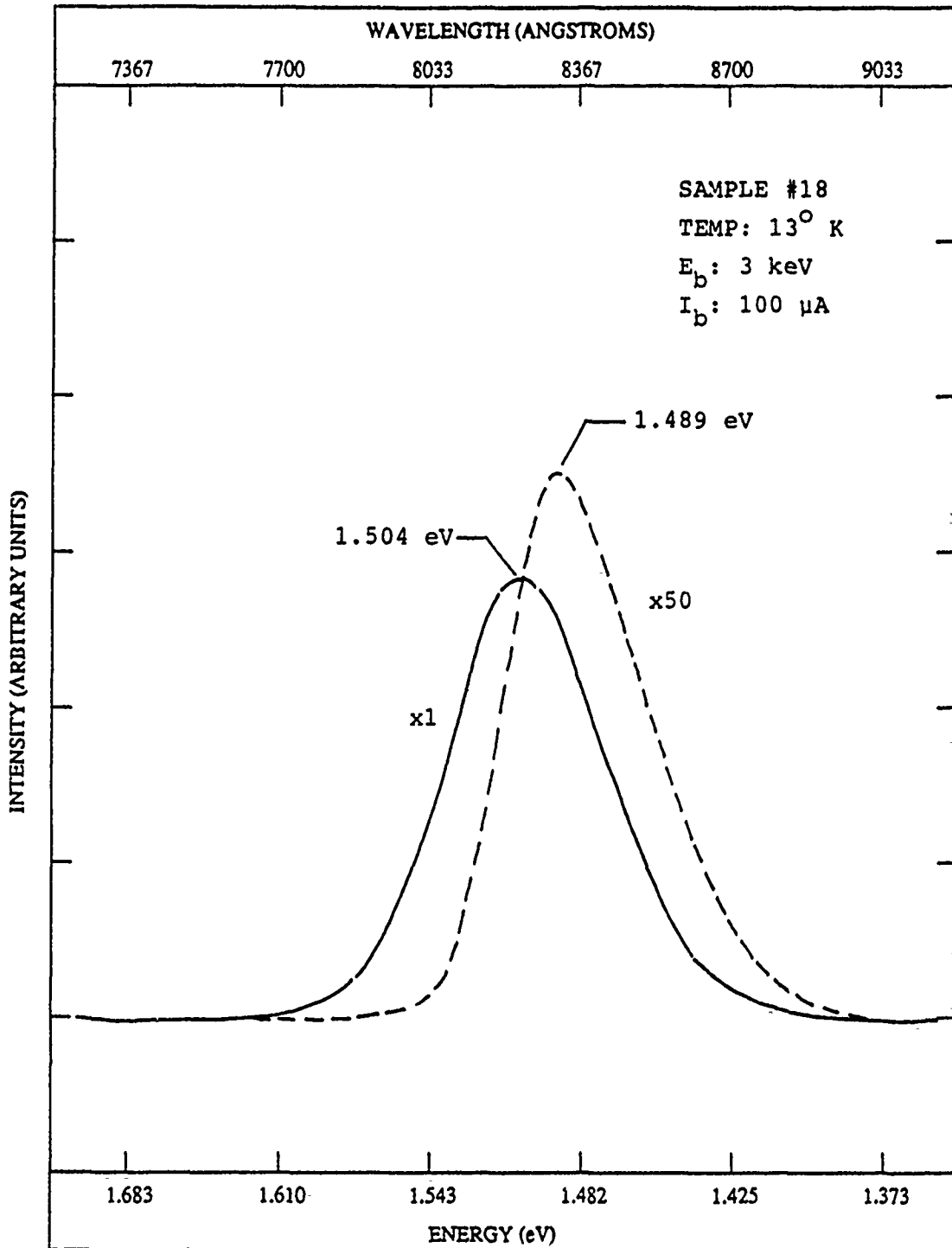


Figure 35. Cathodoluminescence spectra of sample #18; Si-doped GaAs ($2.9 \times 10^{18}/\text{cm}^3$) control and exposed samples. Dashed line represents exposed (irradiated) sample; solid line represents control (unirradiated) sample

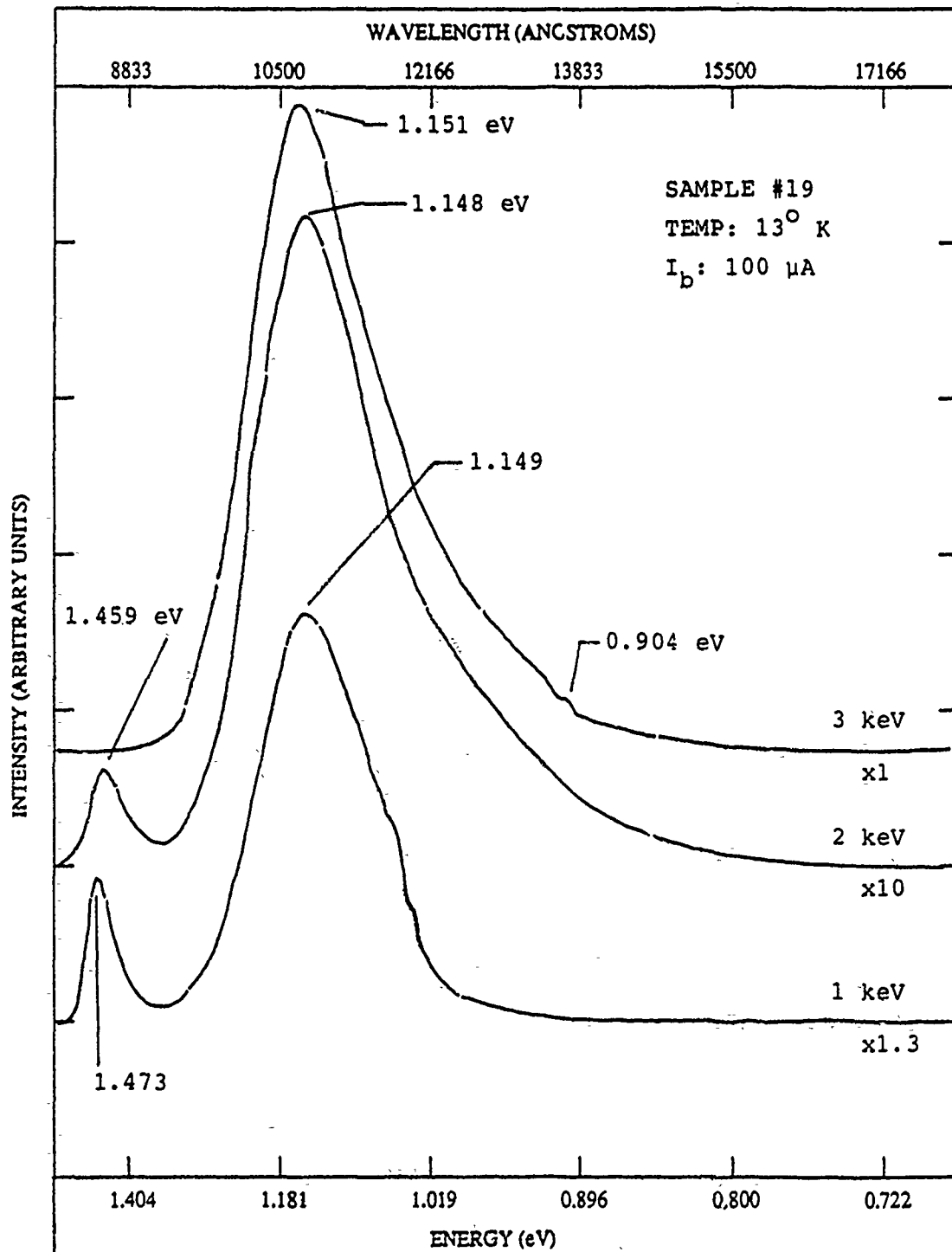


Figure 36. Cathodoluminescence spectra of sample #19; Si-doped GaAs ($2.1 \times 10^{18}/\text{cm}^3$) control sample at 100 μA and varying beam energy

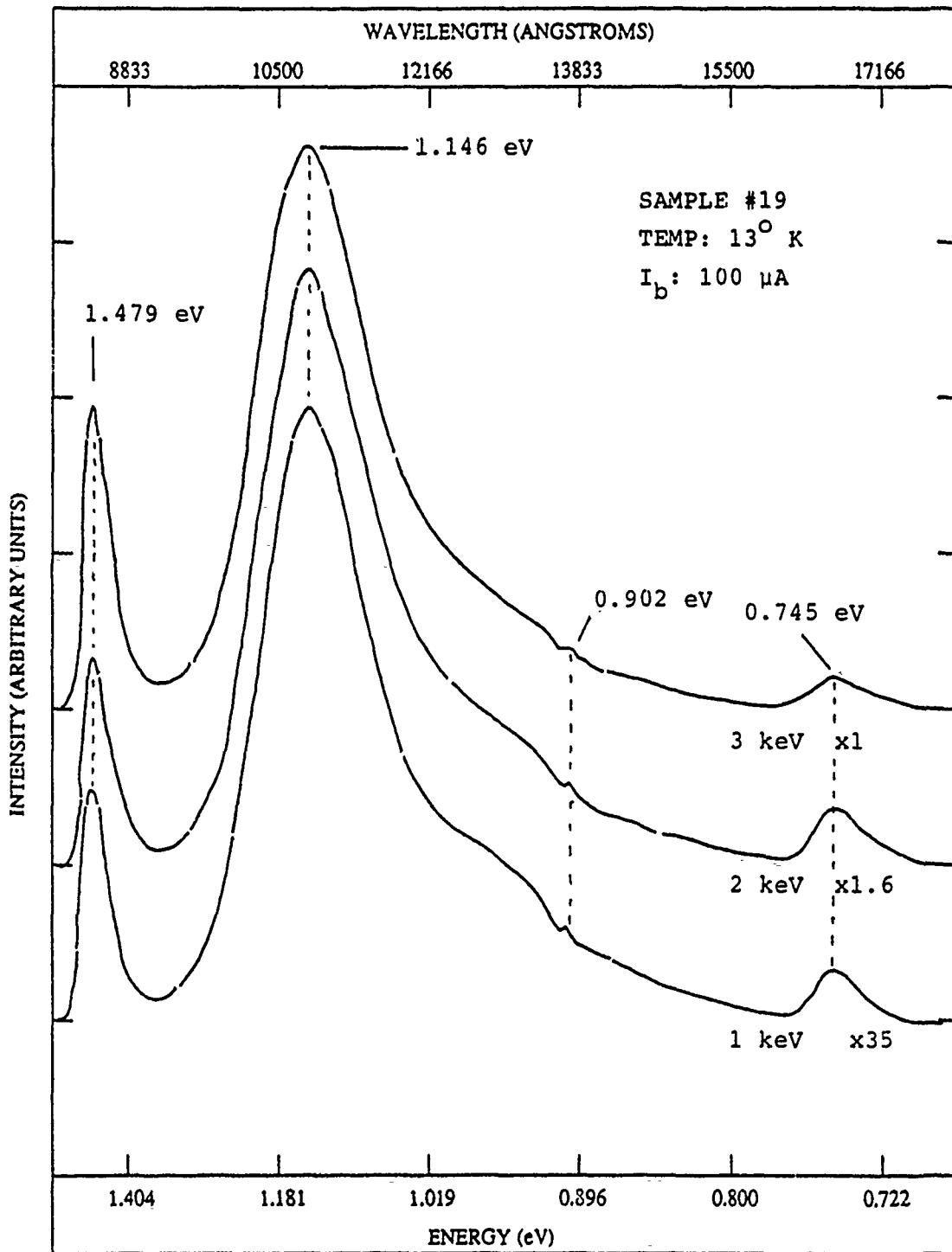


Figure 37. Cathodoluminescence spectra of sample #19; Si-doped GaAs ($2.1 \times 10^{18}/\text{cm}^3$) exposed sample at 100 μ A and varying beam energy

The 5 μ A control and exposed samples displayed several additional peaks in the region 1.0 eV to 0.745 eV, similar to the results shown for Sample #17. Figure 38. shows how those peaks are readily apparent in the 1 keV - 100 μ A exposed sample, but absent in the control sample.

5.1.10 Sample #20; GaAs:Si, $N = 0.92 \times 10^{18}/\text{cm}^3$ The only feature is the combined result of free-to-bound transitions involving a Si acceptor and carbon donor-acceptor pair transition, which is located at 1.490 eV for the control sample, and the luminescence peak has shifted to 1.476 eV for the exposed sample, which may be associated with Si donor-acceptor pair transitions. The exposed samples showed a shift towards longer wavelengths with increasing beam flux as shown in Figure 40, whereas, Figure 39 shows the constant peak location for the control sample with changing beam flux. Figure 41 shows a typical peak relationship between control and exposed samples. Notice the shift in peak location, which increases with increasing electron current.

5.1.11 Sample #21; GaAs:Si, $N = 0.66 \times 10^{18}/\text{cm}^3$ The exposed sample was damaged too extensively during removal from it's tray that luminescence measurements could not be taken from it.

5.2 Discussion

As a group, the exposed samples display many radiation effects described in the literature review. Seven of the nine exposed samples demonstrate changes in their spectra, which can be attributed to their space radiation exposure. Some of the similar samples share similar radiation effects.

A review of the literature gathered on irradiation of GaAs and CdSe yielded only limited success in finding correlations between observed changes and a particular type of irradiating particle. This is obviously a very complicated matter to pursue. Part of the problem is that different particles may produce the same type of radiation

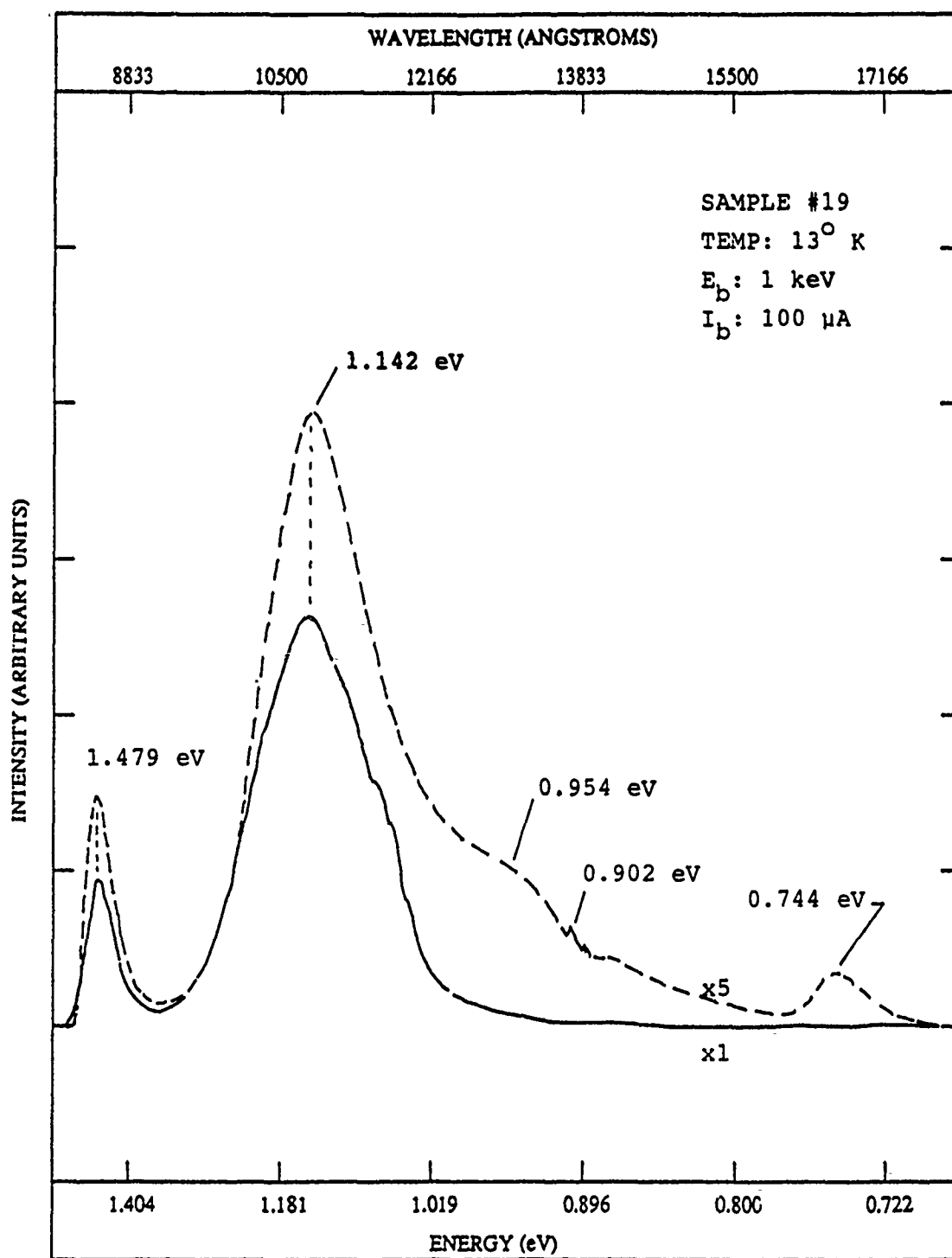


Figure 38. Cathodoluminescence spectra of sample #19; Si-doped GaAs ($2.1 \times 10^{18}/\text{cm}^3$) control and exposed samples at 1 keV and 100 μA . Dashed line represents exposed (irradiated) sample; solid line represents control (unirradiated) sample

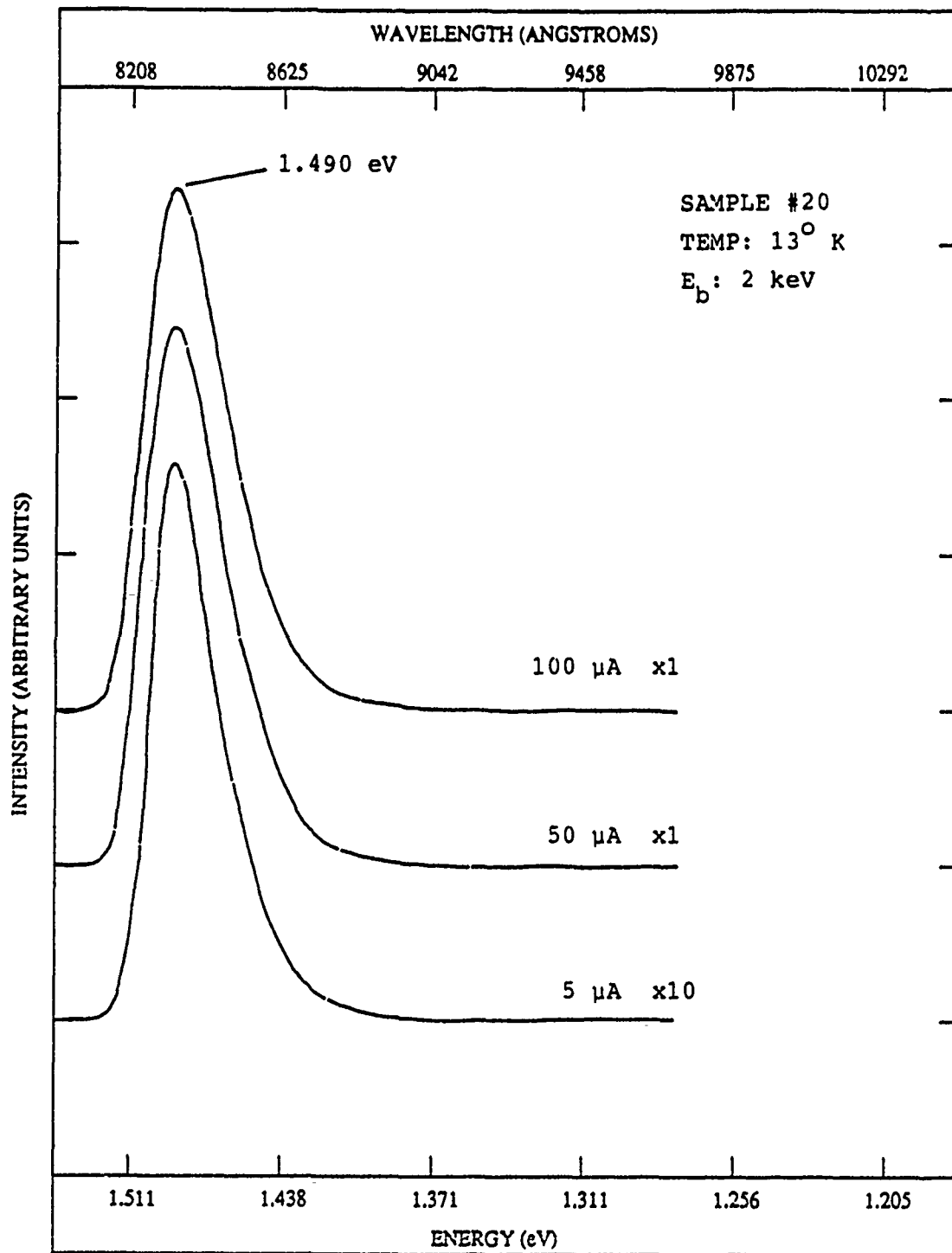


Figure 39. Cathodoluminescence spectra of sample #20; Si-doped GaAs ($0.92 \times 10^{18}/\text{cm}^3$) control sample at 2 keV and varying beam current

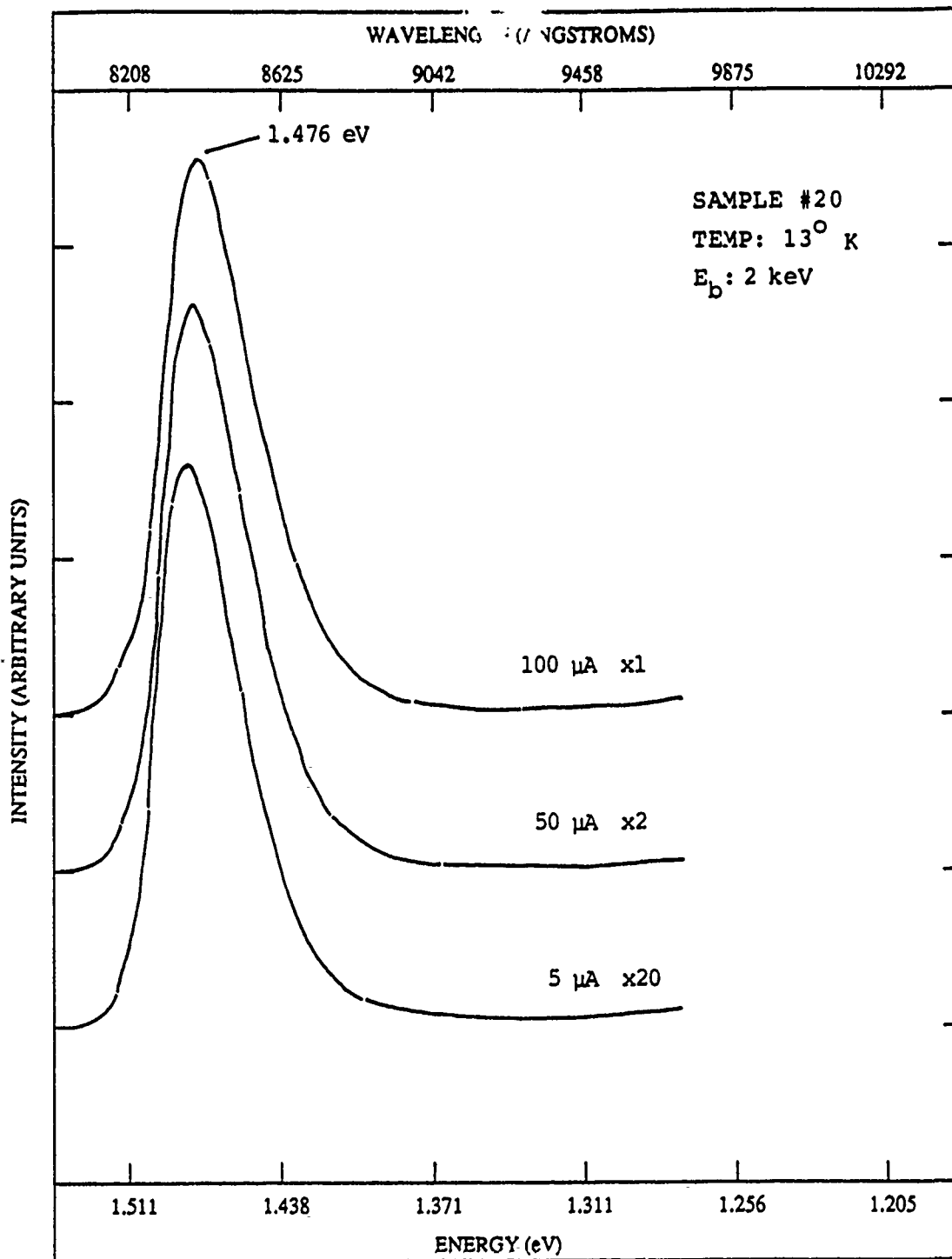


Figure 40. Cathodoluminescence spectra of sample #20; Si-doped GaAs ($0.92 \times 10^{18}/\text{cm}^3$) exposed sample at 2 keV and varying beam current

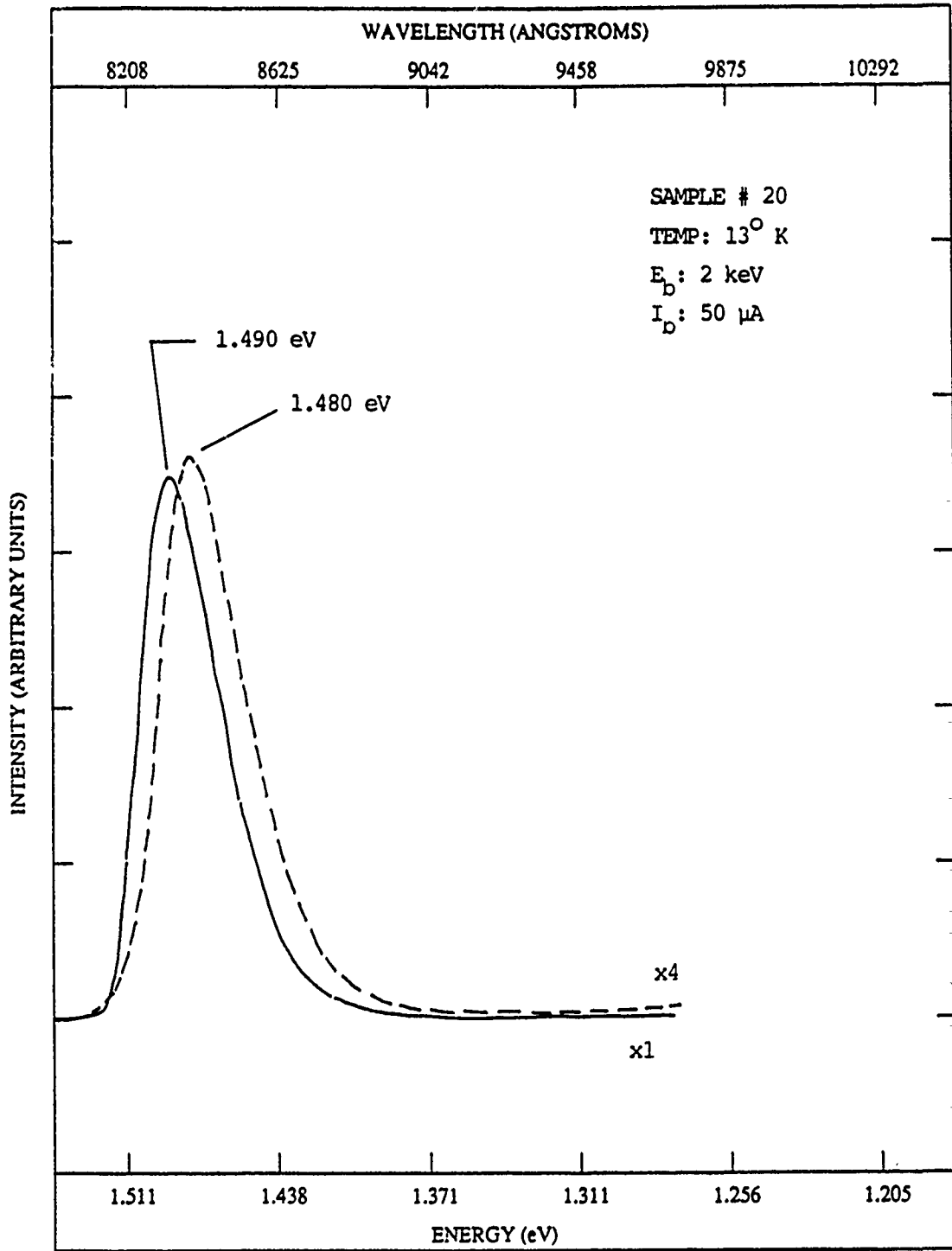


Figure 41. Cathodoluminescence spectra of sample #20; Si-doped GaAs ($0.92 \times 10^{18}/\text{cm}^3$) control and exposed samples at 2 keV and 50 μ A. Dashed line represents exposed (irradiated) sample; solid line represents control (unirradiated) sample

effect. For example, analysis would become trivial if protons produced only higher energy peak shifts, and neutrons produces only lower energy peak shifts.

Examining samples #17 and #19 reveals a very similar spectrum, but with the exception of the loss of a peak through quenching, although they both have similar Si impurity concentrations. This kind of a subtle difference is hard to understand.

Additional information about the nature of the radiation effect can be gleaned from what hasn't occurred. For example, it is known that protons and neutrons of 4 MeV energies and fluxes of 10^{13} particles/cm² will totally quench the spectrum of a semiconductor. Because the exposed samples still have a spectra, it can be said that the space environment did not present these types of particles during the mission.

The GaAs exposed samples showed decreases in luminescent intensity and some of the samples showed shifts of spectral peaks toward longer wavelengths. The exposed CdSe samples showed increases in luminescent intensity. Some of these changes are well documented in artificially irradiated laboratory samples. The samples have obviously underwent complex and defect center generation as a result of energetic particle collisions above the threshold energy.

VI. *Conclusions and Recommendations*

6.1 *Conclusions*

In this thesis, GaAs and CdSe semiconductors exposed to a low earth orbit space environment were studied using cathodoluminescence and photoluminescence to determine if radiation effects were present. Based upon the results presented in the previous chapter, the following conclusions have been reached:

1. Seven of the nine exposed samples examined displayed changes in their spectra when compared to the control samples.
2. The most prevalent changes in the GaAs samples were decreases in luminescent intensity and shifts of certain spectral peaks toward longer wavelengths.
3. The most prevalent changes in the CdSe samples were increases in luminescent intensity and slight shifts in peak positions toward shorter wavelengths.
4. Similar changes as in the exposed samples have been observed in artificially irradiated laboratory samples.
5. Because different types of radiation particles bombarded the sample simultaneously, luminescence alone generally will not enable effects to be assigned to specific types of space radiation, nor will it enable the magnitude of the effects to be quantified.
6. The majority of changes observed in the exposed sample occurred at wavelengths greater than 0.8μ .

6.2 *Recommendations*

1. Future analysis of the samples should involve electrical aspects of the irradiation changes in conjunction with further optical examinations.

2. The samples should be further examined with the Ge detector to provide damage information in longer wavelenghts.
3. The LEG32 electron gun should be modified to permit stable operations with better beam focus.
4. Because of inadvertant damage done to the exposed samples during removal from the tray, future LDEF samples should be held in place by other means than Torrseal to permit non-destructive removal.

Bibliography

1. Adams, J. H. and others. *Cosmic Ray Effects On Microelectronics, Part I: The Near-Earth Particle Environment*. 25 August 1981. Naval Research Laboratory Memorandum Report 4506-P. Washington: Office of Naval Research, August 1981 (AD-A103897).
2. American Society For Testing And Materials Special Study Group on Space Radiation and Matter. *Space Radiation Effects On Materials*. ASTM Special Technical Publication No. 330. Sponsored by ASTM Committee E-10 on Radioisotopes and Radiation Effects. ASTM, Philadelphia PA, October 1962.
3. Anderson, Kinsey A. "Energetic Solar Particles," *Space Physics*, University of California Engineering and Physical Sciences Extension Series, edited by Donald P. Le Galley and Alan Rosen. New York: John Wiley & Sons, Inc., 1964.
4. Arnold, G. W. "Luminescence in Intrinsic and Annealed Electron-Irradiated GaAs: Cd," *Physical Review*, 183: 777-783 (July 1969).
5. Arnold, George W. "Radiative Recombination in Annealed Electron-Irradiated GaAs," *Physical Review*, 149: 679-680 (September 1966).
6. Arora, B. M. and Compton, D. W. "Luminescence From Impurities and Radiation Defects in CdSe and CdS," *Journal of Applied Physics*, 43: 4499-4507 (May, 1972).
7. Baranowski, J. M. and Phuong An. "The Ni Donor and Acceptor Levels in CdSe," *Physica Status Solidi (B)*, 122: 331-335 (August 1983).
8. Benton, E. V. and Heinrich, W. (editors). "Ionizing Radiation Exposure Of LDEF," LDEF Pre-Recovery Estimates. Physics Department, University of San Francisco CA, August 1990.
9. Biswas, S. and others. "Nuclear Composition and Rigidity Spectra of Solar Cosmic Rays," *Astrophysics Journal*, 139: 941-950 (May 1964).
10. Brehm, G. E. and Pearson, G. L. "Gamma-Radiation Damage in Epitaxial Gallium Arsenide," *Journal of Applied Physics*, 43: 568-573 (February 1972).
11. Brodin, M. S. and others. "Nonlinearities in Excitonic Luminescence of Direct-Gap Semiconductors under Very Low Optical Excitation Levels," *Physica Status Solidi (B)*, 144: 863-873 (April 1987).
12. Brozel, M. R. "Defect Densities In SI LEC GaAs," *Properties of Gallium Arsenide*, Electronic Materials Information Service Datareviews Series No. 2. London: The Institution of Electrical Engineers (INSPEC), 1986.
13. Bryant, F. J. and Radford, C. J. "Electron Radiation Damage and the Green Edge Emission of CdS," *Journal of Physics C: Solid State Physics*, 3: 1264-1274 (January 1970).

14. Burrell, M. O. and Wright, J. J. *The Estimation of Galactic Cosmic Ray Penetration and Dose Rates: Technical Note*, March 1972. NASA TN D-6600. Marshall Space Flight Center AL: George C. Marshall Space Flight Center, March 1972.
15. Cherednichenko, A. S. and others. "Characteristics of Exciton Spectra of CdSe Crystals Due to Excitons Localized at Surface Fluctuations of the Potential," *Soviet Physics - Solid State*, 29: 1945-1946 (November 1987).
16. Clark, Lenwood G. and DiBattista, John D. "LDEF/Shuttle Capabilities For Environmental Testing In Space," *The Industrialization of Space*, Volume 36, Part 1, *Proceedings of the 23rd American Astronautical Society Annual Meeting*, October 18-20, 1977. 297-308. California: AAS Publications Office, 1978.
17. "Columbia Crew Retrieves LDEF, Conducts Medical Experiments," *Aviation Week & Space Technology*, 4: 35 (January 22, 1990).
18. Daly, E. J. "Radiation Environment Evaluation For ESA Projects," *American Institute of Physics*, 483-499 (1989) (A90-2530509-93).
19. Department of the Air Force. *Handbook of Geophysics And The Space Environment*. Edited by Adolph S. Jursa. Andrews AFB MD: Air Force Geophysics Laboratory, 1985 (AD-A1670000).
20. Department of the Air Force. *Space Handbook*. UA-18. Air Command and Staff College. Maxwell AFB AL: Air University Press, January 1985.
21. Dessler, A. J. and O'Brien, B. J. "Penetrating Particle Radiation," *Satellite Environment Handbook* (Second Edition), edited by Francis S. Johnson. Stanford: Stanford University Press, 1965.
22. Dunlap, W. Crawford, Jr. *An Introduction to Semiconductors*. New York: John Wiley & Sons, Inc., 1957.
23. Elsby, C. N. and Meese, J. M. "Luminescence in Electron Irradiated CdS," *IEEE Transactions on Nuclear Science*, Vol. NS-21: 14-20 (December 1974).
24. Feldman, Charles. "Range of 1 - 10 keV Electrons in Solids," *Physical Review*, 117: 455-459 (January 1960).
25. Fu, J. H. and Graves, G. R. "Thermal Environments For Shuttle Payloads," *AIAA Shuttle Environment And Operations II Conference*, AAIA No. 85-6055. 18-37. New York: AIAA Press, 1985.
26. Garlick, G. F. "Cathodo- and Radioluminescence," *Luminescence of Inorganic Solids*, edited by Paul Goldberg. New York: Academic Press, 1966.
27. Garrido, J. and others. "Photoluminescence in Gallium Arsenide Irradiated with Thermal Neutrons," *Physica Status Solidi (A)*, 65: 103-106 (January 1981).

28. Glinchuk, K. L. and Vovnenko, V. I. "Effect of Electron Irradiation on Recombination Characteristics of Deep Radiative Centres in GaAs," *Physica Status Solidi (A)*, 69: K43-47 (January 1982).
29. Gregory, J. C. and Peters, P. N. "A Measurement Of The Angular Distribution Of 5 eV Atomic Oxygen Scattered Off A Solid Surface In Earth Orbit," *Proceedings of the 15th International Symposium on Rarefied Gas Dynamics*. Volume 1. 644-657. Italy: B. G. Teubner Stuttgart, 1986.
30. Gregory, J. C. *Surface Interaction Mechanisms of 5 eV Atomic Oxygen: Data Analysis From The UAH Experiment On STS-8: Final Report*. NASA Grants NAGW-823. Huntsville AL: Alabama University, August 1987 (NASA 87N25447).
31. Hamilton, B. "Photoluminescence Spectra Of Group VI Doped GaAs," *Properties of Gallium Arsenide*, Electronic Materials Information Service Datareviews Series No. 2. London: The Institution of Electrical Engineers (INSPEC), 1986.
32. Hanson, W. B. "Structure of the Ionosphere," *Satellite Environment Handbook* (Second Edition), edited by Francis S. Johnson. Stanford: Stanford University Press, 1965.
33. Heitman, James M. *Photoluminescence Study of Laser Interaction With GaAs*. MS thesis, AFIT/GEO/PH/80-6. School of Engineering, Air Force Institute of Technology (AU), Wright-Patterson AFB OH, December 1980.
34. Henry, C. H. and others. "Optical Studies of Shallow Acceptors in CdS and CdSe," *Physical Review B*, 4: 2453-2463 (October 1971).
35. Herron, Russell G. "Proton Measurements On A Verticle Probe Into The South Atlantic Radiation Anomaly," *Space Research VI, Proceedings of the Sixth International Space Science Symposium*. 132-147. Edited by R. L. Smith-Rose. Washington: Spartan Books, 1966.
36. Hunton, D. E. and Calo, J. M. "Gas Phase Interactions In The Space Shuttle Environment," *AIAA Shuttle Environment And Operations II Conference*, AIAA No. 85-6055. 1-5. New York: AIAA Press, 1985.
37. Jeong, M. and others. "Photoluminescence Studies in Irradiated Si-Doped Gallium Arsenide," *Japanese Journal of Applied Physics*, 12: 109-119 (January 1973).
38. Johnson, Francis S. "Structure of the Upper Atmosphere," *Satellite Environment Handbook* (Second Edition), edited by Francis S. Johnson. Stanford: Stanford University Press, 1965.
39. Kalma, A. H. and others. "Electron Irradiation of GaAs," *Proceedings of the XI International Conference on the Physics of Semiconductors*. 364-370. Warsaw: Polish Scientific Publishers, 1972.

40. Kelso, Maj T. S., Compiled from orbital element sets obtained from NASA. Operational Sciences Department, School of Engineering, Air Force Institute of Technology (AU), Wright-Patterson AFB OH, May 1990.
41. Kittel, Charles. *Introduction to Solid State Physics* (Sixth Edition). New York: John Wiley & Sons, Inc., 1986.
42. Kozanecki, A. and others. "The Effect of High-Energy Electron Irradiation On The Edge Emission in CdSe," *International Conference on Defects and Radiation Effects in Semiconductors, Conference Series Number 46*. 406-413. Bristol and London: The Institute of Physics, 1979.
43. Kulp, B. A. "Displacement of the Cadmium Atom in Single Crystal CdS by Electron Bombardment," *Physical Review*, 125: 1865-1869 (November 1963).
44. Larin, Frank. *Radiation Effects in Semiconductor Devices*. New York: John Wiley & Sons, Inc., 1968.
45. Leverenz, Humboldt W. *An Introduction To Luminescence Of Solids*. New York: Dover Publications, Inc., 1968.
46. Loferski, J. J. and Ming Hsien Wu. "Studies of Radiation Defects in GaAs Based on Proton - and Electron - Bombardment Induced Light Emission," *Proceedings of the 7th International Conference on the Physics of Semiconductors*. 213-217. New York: Academic Press, 1964.
47. Maclin, Capt Myron T. *Depth-Resolved Luminescence of Gallium Arsenide Using Ion Etching*. MS thesis, AFIT/GEP/PH/81D-6. School of Engineering, Air Force Institute of Technology (AU), Wright-Patterson AFB OH, December 1981 (AD-A111 139).
48. Martinelli, R. U. and Wang, C. C. "Electron-beam Penetration in GaAs," *Journal of Applied Physics*, 44: 3350-3351 (July 1973).
49. Mathews, T. and Vekatesan, D. "Unique Series of Increases in Cosmic-Ray Intensity Due to Solar Flares," *Nature*, 345: 600-602 (1990).
50. McIlwain, C. E. "Measurements Of Trapped Electron Intensities Made By The Explorer XV Satellite," *Radiation Trapped In The Earth's Magnetic Field, Proceedings of the Advanced Study Institute*, 593-609. Volume V, edited by Billy M. McCormac. New York: Gordon and Breach, 1966.
51. Medland, J. and EMIS Group. "Photoluminescence Spectra Of LPE GaAs," *Properties of Gallium Arsenide*, Electronic Materials Information Service Datareviews Series No. 2. London: The Institution of Electrical Engineers (IN-SPEC), 1986.
52. Nahra, H. K. "Low Earth Environmental Effects On The Space Station Photovoltaic Power Generation Systems," *Proceedings of the Tenth Annual ASME Solar Energy Conference*. 499-507. New York: American Society of Mechanical Engineers, 1988 (A89-291111-20).

53. National Aeronautics and Space Administration, *The Long Duration Exposure Facility (LDEF)*. NASA SP-473. Washington: Scientific and Technical Information Branch, 1984.
54. Neuberger, M. *Cadmium Selenide Data Sheets*. Contract AF 33(616)-8438. Electronic Properties Information Center, Hughes Aircraft Company, Culver City CA, November 1963.
55. Newman, R. C. and Woodhead, J. "The Selective Trapping of Mobile Group-V Interstitials by Impurities in Electron-Irradiated GaAs and GaP," *Journal of Physics C: Solid State Physics*, 17: 1405-1419 (1984).
56. Owen, 2Lt Kelli and others. "Effects of CH_2Cl_2 on GaAs and UV-Irradiated Torrseal." Summary of Physics 688 Research. Air Force Institute of Technology (AU), Wright-Patterson AFB OH, June 1990.
57. Peaker, A. R. "Defect Energy Levels In VPE GaAs," *Properties of Gallium Arsenide*, Electronic Materials Information Service Datareviews Series No. 2. London: The Institution of Electrical Engineers (INSPEC), 1986.
58. Pedrotti, Frank L. *Optical Properties of CdS:Se Solid Solutions*. PhD dissertation. School of Engineering, Air Force Institute of Technology (AU), Wright-Patterson AFB OH, 1962.
59. Pogrebnyak, A. D. and others. "Positron Annihilation and Profiles of Radiation Damages in GaAs and Si Crystals Irradiated by Supercurrent Proton or Electron Beams," *Physica Status Solidi (A)*, 81: 217-225 (1984).
60. Pons, D. and others. "Electron Traps in Irradiated GaAs: Comparison With Native Defects," *International Conference on Defects and Radiation Effects in Semiconductors, Conference Series Number 46*. 406-413. Bristol and London: The Institute of Physics, 1979.
61. "Prompt Reports," *Solar-Geophysical Data*, 498: 10-12 (February 1986).
62. Roederer, Juan G. "Southern Hemisphere Anomalies," *Space Research VI, Proceedings of the Sixth International Space Science Symposium*. 117-129. Edited by R. L. Smith-Rose. Washington: Spartan Books, 1966.
63. Schulz, H. J. and Kulp, B. A. "Electron Radiation Damage in Cadmium-Selenide Crystals at Liquid-Helium Temperature," *Physical Review*, 159: 603-609 (July 1967).
64. Sharp, G. W. and others. "Direct Evidence For Copuscular Radiation Effects On The Ionosphere In The Southern Anomaly Region," *Space Research VI, Proceedings of The Sixth International Space Science Symposium*. 203-216. Edited by R. L. Smith-Rose. Washington: Spartan Books, 1966.
65. Singer, S. F. "On The Nature And Orgin Of The Earth's Radiation Belts," *Space Research I, Proceedings of the First Space Science Symposium*. 797-820. Edited by Hilde Kallman Bijl. Washington: Spartan Books, 1960.

66. Smith, Robert E. and West, George S. *Space And Planetary Environment Criteria Guidelines For Use In Space Vehicle Development*, 1982 Revision (Volume 1). National Aeronautics and Space Administration Technical Memorandum, TM 82478. Marshall Space Flight Center AL: George C. Marshall Space Flight Center, January 1983.
67. Sowle, D. H. and Lowen, R. W. "A Method For Calculation Of Average Radiation Fluxes On Satellites," *Radiation Trapped In The Earth's Magnetic Field, Proceedings of the Advanced Study Institute*, 808-814. Volume V, edited by Billy M. McCormac. New York: Gordon and Breach, 1966.
68. Srour, J. R. *Radiation Effects on and Dose Enhancement of Electronic Materials*. Park Ridge NJ: Noyes Publications, 1984.
69. Stassinopoulos, E. G. and Barth, J. M. *Non-Equatorial Terrestrial Low Altitude Charged Particle Radiation Environment: Version 2* (Revised Edition). NASA X-600-97-7. Goddard Space Flight Center MD: Goddard Space Flight Center, May 1987.
70. Tkachev, V. D. and others. "Radiative Recombination In GaAs With Residual And Radiation Defects," *Soviet Physics - Semiconductors*, 1: 825-827 (January 1968).
71. van Lint, V. A. J. and others. *Mechanics of Radiation Effects in Electronic Materials*. Volume 1. New York: John Wiley & Sons, Inc., 1980.
72. Varni, Capt Jamie G. G. *The Cathodoluminescence Of Cleartran: A Novel Form Of Polycrystalline ZnS*. PhD dissertation. AFIT/DS/ENP/86-2. School of Engineering, Air Force Institute of Technology (AU), Wright-Patterson AFB OH, December 1986.
73. Vavilov, V. S. and Ukhin, N. A. *Radiation Effects In Semiconductors And Semiconductor Devices*. New York: Plenum Publishing Company, 1977.
74. West, G. S. and Wright, J. J. *Natural Environment Design Requirements for the Space Telescope*. National Aeronautics and Space Administration Technical Memorandum, TM X-73316. Marshall Space Flight Center AL: George C. Marshall Space Flight Center, July 1976 (NASA 76N27137).
75. White, O. R. (editor). *The Solar Output and its Variation*. Boulder: Colorado Associated University Press, 1977.
76. Williams, E. W. and Bebb, H. Barry. "Photoluminescence II: Gallium Arsenide," *Semiconductors and Semimetals*, Volume 8, Transport and Optical Phenomena, edited by R. K. Willardson and Albert C. Beer. New York: Academic Press, 1972.
77. Williams, Ferd. "Theoretical Basis for Solid-State Luminescence," *Luminescence of Inorganic Solids*, edited by Paul Goldberg. New York: Academic Press, 1966.

78. Yacobi, B. G. and Holt, D. B. *Cathodoluminescence Microscopy of Inorganic Solids*. New York: Plenum Press, 1990.
79. Yeo, Y. K. and Ehret, J. E. "Amphoteric behavior of Ge implants in GaAs," *Applied Physics Letters*, *35*: 197-199 (15 July 1979).
80. Zimcik, D. G. and Maag, C. R. "Results Of Apparent Atomic Oxygen Reactions With Spacecraft Materials During Shuttle Flight STS-41G," *AIAA Shuttle Environment And Operations II Conference*, AIAA No. 85-7020. 181-189. New York: AIAA Press, 1985.

REPORT DOCUMENTATION PAGE

Form Approved
GMB No. 0704-0188

Public reporting burden for this collection of information is estimated to average 1 hour per response, including the time for reviewing instructions, searching existing data sources, gathering and maintaining the data needed, and completing and reviewing the collection of information. Send comments regarding this burden estimate or any other aspect of this collection of information, including suggestions for reducing this burden, to Washington Headquarters Services, Directorate for Information Operations and Reports, 1215 Jefferson Davis Highway, Suite 1204, Arlington, VA 22202-4302, and to the Office of Management and Budget, Paperwork Reduction Project (0704-0188), Washington, DC 20503

1. AGENCY USE ONLY (Leave blank)	2. REPORT DATE December 1990	3. REPORT TYPE AND DATES COVERED Master's Thesis	
4. TITLE AND SUBTITLE ANALYSIS OF SPACE RADIATION EFFECTS IN GALLIUM ARSENIDE AND CADMIUM SELENIDE SEMICONDUCTOR SAMPLES USING LUMINESCENCE SPECTROSCOPIC TECHNIQUES		5. FUNDING NUMBERS	
6. AUTHOR(S) Brad Lee Shaffer, Captain, USA		8. PERFORMING ORGANIZATION REPORT NUMBER AFIT/GSO/ENP/90D-2	
7. PERFORMING ORGANIZATION NAME(S) AND ADDRESS(ES) Air Force Institute of Technology, WPAFB OH 45433-6583		10. SPONSORING / MONITORING AGENCY REPORT NUMBER	
9. SPONSORING / MONITORING AGENCY NAME(S) AND ADDRESS(ES)		11. SUPPLEMENTARY NOTES	
12a. DISTRIBUTION / AVAILABILITY STATEMENT Approved for public release; distribution unlimited		12b. DISTRIBUTION CODE	
13. ABSTRACT (Maximum 200 words) Analysis of space radiation effects in gallium arsenide and cadmium selenide semiconductor samples using luminescence spectroscopic techniques. The M0006 semiconductor samples were placed into a 28.5 degree inclination, 480 km altitude, near-circular orbit aboard the Long Duration Exposure Facility satellite and exposed to direct space environment for a period of 11 months, and were shielded by 0.313 inches of aluminum for another 58 months. The samples were examined for changes using cathodoluminescence and photoluminescence in various wavelength regions from 0.5 to 1.8 microns. Samples were cooled to approximately 10 degrees Kelvin in a vacuum of 10 ⁻⁸ torr. Cathodoluminescence was performed with 1-3 keV electron energies at beam currents of 5-100 microamperes (2.5 x 10 ¹⁴ to 5.0 x 10 ¹⁵ electrons/cm ² -sec). The photoluminescence excitation source was a 20 mW Argon laser. Changes were detected in some of the sample pairs which could be attributed to radiation induced effects. The changes primarily manifested themselves in three different categories: 1) decrease or increase of luminescent intensity; 2) shifts in peak locations; and 3) quenching of a peak. Special changes noted by sample and category were: #12 (CdSe:S), 1) exposed sample increased five times in luminescent intensity, and the luminescence lines shifted slightly towards shorter wavelengths; #13 (CdSe:S), 1) the exposed sample had about five times greater luminescence than the control sample, additionally, the exciton related emission increased much more strongly than the donor-acceptor pair emission did for the exposed sample; #14 (p-GaAs:Zn), no changes; #15 (n-GaAs), 1) the relative intensity of carbon donor-acceptor pair emission increased slightly than that of the carbon free-to-bound transition from the exposed sample; #16 (GaAs), compensated material provided no signal in either control or exposed samples to evaluate; #17 (n-GaAs:Si), 3) the 1.479 eV Si donor-acceptor pair transition and 0.77 eV arsenic antisite related lines were quenched; #18 (GaAs:Si), 1) decrease in luminescence intensity, 2) peak shift towards longer wavelengths; #19 (GaAs:Si), 1) decrease in luminescence intensity; #20 (GaAs:Si), 2) peak shift towards longer wavelengths from 1.489 eV for control sample to 1.476 eV for the exposed sample; #21 (GaAs:Si), exposed sample was too damaged from unmounting process to be examined.			
14. SUBJECT TERMS LDEF, Space Radiation Effects, Space Environment, Radiation Effects on Semiconductors, Gallium Arsenide, Cadmium Selenide		15. NUMBER OF PAGES 119	16. PRICE CODE
17. SECURITY CLASSIFICATION OF REPORT UNCLASSIFIED	18. SECURITY CLASSIFICATION OF THIS PAGE UNCLASSIFIED	19. SECURITY CLASSIFICATION OF ABSTRACT UNCLASSIFIED	20. LIMITATION OF ABSTRACT UL